UNIVERSITY OF CALIFORNIA, SAN DIEGO

Structures of PKA RII Beta Holoenzymes Define Isoform Diversity

A dissertation submitted in partial satisfaction of the requirements for the degree Doctor of Philosophy

in

Chemistry

by

Simon Hugh Jolyon Brown

Committee in charge:

Professor Susan S. Taylor, Chair
Professor Timothy S. Baker
Professor Gourisankar Ghosh
Professor Paul A. Insel
Professor Yoshihisa Kobayashi
Professor Roger Y. Tsien

2008

The dissertation of Simon Hugh Jolyon Brown is approved, and it is acceptable in quality and form for publication on microfilm and electronically:

_____

_____

_____

_____

_____

_____

Chair

University of California, San Diego

2008

Table of Contents

List of Abbreviations

Å. Angstrom

AKAP. A-kinase anchoring protein

ATP. adenosine triphosphate

cAMP. adenosine 3',5'-cyclic monophosphate.

C-subunit. The Catalytic Subunit of PKA.

CNB. Cyclic nucleotide binding.

C-terminus. Carboxy-terminus.

D/D. Dimerization Docking domain.

D-AKAP2. Dual A-kinase anchoring protein-2.

DNA. Deoxyribonucleic Acid.

DTT. Dithiothreitol.

E. coli. *Escherichia coli*

EDTA. Ethylenediaminetetraacetic acid.

EGTA. [ethylenebis(oxyethylenenitrilo)] tetraacetic acid

IP20. Residues 5-24 of PKI.

kDa. Kilodaltons.

MALDI. Matrix-Assisted Laser Desorption/Ionization

MES. 2-(N-morpholino) ethanesulfonic acid

mg. milligram

µl. microliter

$MgCl_2$. Magnesium chloride.

mM. millimoles/liter

MOPS. 3-(N-morpholino) propanesulfonic acid.

mRNA. Messenger ribonucleic acid.

NaCl. Sodium chloride

N-terminus. Amino-terminus.

PAGE. Polyacrylamide gel electrophoresis.

PBS. Phosphate buffered solution.

PDB. Protein data bank.

pI. Isoelectric point.

PKA. Protein Kinase A or cyclic-AMP Dependent Protein Kinase

PKI. Protein kinase A inhibitor.

R-subunit. The Regulatory Subunit of PKA.

SDS-PAGE. Sodium dodecyl sulfate

TCEP. Tris(2-Carboxyethyl) phosphine Hydrochloride

TBS. Tris-Buffered Saline

Tris. Tris Hydroxymethylaminoethane.

WT. Wild type.

List of Figures

List of Tables

Acknowledgements

I would like to thank my parents for their continuous support. From the moment I started asking questions my parents have been there, patiently answering and explaining the world around me. Even though they lived thousands of miles away during the past decade, their constant support and encouragement in life have been crucial, especially in the past few years.

I would like to thank everyone in the Taylor lab. The people in the Taylor lab what makes it really special, and from my early days as a lab assistant all the way to the past few months as a frantic graduate student, everyone in the Taylor lab has been great. When I first joined the lab, Tom Diller and Xiadong Cheng gave me my first introduction into lab techniques that I still use today. John Jones taught me how to manage equipment in a lab full of independent scientists, as well as introducing me to backpacking. Ganesh Anand and Adrian Saldanha have been great teachers during graduate school, teaching me how to effectively design experiments and analyze data. Choel Kim has been my crystallography mentor over the years, teaching me everything from the mysterious uses of cat whickers to optimizing data collection.

Working with undergraduates throughout the past years has been a great joy. Laura Ellis and Kimberly Alberto were both fantastic to work with and provided invaluable support over their time in the lab. I learned more while trying to teach them than I learned anywhere else.

All the other members of the Taylor lab have been teachers, mentors, and friends. Peter Carmichael and Mike Moore kept me laughing, and provided motivation to finish graduate school. Francis Kinderman taught me everything I needed to know about hip-hop music, and showed the lab that all you need is one crystal. Cecilia Cheng has been my buddy for Friday afternoon beers, a travel partner, and just a great friend. Cecilia and I have been lucky to enough to bump ideas off each other for most of our time in graduate school and I have learned a lot from her.

Donald Blumenthal has been a friend and mentor ever since we first shared a beam line together. Don has been a great teacher every time we have done experiments together, and his advice as an outside observer of UCSD has always been of great value to me. I will miss the late nights at the beam line and the powder days at Alta.

I would like to thank my friends that have been so important to me during the last few years. I thank Justin Haas for his support and friendship over the past decade, and for giving me sense of perspective on life. I thank Laura Doolittle for her companionship and friendship, and especially for all the ways she taught me what is truly important in life.

I thank my advisor Susan Taylor for the years she has spent teaching me how to think about science. She has been my mentor ever since I started doing research at UCSD. I joined her lab as an undergraduate with barely a summer of experience. She gave the support and trust that enabled me to learn science in the lab, and opened new doors and opportunities for me

constantly. Susan has always supported my choices and has respected my opinions, scientific or otherwise, and I thank her especially for this respect.

Chapter 2 and Chapter 5 in part have been published as it may appear as R-subunit Isoform Specificity in Protein Kinase A: Distinct Features of Protein Interfaces in PKA Types I and II by Amide H/(2)H Exchange Mass Spectrometry. *J Mol Biol.* 374(2):487-99 (2007). Anand GS, Hotchko M, Brown SH, Ten Eyck LF, Komives EA, Taylor SS. The dissertation author was a secondary investigator and author of this paper.

Chapters 2 and 3 are in preparation for publication as it may appear as AMP-PNP Traps PKA RIIβ Holoenzyme in a Transition State Complex. Brown SHJ, Kim CW, Taylor SS. The dissertation author is the primary investigator and author of this paper.

Chapter 6 is in preparation for publication as it may appear as Protein Kinase A Isozyme Assays Reveal True Selectivity of Commonly Used cAMP Derivatives. Brown SHJ, Saldanha AS, Cottam H, Taylor SS. The dissertation author was the primary investigator and author of this paper.

Vita

Education

2008	Ph.D., Chemistry University of California, San Diego.
2001	M.S., Chemistry University of California, San Diego.
2000	B.S., Chemistry/Biochemistry University of California, San Diego.

Publications

Brown SHJ, Kim CW, Taylor SS. *AMP-PNP Traps PKA RIIβ Holoenzyme in a Transition State Complex*. In preparation.

Brown SHJ, Saldanha AS, Cottam H, Taylor SS. *Protein Kinase A Isozyme Assays Reveal True Selectivity of Commonly Used cAMP Derivatives.* In preparation.

Taylor SS, Kim C, Cheng CY, **Brown SHJ**, Wu J, Kannan N. *Signaling through cAMP and cAMP-dependent protein kinase: Diverse strategies for drug design.* Biochim Biophys Acta. 1784(1):16-26 (2007)

Wu J, **Brown SHJ**, Daake S, Taylor SS. *PKA Type IIα Holoenzyme Reveals a Combinatorial Strategy for Isoform Diversity* Science 318(5848):274-9 (2007)

Anand GS, Hotchko M, **Brown SHJ**, Ten Eyck LF, Komives, EA, Taylor SS. *R-subunit Isoform Specificity in Protein Kinase A: Distinct Features of Protein Interfaces in PKA Types I and II by Amide H/2H exchange Mass Spectrometry.* J Mol Biol 374(2):487-99 (2007)

Esposito V, Sjoberg T, Das R, **Brown S**, Taylor SS, Melacini G. *NMR assignment of the cAMP-binding domain A of the PKA regulatory subunit.* Journal of Biomolecular NMR 36 Suppl 1:64 (2006)

Wu J, **Brown S**, Xuong NH, Taylor SS. RIα Subunit of PKA: *A cAMP-free Structure Reveals a Hydrophobic Capping Mechanism for Docking cAMP into Site B.* Structure 12(6):1057-65 (2004)

Vigil D, Blumenthal DK, **Brown S**, Taylor SS, Trewhella J. *Differential Effect of Substrate Binding on Type I and Type II PKA Holoenzyme Dissociation.* Biochemistry 43(19):5629-36 (2004).

Vigil D, Blumenthal DK, Heller WT, **Brown S**, Canaves JM, Taylor SS, Trewhella J. *Conformational differences among solution structures of the type I alpha, II alpha and II beta protein kinase A regulatory subunit homodimers: role of the linker regions.* J Mol Biol. 337(5):1183-94 (2004).

Heller WT, Vigil D, **Brown S**, Blumenthal DK, Taylor SS, Trewhella J. *C-subunits Binding to the Protein Kinase RIα Dimer Induces a Large Conformational Change.* J. Biol. Chem. 279:19084-19090 (2004).

ABSTRACT OF THE DISSERTATION

Structures of PKA RII Beta Holoenzymes Define Isoform Diversity

by

Simon Hugh Jolyon Brown

Doctor of Philosophy in Chemistry

University of California, San Diego, 2008

Professor Susan S. Taylor, Chair

Protein phosphorylation is a major mechanism of enzyme control in cell signaling systems. Phosphoryl transfer activity by cyclic adenosine mono-phosphate (cAMP) dependant protein kinase A (PKA) is inhibited by the regulatory (R) subunits. The binding of cAMP to the R-subunit disassociates the PKA holoenzyme complex and releases the C-subunit inhibition. The R-

subunits consist of four non-redundant isoforms that vary in molecular weight, cAMP affinity, localization, and in their potential as PKA substrates. Although all known cAMP binding domains share the same basic structure, there is significant diversity among protein families and isoforms. RIIβ is implicated in both Lupus and cancer, and knockout of RIIβ in mice has unique phenotypes of obesity resistance and alcohol consumption.

The crystal structure of the RIIβ deletion mutant 108-268 bound to the C-subunit was determined at 1.6 Å. Crystallization of the holoenzyme complex with the non-hydrolyzable ATP analogue AMPPNP trapped the RIIβ substrate in a transition state. This structure revealed the conserved and non-conserved regions between RIIβ holoenzyme and previous structures of PKA holoenzymes. Biochemical affinity analysis determined the contribution of each domain of RIIβ in holoenzyme formation. The RIIβ linker region 102-107 was determined to be important for high affinity complex formation. The crystal structure of the RIIβ deletion mutant 102-265 bound to the C-subunit was determined at 2.9 Å. This structure highlighted the structurally unique docking of RIIβ 102-107 to the C-subunit. Solution based methods of hydrogen-deuterium exchange and small angle X-ray scattering demonstrated the isoform diversity of RIIβ and allosteric communication in the holoenzyme complex.

The cyclic nucleotide binding (CNB) domain is a highly conserved module that serves as the primary intracellular receptor for cAMP. Although

similar in sequence and overall structure, cAMP binding domains vary in affinity and binding rates for cAMP. Additionally, analogues of cAMP show distinct preferences for binding different CNBs. A high throughput, isoform specific assay to screen cAMP analogues demonstrated the RIIβ preference for N6 substituted analogues and RIα preference for C8 substituted analogues. The combination of X-ray structures and high throughput screening is a powerful technique to develop highly isoform specific cAMP analogues.

Chapter I

Introduction

Signal transduction is the communication system of life. Signals are passed from one part of an organism to another through an intricate system of hormones, nerves, primary and secondary messengers, and protein enzyme components. Signals go through many steps of modification, amplification, feedback and crosstalk on the way to producing downstream effects. Modulation of signaling cascades through systems of feedback and crosstalk are highly complicated and largely not understood. Simple signaling pathways have been described but the full extent of the complicated networks in an organism are just starting to be touched upon by the scientific community.

One element of signal transduction pathways is the transfer of a signal through the cell membrane into the cell, and the amplification of this signal upon its register on the outside of the cell. Many systems exist for this signal reception and amplification, including phosphorylation, calcium and sodium fluxes, and small molecule signaling. Protein phosphorylation is the process of transferring the γ-phosphate of ATP to a serine, tyrosine or threonine residue of the substrate. Phosphorylation by protein kinases often acts as a molecular on and off switch, switching substrate molecules between active and inactive states. Kinases themselves are an example of this effect, with the addition of a phosphate to the activation loop often necessary for kinase activity. In addition, phosphorylation can act to change binding affinities of a protein for partner molecules, affecting both activity and localization.

The protein kinases are one of the largest gene families, consisting of over 500 members and representing approximately 2% of the human genome.

[1, 2]. Even though substrates and regulation are highly diverse among members of this superfamily, all protein kinases in this large family share a conserved structural core. The first structural determination of a kinase in a fully active form was of the cyclic adenosine monophosphate (cAMP) dependent Protein Kinase (PKA) catalytic (C) subunit [3]. This crystal structure defined the kinase core and has served as a prototypical model for the entire family of kinases.

Regulation of PKA is achieved through both phosphorylation and cAMP release of inhibition of the regulatory (R) subunits, shown in Figure 1.1. The R-subunits of PKA are the major cellular receptors of cAMP in mammalian cells and serve to regulate and localize PKA in the cell. In the absence of cAMP, the R-subunits bind to the C-subunit, rendering the kinase inactive through blockage of the catalytic cleft of the kinase. Interaction between the R and C-subunits of PKA is a high affinity (<1nM) interaction, and conformational changes upon cAMP binding to the R subunit reduces this affinity by 3-4 orders of magnitude and allows for release of the active C-subunit for phosphorylation. The role of PKA in signal transduction is to act as a signal amplifier that can be easily modulated by a small molecule second messenger. Amplification of a signal occurs though the catalytic activity of PKA. Active PKA binds to substrates and transfers a phosphate from ATP to the substrate. This phosphorylation event modulates the activity of the substrate and downstream signaling. As a single active PKA molecule can

phosphorylation many substrate molecules, amplification of the cAMP signal occurs following PKA activation.

PKA subunits and subdomains are organized in a modular fashion. Basic subunit organization of the inactive form of PKA consists of a tetramer of four subunits, two C-subunits bind a dimer of identical regulatory subunits. The PKA C-subunit has a simple bi-lobal subdomain organization, consisting of an N-terminal (small) and C-terminal (large) lobe, shown in Figure 1.2. Each lobe is flanked by a short N- and C- terminal tail. The active site of the enzyme is located in the cleft between the two lobes, with the residues critical for catalysis located on the surface of the large lobe at the active site cleft. The binding site for adenosine tri-phosphate (ATP) is also located in the cleft between the large and small lobes, shown in Figure 1.3.

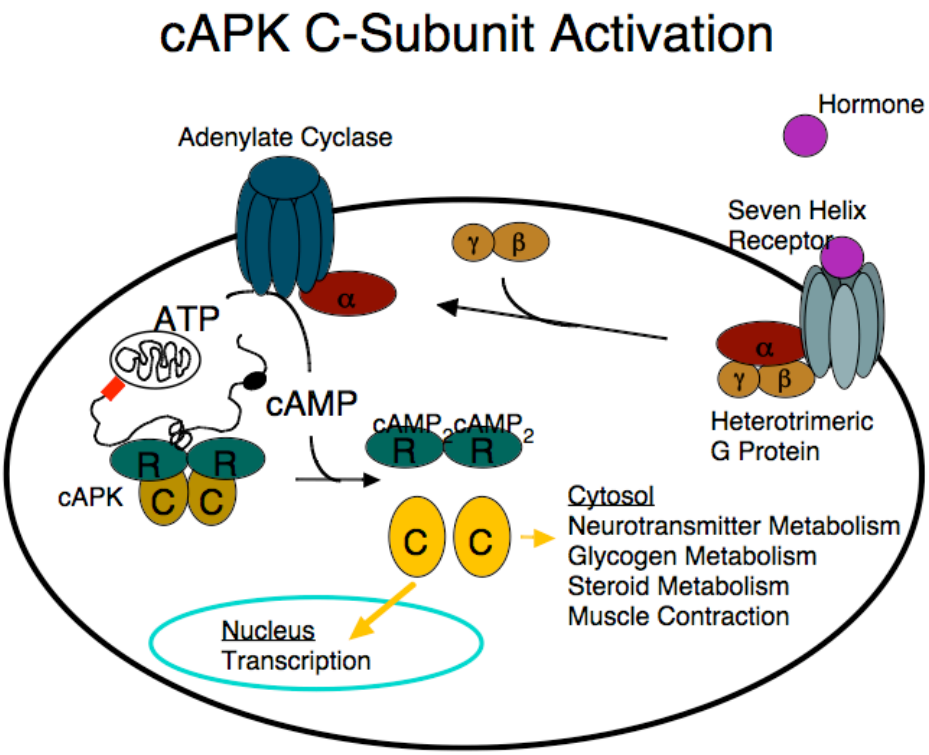

Figure 1.1: Activation of PKA by cAMP

In addition to the regulation of the catalytic activity by the regulatory subunits and cAMP, PKA is often localized to specific sites by A-Kinase Anchoring Proteins (AKAPs).

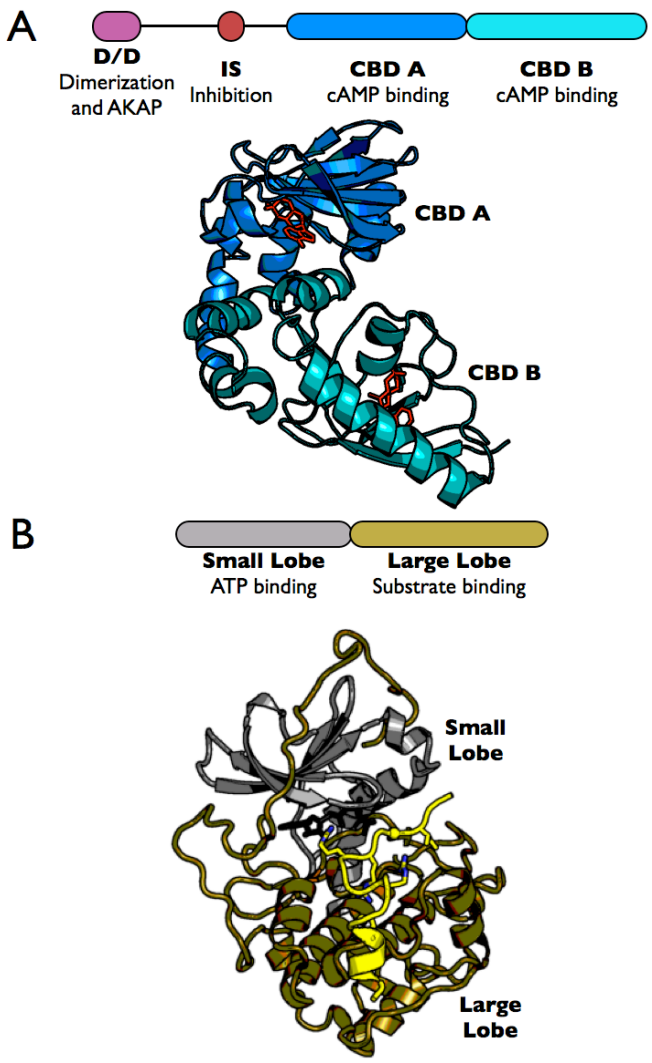

Figure 1.2: PKA Subdomain Organization.

Panel A shows the regulatory subunit: Domain A is shown in dark teal, Domain B is shown in light teal. The cAMP bound structure (PDB ID 1CX4) is rendered as a cartoon. Panel B shows the domains of the catalytic subunit. The N-terminal large lobe in tan, and the C-terminal small lobe in grey. Structure of ATP and PKI-bound PKA (PDB ID 1ATP) is rendered as cartoon.

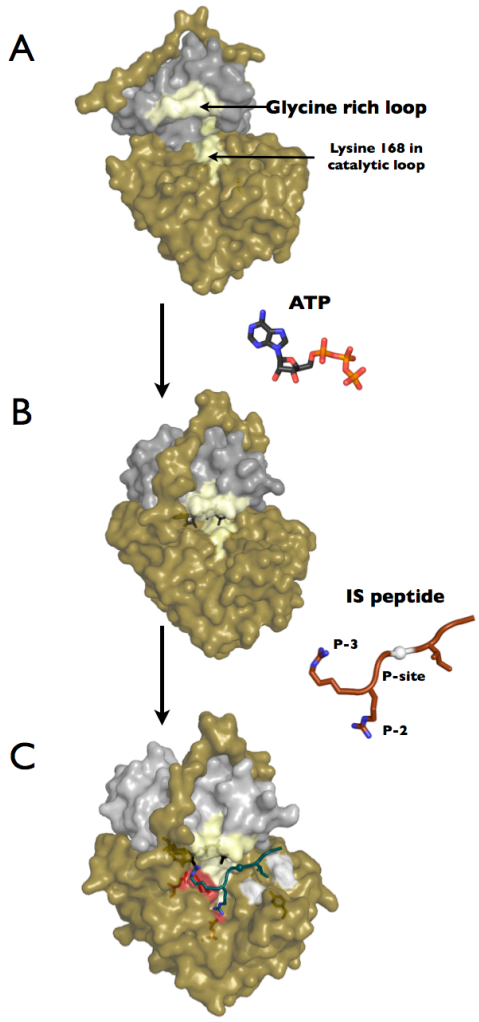

Figure 1.3: Conformational States of the Catalytic Subunit

Panel A shows an apoenzyme PKA catalytic subunit with ATP binding surfaces highlighted (PDB ID 1J3H). Panel B shows the catalytic subunit bound to ATP. Panel C shows the catalytic subunit bound to ATP and an Inhibitor Site (IS) peptide, and peptide binding surfaces highlighted. Panels B and C are visualized from a structure that contains ATP and IP20 (PDB ID 1ATP) to mimic a catalytic cycle.

The regulatory subunits of PKA have a more complicated modular subdomain organization shown in Figure 1.2. The R-subunits consist of 3 main subdomains separated by two flexible linkers. At the N-terminus is the dimerization and docking (D/D) domain that is necessary for the localization of PKA by anchoring proteins. This approximately 50-residue D/D segment forms an anti-parallel X type helical bundle that dimerizes the two R-subunits [4-6].

The dimerization of the R-subunits at the D/D domain creates a hydrophobic surface that is utilized for docking of A-Kinase Anchoring Proteins (AKAPs). AKAPs are scaffolding proteins that bring together multiple enzymes into higher order signaling complexes [7]. AKAPs bind a variety of proteins in addition to PKA, including PKA substrates, phosphatases, phosphodiesterases, and other components of the signaling pathway. Through localization to specific compartments in the cell, PKA is exposed to cAMP gradients allowing for activation of specific PKA isoforms and accurate phosphorylation of target proteins [7, 8].

C-terminal to the D/D domains is the inhibitor site of the R-subunits. This region consists of the 5 residues of the PKA substrate recognition sequence. This region extends 3 amino acids N-terminal (P-3) and 1 amino acid C-terminal (P+1) to the substrate site, is defined as the inhibitor site (IS). The IS region is flanked by two flexible linker regions. The linker that lies N-terminal to the IS is disordered in the free regulatory subunits, but becomes partially ordered upon forming the inactive tetramer [9, 10]. The 20 residue linker

between the IS and cAMP binding domains is only partially ordered in the free R-subunit, and becomes fully ordered in the presence of the C-subunit.

Following this flexible linker are two tandem cAMP binding domains. The cyclic nucleotide binding domains (CNB domains) are the primary functional units for regulating PKA activity. The CNB domains undergo significant conformational changes upon cAMP binding and transmit the signal of cAMP binding into the release of the C-subunit. The CNB domain's are highly conserved domains, with conservation held across domains of each R-subunit, across PKA isoforms, and across other cyclic nucleotide binding proteins [11, 12]. Comprised of about 120 amino acids, the general domain organization consists of an eight stranded beta sandwich that forms a basket-like structure. The cAMP molecule docks the functional phosphate in the bottom of this 'basket'. The Phosphate Binding Cassette (PBC) is the core of the cAMP binding site. Consisting of two β-strands attached by a small helical turn, the PBC contains critical arginine and glutamic acid residues for cAMP binding. Conformational changes that occur upon cAMP binding to the PBC are transmitted across the PBC into the entirety of the CNB domain and lead to PKA holoenzyme disassociation. The N-terminal CNB domain A has extended interactions with the C-subunit [13], while CNB domain B plays a role modifying the cAMP affinity of CNB domain A and as a secondary holoenzyme binding surface [14, 15].

There are four different isoforms of the PKA R-subunits that vary in sequence, molecular weight, pI, and cAMP binding affinity. Sequence

alignments of the four isoforms of the R-subunits are shown in Figure 1.4. Initially characterized by elution time from an ion exchange DEAE column, PKA types RI and RII were identified and isolated [16]. The most significant difference between RI and RII isoforms of PKA is the autophosphorylation potential of the inhibitor site. The RII subunits contain a serine at the inhibitor site making them substrates as well as inhibitors for the C-subunit, while RI subunits contain a glycine or alanine rendering them pseudosubstrates. This difference in phosphorylation potential will be discussed further and has major implications for the R-C interaction and PKA's role in signal transduction. Additionally, Type I PKA has an absolute requirement for two magnesium ions and ATP to form a tight holoenzyme complex, while Type II PKA can form a high affinity complex (<1nM) in the absence of nucleotide [15].

PKA isoforms also vary in subcellular localization, tissue expression, and cell type expression [17]. In general, RIα and RIIα are ubiquitous, while the RIβ and RIIβ isoforms are more tissue specific. RIβ has been detected mainly in neuronal tissues, while RIIβ has the highest expression in neuronal, adipose, testes and heart tissues. RII subunits have higher affinity than RI subunits for AKAP scaffold proteins, and are often found localized to subcellular organelles, especially the nuclear envelope, the Golgi, and the cytoskeleton. Conversely, RIα and RIβ are typically cytoplasmic in most cell types but can be dynamically recruited to AKAPs [18].

Figure 1.4: Sequence comparison of PKA R Isoforms.

PKA sequences are represented by single letter code. Sequences are aligned using in house software. (Kannan Natarajan)

Table 1.1: Properties of PKA Regulatory Isoforms

	RIα	RIβ	RIIα	RIIβ
Tissue	ubiquitous	brain, spinal cord, testes	ubiquitous	brain, adipose, heart, testes
Localization	cytoplasmic	cytoplasmic	targeted	targeted
PI	5.27	5.64	4.78	4.90
MW	42762	43027	45258	45992
Ka (cAMP)	101 nM [19]	24 nM [20]	63 nM [21]	610 nM [22]
PKA substrate	no	no	yes	yes
R-C Affinity	0.19 nM [19]	0.13 nM [23]	< 1 nM [15]	0.2 nM [22]

Table 1.2: RIIβ Construct Summary

	RIIβ (108-268)	RIIβ (102-265)	RIIβ (108-402)	RIIβ Full-length
CNB Domains	A	A	AB	AB
R-C Affinity				
+ AMPPNP	11.3 nM	0.6 nM	0.2 nM	0.2 nM
- AMPPNP	n.d.	n.d.	1.6 nM	n.d.
MW (Da)	18349	18713	33140	45992

PKA regulatory subunits are shown by targeted gene replacement to not be interchangeable. For example, unlike the other three isoforms, targeted gene replacement of RIα is embryonically lethal in mice, through a failure of mesoderm-dependent cardiovascular development. Addition of a targeted disruption of the Cα isoform to the deficient RIα mice results in restoration of viability [24]. Therefore, it is presumed that it is unregulated Cα subunit in the RIα targeted gene replacement mice that causes developmental failure.

RIIβ targeted gene replacement in mice creates a number of interesting phenotypes that are mainly focused on the adipose and neuronal roles for RIIβ. RIα over expression is observed in RIIβ knockout mice; however, the mice have a phenotype of small fat cells and resistance to obesity [25]. Recent studies have shown that these RIIβ targeted gene replacement mice are also resistant to diet-induced diabetes [26], and RIIβ targeted gene replacement in obesity model agouti mice restores a normal phenotype [27]. Leanness does not result from a decrease in caloric intake or absorption, and mutants are slightly hyperphagic. The reduction of fat in adipose tissue results from a decrease in the storage of triglycerides.

The exact mechanism of obesity resistance is unknown; however, a functional correlation between RIα compensation and RIIβ targeted gene replacement has been hypothesized. RIIβ is primarily expressed in BAT and WAT fat cells, and targeted gene replacement of RIIβ causes a compensatory increase in RIα in both cell types. Since the RIIβ holoenzyme has a higher

activation K_A for cAMP, it requires higher levels of cAMP for activation than the RIα holoenzyme. Increases in PKA activity has also been observed in BAT and WAT of mice that are depleted of RIIβ. Deficient mice also have reduced levels of leptin, indicating a link between satiety and expression of RIIβ subunit [28].

Targeted gene replacement of RIIβ in mice also causes an increase in alcohol consumption and a lack of response to alcohol intoxication [29]. Mice missing RIIβ voluntarily drink nearly twice as much ethanol as compared to control mice but were much more resistant to the sedative effects of ethanol consumption. RIIβ is the primary R-subunit in many brain regions, and targeted gene replacement of RIIβ is only partially compensated for by increases in RIα and RIβ. R-subunit serves two roles for the C-subunit; they regulate its activity and protect it from degradation [30]. The effects of the lack of RIIβ are therefore two fold: there is an increase in PKA activity due to lack of RIIβ regulation, and there is a decrease in steady state C-subunit activity due to loss of proteolytic protection. The effects of loss of RIIβ in the brain is complicated, with changes in both the levels of C-subunit activity and degradation, and further understanding of the changes of levels of dynamic PKA activity is still needed to understand the ethanol-resistance phenotype.

In addition to the targeted gene replacement studies described above, other studies have shown that the balance of type I and type II activity and expression plays a role in cell growth and differentiation [31, 32]. Loss of this

balance between the activities of the R-subunit isoforms has roles in disease mechanisms, including the autoimmune disease Systemic Lupus Erythematosus (SLE/Lupus), Carney complex, and breast cancer [33-37].

Carney complex is an autosomal dominant condition that causes tumors in the heart and skin, hyperpigmentation of the skin, and endocrine problems. The primary cause of Carney complex is mutations in the RIα subunit of PKA, causing nonsense-mediated mRNA decay and reduction in expression of the RIα subunit; however, the exact mechanisms remain unclear. It is hypothesized that RIα acts as a tumor suppressor function based on studies of the Carney complex syndrome [33, 34].

Systemic lupus erythematosis (SLE) is an autoimmune disease characterized by a serious dysfunction in the immune response. Recent reports have indicated that PKA is an important enzyme in the negative regulation of immune response. PKA has shown to be a legitimate target for autoimmune reactive T-cells due to deficiencies in PKA phosphorylation in these cells. Levels of both PKA I and II proteins and phosphorylation activity are decreased 3-4 fold in SLE T-cells, and PKA acts to down regulate immune response through the inhibitory PKA-SRC pathway. Activation of PKA by a cAMP agonist showed that the restoration of PKA activity induces down regulation of T-cell response. Therefore, PKA is a legitimate target for reduction of abnormal autoimmune response in SLE T-cells [35, 38-40].

Differential expression and mRNA levels of PKA isoforms also have been correlated with clinical human tumors and cell lines. Increased

expression of RI over RII has been shown in breast, renal, and colon cancer carcinomas, and well as in a number of human cancer cell lines [41, 42]. Additionally, RIα overexpression has also been associated with an increase in growth advantages for HL60 and MCF-7 cell lines [36]. RIα overexpression in normal cells only occurs under conditions of cell proliferation, while in cancer cells RIα is constitutively overexpressed.

Targeting RIα through use of antisense techniques has been shown to inhibit growth in both cancer cell lines and mouse models [43]. A second approach for altering the RI/RII balance in cancer cells is to modulate the levels of RIIβ. Antisense reduction in RIIβ levels produces cell lines that are resistant to cAMP-induced growth inhibition and differentiation [44]. Interestingly, a mutant form of RIα containing a phosphorylation site at the inhibitor site that mimics RIIβ shows a phenotype similar to RIIβ overexpression. Therefore, the single mutation of the P-site phosphorylation site between RIα and RIIβ to produce a RIα-P can confer a phenotype similar to reducing RIα levels through site selective analogues or antisense therapy [45].

To understand the role that RIIβ plays in disease, investigation of the structural and functional features that make RIIβ unique is necessary. Furthermore, in order have a complete understanding of the mechanism of cAMP activation; both the cAMP bound and C-subunit bound states of RIIβ are needed. Shown in Figure 1.5, crystal structures of RIIα and RIα bound to the

C-subunit demonstrated differences between the RII and RI isoforms, defined the mechanisms of inhibition and cAMP-induced activation, and allowed investigation of roles of key residues in each state of the R-subunit. Crystal structures of cAMP bound RIα and RIIβ defined the mechanism of cAMP binding and the role of the PBC in ligand binding, but the structures of both a cAMP bound and C-subunit bound RII isoform is needed for complete understanding of RII specific features.

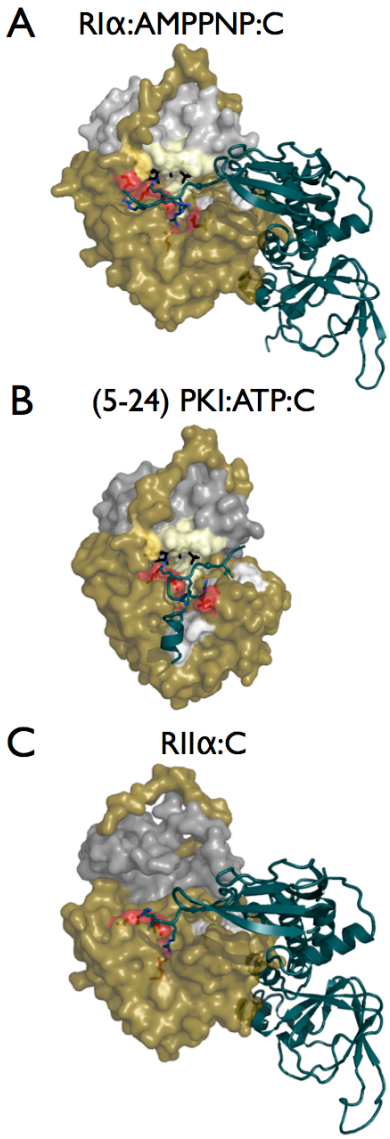

Figure 1.5: Binding of Inhibitors to the Catalytic Subunit

Panel A shows RIα (91-376) bound the catalytic subunit in the presence of Mn^{2+}: AMPPNP. Panel B shows the 20-mer IP20 peptide from Protein Kinase Inhibitor (PKI) bound to the catalytic subunit in the presence of Mg^{2+}: ATP. Panel C shows RIIα (91-400) bound to the catalytic subunit in the absence of nucleotide.

The overall goal of this thesis is to define the molecular features of RIIβ and in particular to determine how it differs from both RIα and RIIα. Studies will elucidate the structural and biochemical properties of RIIβ to specifically define the role of the RIIβ subunit as an inhibitor of the C-subunit and the mechanism of cAMP activation at the molecular level. Elucidation of the isoform specific characteristics of the RIIβ isoform in both the holoenzyme and cAMP bound forms will also define mechanisms behind the importance of RIIβ in disease, and may allow development of future therapies. Comparison of RIIβ and RIα holoenzymes will elucidate the importance of isoform-specific characteristics of the CNB domains and will define the role of the phosphorylation site of the RII subunits in PKA inhibition.

In Chapter Two, the design of stable RIIβ constructs is described. Surface Plasmon Resonance (SPR) is used to define the roles of each subdomain of RIIβ for inhibition of C-subunit and elucidate the importance of ATP in the R-C interaction interface.

Chapter Three describes the crystal structures of two RIIβ-C holoenzymes co-crystallized with AMPPNP, a non-hydrolyzable ATP analogue. AMPPNP traps the RIIβ holoenzyme in a transition-like state that highly resembles RIα. A second RIIβ holoenzyme crystal structure demonstrates the surprising importance of the 6 residues N-terminal to the inhibitor site and defines a new binding surface for RII subunits.

Chapter Four summarizes structural work on the linker regions of RIIβ and the importance of this region for explaining differences between RIIα and RIIβ. Small angle X-ray scattering analysis (SAXS) defines the global shape of RIIβ in solution. Peptide scanning of D/D domain binding D-AKAP2 peptides demonstrates RIIα and RIIβ specificity in the D/D interactions with D-AKAP2.

Chapter Five describes the application of another solution-based technique to investigate the RIIβ-C interaction. This study using amide $H/^{2}H$ exchange mass spectrometry complements the crystallography and SPR results. A potential mechanism for allosteric communication in the C-subunit and the role of the RIIβ B-domain are discussed

In Chapter Six, an isoform specific activation assay is described and the results of cAMP analogue screening for isoform specificity are presented. Structural analysis of the crystal structure of RIIβ (108-402) bound to HE33 reveals a possible mechanism for selectivity. Future chemical modifications of the selectivity features of the cAMP analogues are likely to yield highly selective PKA agonists and antagonists.

Chapter II

Engineering of RIIβ Deletion Mutants

Crystal structures of the C-subunit bound to both ATP and a peptide inhibitor [46, 47] defined the functional domains of the C-subunit and allowed investigation of the catalytic mechanism. The structure of the RIIβ subunit bound to cAMP [48] defined the cAMP binding domains of the R-subunit. However, in order to understand the RIIβ inhibition of C-subunit and the cAMP-induced activation of the RIIβ holoenzyme at a molecular level, higher order structures of the proteins together in a holoenzyme complex were needed.

The RIIβ cAMP bound structure was solved by using an N-terminal deletion mutant of RIIβ [49]. Initial purifications of the deletion RIIβ subunit were based on constructs used for RIα cAMP bound structures, and a construct containing the IS and both CNB domains was cloned and expressed. This construct was unstable during purification, and the final construct used for the RIIβ cAMP bound structure was RIIβ (112-416), a construct that was missing both the N-terminal linker region and four residues at the inhibitor site. The final structure had significant disorder at the N-terminus, and order of the N-terminus began at residue 130.

Small angle X-ray scattering (SAXS) experiments defined the general shapes and provided low-resolution models for the tetramer and dimer forms of the PKA holoenzymes [50-52]. The RIα dimer has a general Y shape configuration, with the addition of the C-subunit changing the overall shape only slightly. The C-subunits only induce a moderate overall conformational

change even though there are many changes within the CNB domains of RIα. The RIIα and RIIβ subunits are much more extended as dimers, with both isoforms forming a dumbbell-like shape. The RIIα holoenzyme maintains this extended structure following C-subunit binding, while surprisingly the RIIβ subunit undergoes a large compaction during holoenzyme formation [51]. This globular shape of the RIIβ holoenzyme indicated that crystallization of a full-length RIIβ holoenzyme complex may be feasible, and this was a major motivator for ongoing structural studies of the holoenzyme.

The high affinities between the R and C-subunits of PKA are the result of a large protein-protein binding surface with a combination of hydrophobic and charged interactions between these two surfaces [14, 15]. The binding of cAMP to the R-subunit is able to induce a conformational change that can release this interaction. In this way specific cAMP-induced changes of the R-C interaction surface cause a decrease in the R-C affinity to the point of C-subunit release. Most of the interactions between R and C-subunits are associated with the C-terminal regions of R including the inhibitor site and the CNB domains.

A primary goal of the RIIβ holoenzyme project was to engineer constructs of the RIIβ subunit that could form high affinity complexes with the C-subunit. A stepwise approach utilizing modular constructs was highly successful in determining the functions of each domain of RIα [53-56], and a similar strategy was used for RIIβ. To investigate the role of the domains of

RIIβ, three stable monomeric forms of RIIβ with high affinity for the C-subunit were engineered. Surface Plasmon Resonance (SPR) was used to characterize the affinities of these RIIβ constructs for the C-subunit in the presence and absence of AMPPNP.

Results:

Design of Constructs: To understand the importance of isoform differences in regulation of PKA activity, structural and biochemical information of multiple isoforms for PKA holoenzyme must be obtained. Goals for designing constructs of RIIβ were three-fold. We wanted to obtain monomeric forms of the RIIβ subunit, both an A domain and an AB domain construct, that were stable, expressed at high levels, and formed a tight complex with the C-subunit. To achieve this, a stepwise process of purification and mass spectrometry (MS) analysis was used to obtain proteolytically stable RIIβ constructs. These constructs were then used for crystallization and for hydrogen deuterium exchange experiments.

RIIβ (108-402): Due to the lack of a complete inhibitor site, the deletion RIIβ used for the elucidation of the cAMP bound structure could not be used for investigation of the holoenzyme states. A construct containing the extra residues of the inhibitor site and the complete B domain was therefore designed and purified. Shown in Figure 2.1, this construct, RIIβ (106-416), degraded at both the N and C-terminus and was not suitable for structural studies. Mass Spectrometry (MS) analysis indicated that RIIβ (108-402) was a stable degradation product, and this was confirmed by subsequent cloning and purification.

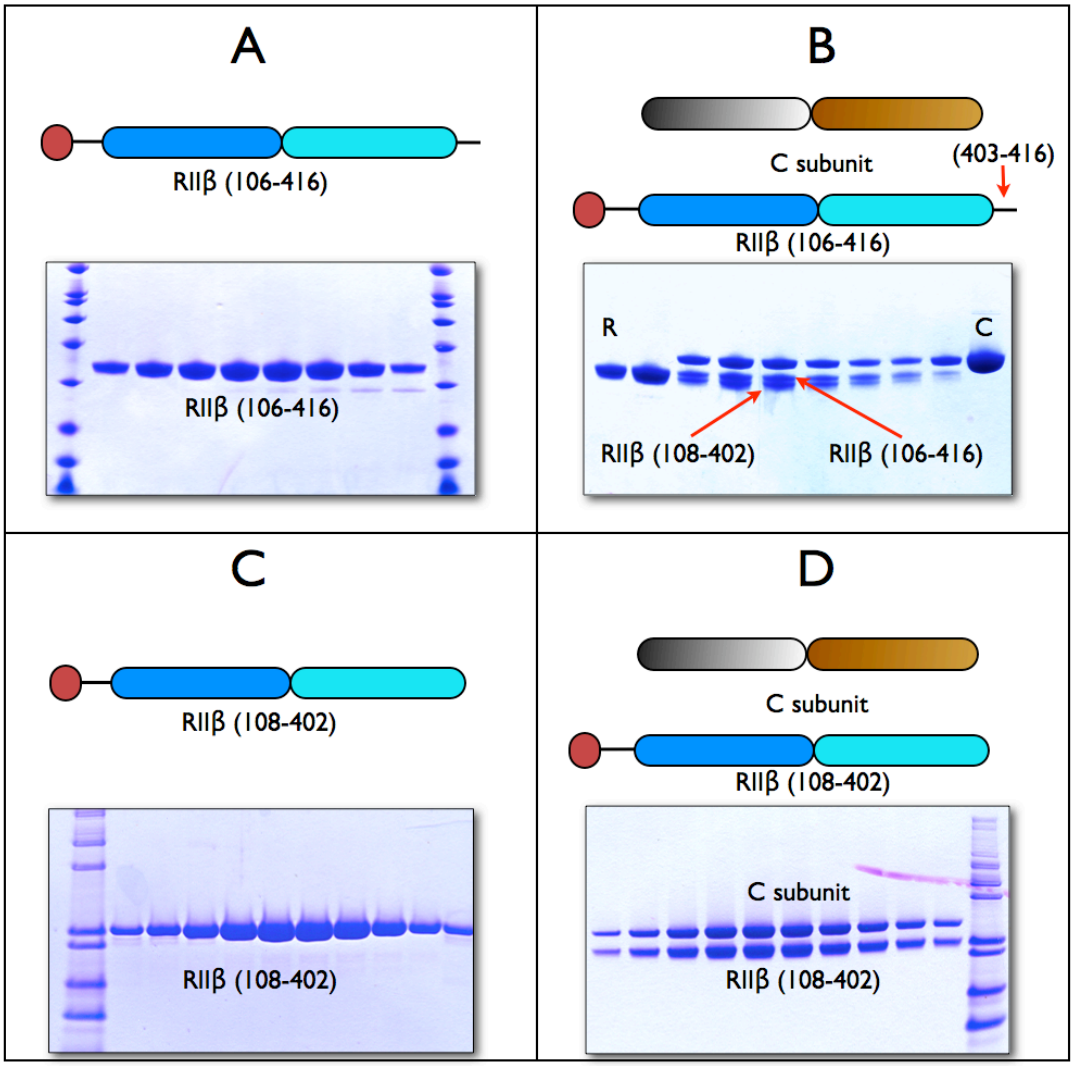

Figure 2.1: Design and Purification of RIIβ (108-402)

Panel A shows an SDS gel of RIIβ (106-416) purified on gel filtration. Panel B the elution of holoenzyme from a gel filtration column. Arrows indicate two bands for R-subunit and identify the faster moving band of RIIβ (108-402). Panel C shows RIIβ (108-402) elution from a gel filtration column. Panel D shows the elution of RIIβ (108-402) holoenzyme.

RIIβ (108-268): Studies of the RIα subunit indicated that a construct containing residues (91-244) that extends from the IS through CNB domain-A contributes most if not all of the affinity between RIα and C [57]. To define the minimal high affinity binding region for RIIβ, a search for a shorter RIIβ construct that retained the ability to inhibit the C-subunit was attempted. The first attempt to form an RIIβ A domain was RIIβ (108-281). The N-terminal truncation was chosen through sequence analysis and comparison with the RIα subunit, while the C-terminal truncation was based on hydrogen deuterium exchange experiments. RIIβ (108-281), however, proved to be susceptible to degradation, and MS analysis indicated that RIIβ (108-268) was a more stable construct. This protein was cloned and expressed, and proved to be a stable form of RIIβ that contained only CNB domain-A as shown in Figure 2.2.

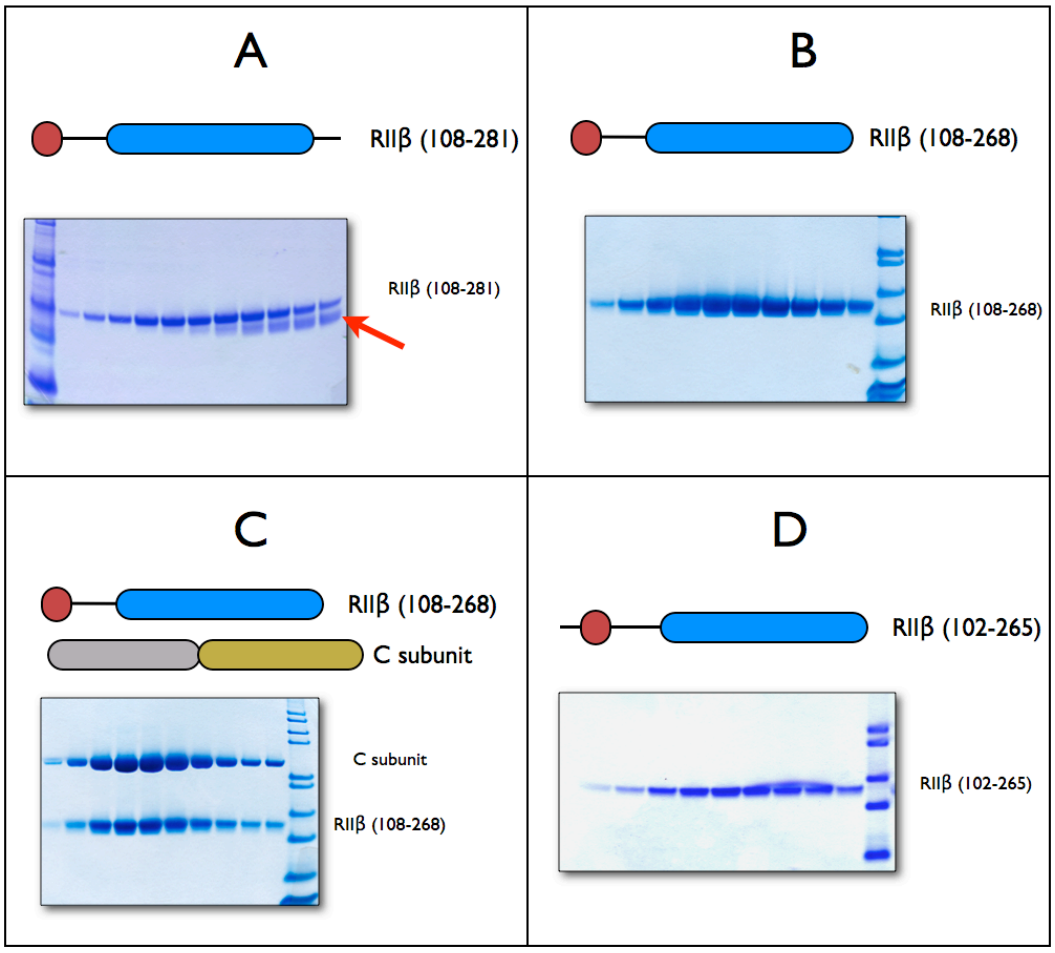

Figure 2.2: Design and Purification of RIIβ A Domains

Panel A shows elution of the initial construct of an RIIβ mutant that included that inhibitor site and domain A. Arrow indicates the degradation product that was identified as RIIβ (108-268) based on mass spectrometry. Panel B shows the purification of RIIβ (108-268). Panel C shows formation of a holoenzyme complex with RIIβ (108-268). Panel D shows a second stable RIIβ construct extending the N-terminus of RIIβ.

Purification of Holoenzymes: Surprisingly, the initial trials of holoenzyme formation with the RIIβ (108-268) indicated that the A domain behaved very differently from the RIIβ (108-402) that contained both CNB domain-A and CNB domain-B. In the absence of nucleotide, RIIβ (108-402) formed a stable dimer that could readily be isolated on a gel filtration column. In contrast, RIIβ (108-268) containing only the A domain formed mixed peaks during size exclusion chromatography. However, when AMPPNP was included in the buffer, RIIβ (108-268) and RIIβ (102-265) both formed high affinity complexes. These results are similar to the RIα isoform which has an absolute requirement for ATP to form a holoenzyme complex. These results indicated that RIIβ has different roles for both ATP and the B domain in holoenzyme formation when compared to RIα.

Surface Plasmon Resonance: To quantify the role that each domain of RIIβ plays in the R-C interaction, SPR was used. Results are shown in Figure 2.3. To elucidate the effects of CNB domain-B, affinity comparisons were made between the RIIβ (108-168) containing only the CNB domain-A and RIIβ (108-402) containing both CNB domain-A and CNB domain-B. Two different buffer conditions were utilized in order to quantify the role that ATP plays in the RIIβ-C interaction. Since ATP would cause autophosphorylation of the RIIβ IS during the experiment, the non-hydrolyzable analogue adenylylimido-diphosphate (AMPPNP) was used.

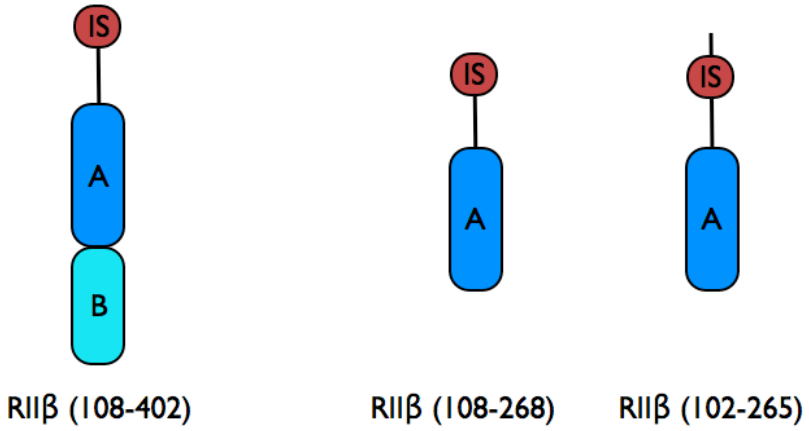

Complex	RIIβ (108-402) APO	RIIβ (108-402) Mn^{2+} AMP-PNP	RIIβ (108-268) Mn^{2+} AMP-PNP	RIIβ (102-265) Mn^{2+} AMP-PNP
k_{assoc} ($M^{-1}s^{-1}$)	1.5 (±0.2) x 10^{5}	4.2 (±0.6) x 10^{5}	3.1 (±0.2) x 10^{6}	8.6 (±1.0) x 10^{6}
K_{diss} (s^{-1})	2.4 (±0.1) x 10^{-4}	8.4 (±2.6) x 10^{-5}	3.5 (±0.1) x 10^{-2}	4.9 (±0.6) x 10^{-3}
K_D	1.6 nM	0.2 nM	11.3 nM	0.6 nM

Figure 2.3: Affinities of RIIβ constructs for the Catalytic Subunit.

Affinities of RIIβ for the catalytic subunit were measured by surface plasmon resonance (SPR). The RIIβ (108-402) was measured both in the presence and absence of AMPPNP. Neither of the shorter constructs could be measured using SPR in the absence of AMPPNP.

The K_D for RIIβ (108-402) in the presence and absence of Mn^{2+}: AMPPNP was 0.2 nM and 1.6 nM, respectively. AMPPNP thus increased the RIIβ (108-402) affinity for C by 8-fold. This increase in affinity was due to both an increase in the association rate and a decrease in the disassociation rate. This binding affinity in the absence of AMPPNP is consistent with previously published SPR analysis of full length RIIβ [22].

The affinity of the minimal binding construct, RIIβ (108-268), for the C-subunit without Mn^{2+} : AMPPNP was too low to be measured by SPR. This is consistent with size exclusion chromatography. In the presence of AMPPNP, however, the affinity increased to 11.3 nM for the RIIβ (108-268)-C interaction. The presence of nucleotide is thus critical for formation of a high affinity holoenzyme complex when only the A domain of RIIβ is present.

The affinity of RIIβ (108-268) compared to RIIβ (108-402) demonstrates the importance of the B domain in the RIIβ holoenzyme complex. The inclusion of the B domain in RIIβ not only increases the R-C affinity from 11.3 nM to 0.2 nM, but also reduces the requirement for AMPPNP. The B domain increases the affinity of the RIIβ-C interaction almost 60-fold in the presence of AMPPNP.

Purification and Characterization of RIIβ (102-265): Analysis of the isoform specific features conserved between RIIα and RIIβ indicated that the region that precedes the IS, up to the P-10 site are conserved in both RII

subunits. Earlier results indicated that RIIβ (102-265) had low affinity for the C-subunit and disassociated when analyzed by gel electrophoresis under non-denaturing conditions where the native state of the protein is preserved.

To determine the importance of this region for binding to the C-subunit, the affinity of RIIβ (102-265) for the C-subunit was measured in the presence of AMPPNP. Surprisingly, addition of this 6-residue region increased the affinity for the C-subunit by almost 20-fold. RIIβ (108-268) has an affinity of 11.3 nM, while extension of RIIβ to (102-265) increases the affinity to 0.6 nM. This demonstrates the importance of the linker region between the inhibitor site and the D/D domain for RIIβ-C affinity.

Discussion:

Role of AMPPNP in RIIβ holoenzyme: The SPR analysis of our RIIβ mutants indicates a surprising role for AMPPNP in the RIIβ-C complex. When only the RIIβ A-domain is present, the affinity of the complex is in the high μM range without nucleotide, but when AMPPNP is present, the affinity decreases into the nM range. This is similar to the A domain of RIα and to PKI, both which show an absolute dependence for ATP to form a tight holoenzyme complex. We are only able to observe the importance of the nucleotide for RIIβ because we are using a non-hydrolyzable analogue of ATP. Under physiological conditions RIIβ would be phosphorylated on Ser 112 in the presence of ATP, and this would facilitate disassociation. Thus, we are trapping a transition intermediate.

Biacore analysis confirms the lack of requirement for Mn^{2+}AMPPNP in the RIIβ AB domain holoenzyme complex, as has been noted as well in the RIIα subunit [15]. Using AMPPNP we show that nucleotide does increase the affinity of RIIβ for C, but the effect is slight. The 8-fold increase in affinity when AMPPNP is present for RIIβ (108-402) is much smaller than the effect ATP has on the RIα complex. In the full length RIα protein, ATP was shown to increase the RIα-C affinity more than 3-orders of magnitude, primarily by a decrease in the off-rate [58, 59]. Additionally, SPR demonstrates the surprising requirement for Mn^{2+}AMPPNP in forming high affinity holoenzyme complexes with RIIβ where the B domain is missing.

Role of Domain B in the RIIβ holoenzyme: The B-domain in RIIβ plays a significant role in the increasing the affinity of RIIβ for C. The K_D goes from 11.3 nM for RIIβ (108-268) to 0.2nM for RIIβ (108-402). This 70-fold increase in RIIβ-C affinity due to addition of the B domain is in stark contrast to the RIα holoenzyme, where the B domain does not contribute significantly to the affinity but rather plays a role as a gatekeeper for cAMP binding to CNB domain-A[14]. Our SPR results further emphasize the role of the B-domain in the RIIβ-C interaction.

RIIβ (P-10 – P-5) Affinity Effects: Shown in Figure 2.4, RIIβ (102-265) binds to the C-subunit with an affinity 20-fold higher than RIIβ (108-268). The region extending from P-5 to P-10 in RIIβ, which is conserved and hydrophobic in RIIα and RIIβ, surprisingly increases the affinity significantly for RIIβ. PKI docks to the large lobe of the C-subunit utilizing an α helix N-terminal to the inhibitor site. The same region in RIIβ significantly increases the affinity of the RIIβ A domain, indicating that a similar mechanism of docking to the C-subunit may be utilized by RIIβ to achieve high affinity. Both RIIβ and PKI also have a P-6 arginine in this region.

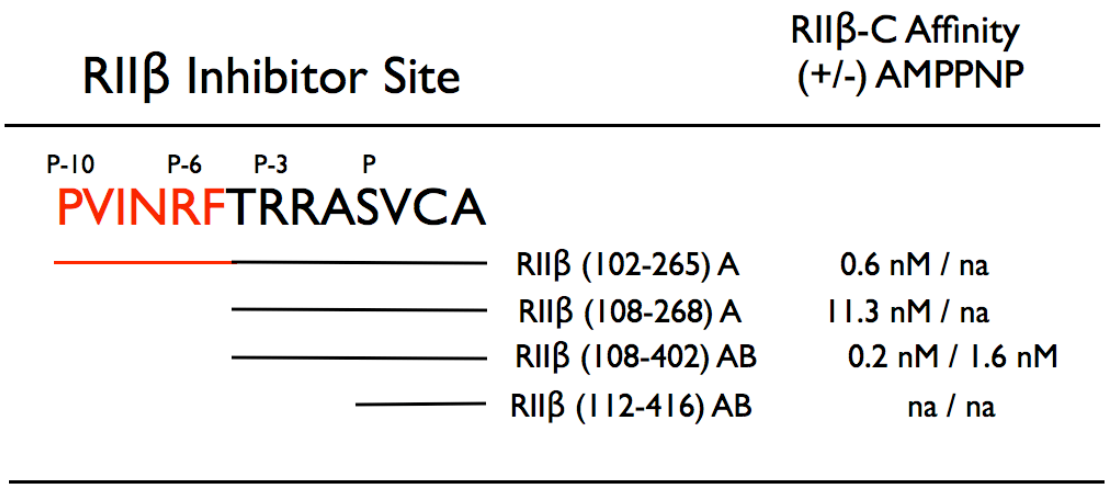

Figure 2.4: Importance of B domain and ATP for RIIβ-C Affinity

N-terminus regions of the RIIβ constructs analyzed by SPR. RII conserved N-terminal residues are highlighted in red. Affinities measured by SPR analysis in the presence and absence of AMPPNP are shown on the right.

Summary: The binding of RIIβ to the C-subunit utilizes a novel set of interactions that build upon the set of combinatorial features that define the surface of the C-subunit. RIIβ binds the C-subunit similar to both RIα and PKI, but surprisingly seems to use a larger set of regions than other known inhibitors to achieve affinity. Biacore analysis shows the importance of four domains for the RIIβ-C affinity. These domains include the RIIβ P-10 region, the IS region, CNB domain-A, and CNB domain-B. Each domain in isolation will not inhibit PKA C-subunit, but when combined high affinity binding is achieved. AMPPNP is required for high affinity binding of the RIIβ A domain to C-subunit, but when the CNB domain-B is added the requirement for AMPPNP is decreased. These results emphasize the differences between RII and RI in the importance of ATP and the CNB domain-B in the R-C interactions.

Methods:

Engineering and Purification of R-subunits: Expression and purification of the R-subunits was carried out as previously described [14, 60]. In short, following *E. coli* expression, cells were lysed and clarified. After 60% ammonium sulfate precipitation, the pellet was resuspended and then bound to cAMP-Sepharose resin overnight. After washing with 0.7 M NaCl, R-subunit was eluted with 30 mM cGMP at pH 5.5. Buffer consisted of 50 mM MES, 200 mM NaCl, 5 mM DTT, 2 mM EDTA and 2 mM EGTA.

The RIIβ (108-281) was PCR cloned out of a longer *E. coli* based expression vector from *R. norvegicus* cDNA. This construct was inserted into a commercial expression vector, pRSET (Invitrogen). The construct was cloned in as an untagged protein, as purification was possible through use of a cAMP-Sepharose resin described previously [61, 62].

Precast Nupage SDS gels (Invitrogen) were used for all SDS gel analysis. Samples were prepared using a commercial 4X sample buffer (Invitrogen), and 5% 1 M DTT was added prior to heating for 10 min at 70 °C.

SPR: Affinities between the R and C-subunits were obtained using Surface Plasmon Resonance (SPR) to quantify the on and off rates of the R subunit in solution binding to an immobilized C-subunit. A Biacore 3000 instrument (Biacore Inc.) was used for all interaction analysis, and Biacore BiAanalysis software was used for analysis of data. Data was fitted using both standard langmuir fitting, and by incorporating limiting mass-transfer correction terms into the langmuir fitting. By checking the absolute rates of K_{on} and K_{off} in both fitting modes, results were confirmed as accurate and mass transfer effects minimal.

C-subunit was attached to a gold sensor CM-5 chip through amine coupling at a concentration of 0.01mg/mL. Immobilization levels of ~300-500 response units (R.U.) were achieved for the C-subunit immobilization. Bound C-subunit was approximately 70% active. Regeneration of the C chip was achieved by application of 50 μL of 100 μM cAMP in the running buffer.

Buffers used for analysis were 20 mM HEPES ph 7.0, 150 mM KCl, 1mM TCEP and 0.05% P20 surfactant for the Apo buffer. 0.2 mM AMPPNP and 1 mM $MnCl_2$ were added for the AMPPNP buffer.

Chapter 2 in part has been published as it may appear as R-subunit Isoform Specificity in Protein Kinase A: Distinct Features of Protein Interfaces in PKA Types I and II by Amide H/(2)H Exchange Mass Spectrometry. *J Mol Biol.* 374(2):487-99 (2007). Anand GS, Hotchko M, Brown SH, Ten Eyck LF, Komives EA, Taylor SS. The dissertation author was a secondary investigator and author of this paper.

Chapters 2 in part is in preparation for publication as it may appear as AMP-PNP Traps PKA RIIβ Holoenzyme in a Transition State Complex. Brown SHJ, Kim CW, Taylor SS. The dissertation author was the primary investigator and author of this paper.

Chapter III

PKA Type II β Holoenzymes

Enzymes are three-dimensional molecular machines that perform specific chemical reactions on a variety of biological molecules. In order to understand the mechanisms of enzyme function, knowledge of the three-dimensional atomic structure is required. Structural information allows us to understand the contribution of individual amino acids to structure and function and to understand kinetic mechanisms on an atomic level. Solving structures of proteins in complex with their biological partner proteins adds another dimension to our understanding of biological function. Such structures give information about the mechanisms of protein-protein interactions, of inhibition, and of allosteric mechanisms for activation or inhibition. PKA is an ideal system for study of protein structures for three key reasons. First, it is an active kinase that phosphorylates a variety of protein and peptide substrates, and therefore the mechanism of enzyme catalysis can be investigated. Second, the kinase is inhibited by independent regulatory subunits, and the protein-protein interactions between kinase and various regulatory molecules give information about general kinase inhibition and protein-protein interactions. Third, binding of a small molecule, the second messenger cAMP, to allosteric sites on the R-subunit releases the inhibition, allowing investigation of small molecule binding and the resulting conformational changes that lead to kinase activation.

To understand the cAMP-induced activation of PKA at an atomic level, at least three structures of the molecules are required. PKA C-subunit alone, PKA R-subunit bound to cAMP, and the R-C holoenzyme complex. Both the

PKA C-subunit and cAMP bound RIIβ subunit have been successfully crystallized and the structures solved [3, 11, 48], but despite repeated attempts, the structure of the RIIβ:C complex remained elusive. The primary focus of this work was to develop new techniques and strategies to crystallize and solve the structure of an RIIβ:C complex.

Crystal structures have been solved for the RIα A domain bound to C-subunit, RIα A and B domains bound to C-subunit, and RIIα A and B domains bound to C [13-15]. Both RIα structures were obtained in the presence of AMPPNP and Mn^{2+}, while RIIα was crystallized in the absence of nucleotide. The RIIα structure engages only the large lobe of the C-subunit, whereas the RIα engages both the large and small lobe of the C-subunit, and formation of the complex has an absolute requirement for ATP or AMPPNP and Mg^{2+}. Crystal structures of the RIIα D/D domains define the dimerization and AKAP binding mechanism [5]. Significant isoform variation between RIIα and RIIβ occurs in the linker region that joins the D/D domain and the IS, and this region will be discussed further in Chapter 4.

This chapter focuses on the inhibitor site and the CNB domains. The major goal was to capture a complex of RIIβ bound to the C-subunit. We describe the structures of two such complexes, RIIβ (108-268) : C and RIIβ (102-265) : C. Both structures were crystallized with Mn^{2+} and AMPPNP and closely resemble a transition state mimic of the phosphoryl transfer from ATP to the RII subunit.

Results and Discussion:

Structure Solutions: The holoenzyme crystal structure of RIIβ (108-268) in complex with the C-subunit, AMPPNP, and two Mn^{2+} ions was solved to 1.63 Å resolution. Additionally, the holoenzyme structure of RIIβ (102-265) in complex with the C-subunit, AMPPNP, and two Mn^{2+} ions was solved to 2.8 Å resolution. Crystals of the complexes and data statistics are shown in Figure 3.1. The C-subunit bound to IP20 was used as a molecular replacement probe to phase the RIIβ (108-268) holoenzyme structure. Initial models were generated using the RIα (91-244) holoenzyme as the model. Both complexes crystallized in the C2 space group. RIIβ (108-268) was refined to an R free value of 22%, and RIIβ (102-265) was refined to an R free value of 29%. The overall structure of RIIβ (108-268) is shown in Figure 3.2.

Global Conformation Changes: The overall conformational changes in the regulatory subunits upon C-subunit binding are conserved among the different isoforms. The orientations of the two CNB subdomains in the holoenzyme are also conserved. In contrast, in the cAMP bound state the relative orientations of the CNB domain-A and CNB domain-B differ between isoforms. While each CNB subdomain in the cAMP bound structures can be superimposed, the orientation of the domains relative to each other is different for RIα and RIIβ [11].

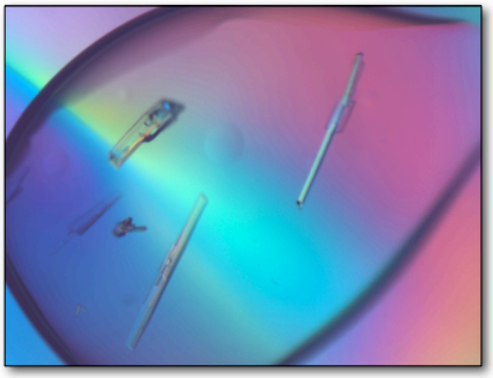

RIIβ (108-268) : C

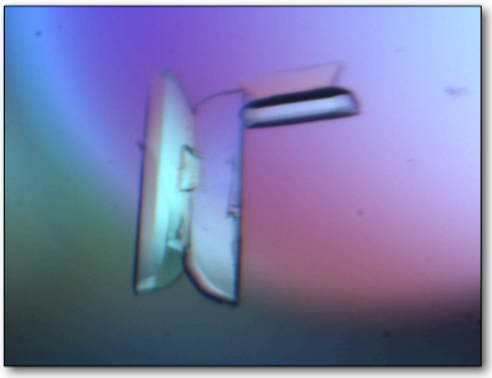

RIIβ (102-265) : C

C2	Space Group	C2
a=173.4, b= 65.7, c= 47.2	Unit cell	a=176.8, b= 67.6, c= 47.2
1.63 – 35.0 (1.63 – 1.67)	Resolution Range	2.79 - 87.1 (2.79-2.86)
61567 (4503)	Unique Reflections	11710 (577)
99.4 % (99.1%)	Completeness	87.8% (59.8 %)
0.068 (0.48)	R_{merge}	0.069 (0.26)
22.1 %	R_{free}	29.8 %

Figure 3.1: Crystallography of RIIβ (108-268) and (102-265)

Panel A shows protein crystals of RIIβ (108-268) holoenzyme. Panel B shows protein crystals of RIIβ (102-265) holoenzyme. Crystal structure statistics shown in panel C.

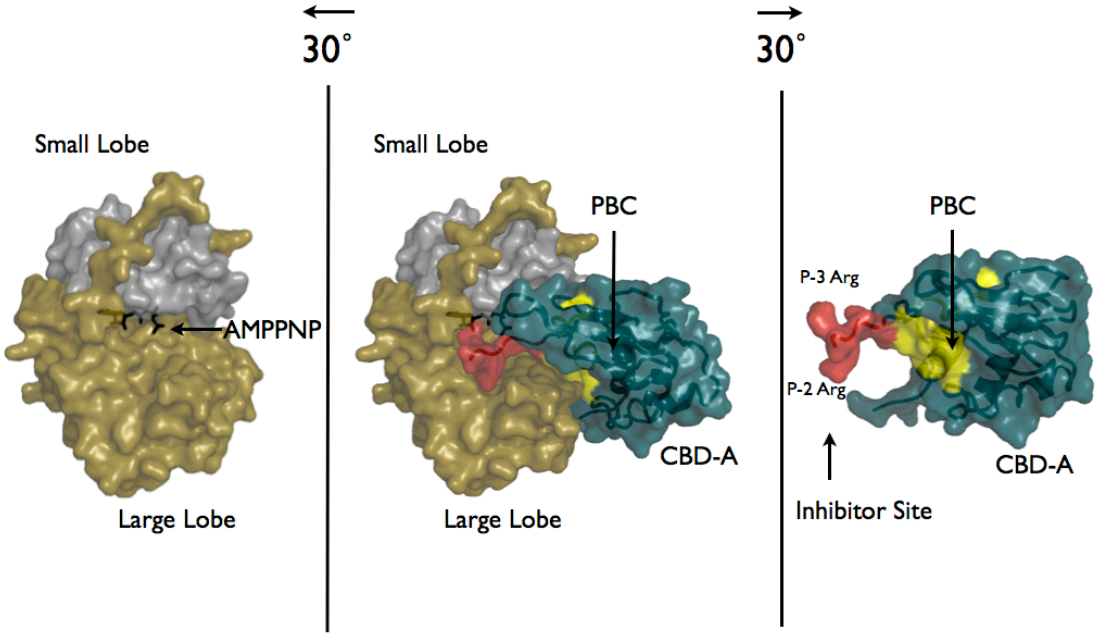

Figure 3.2: RIIβ Overall Crystal Structure

The crystal structure of RIIβ (108-268) holoenzyme shown as space filling surface. The holoenzyme is shown in the middle. Catalytic subunit alone is shown on the left, and regulatory subunit alone is shown on the right. Subunits have been separated and rotated 30 degrees to show the binding surfaces in the holoenzyme. The inhibitor site (red) and phosphate binding cassette (yellow) of the regulatory subunit are highlighted.

This difference is due to variation in the hinge regions of the αBC helix of domain A that causes a rotation of the domains away from each other. This region that is critical for inducing a cAMP response differs in RIα and RIIβ.

The RIIβ regulatory subunit CNB domain-A undergoes major conformational changes upon binding to the C-subunit, with reorganization in all of the subdomains of the R-subunit. In contrast, the C-subunit acts as a stable scaffold for docking of the R-subunit, with almost no differences between the IP20:ATP bound C-subunit and the RIIβ:AMPPNP bound C-subunit. RMSD between PKI and the RIIβ bound C-subunits is only 0.4 Å, demonstrating the impressive stable nature of the C-subunit even when binding such a large molecule as the RIIβ subunit. RMSD between RIα and RIIβ bound C-subunits is only 0.3 Å, while RMSD between RIIα and RIIβ bound C-subunits is 0.9 Å. The C-subunit bound to RIIβ most closely resembles the C-subunit bound to RIα.

The conformational changes in the R-subunit can be correlated with three basic subdomains; changes in the cAMP binding pocket, the C-helix, and the inhibitor site. The most dramatic of these is the extension of the C-helix of RIIβ upon binding C-subunit. Two kinks disappear and a continuous helix forms when the C-subunit is bound. The consequence of this helix switch is that the last 15 residues of the R-subunit move up to 18 Å away from their relative location in the cAMP bound R-subunit, as shown in Figure 3.3 and Figure 3.4.

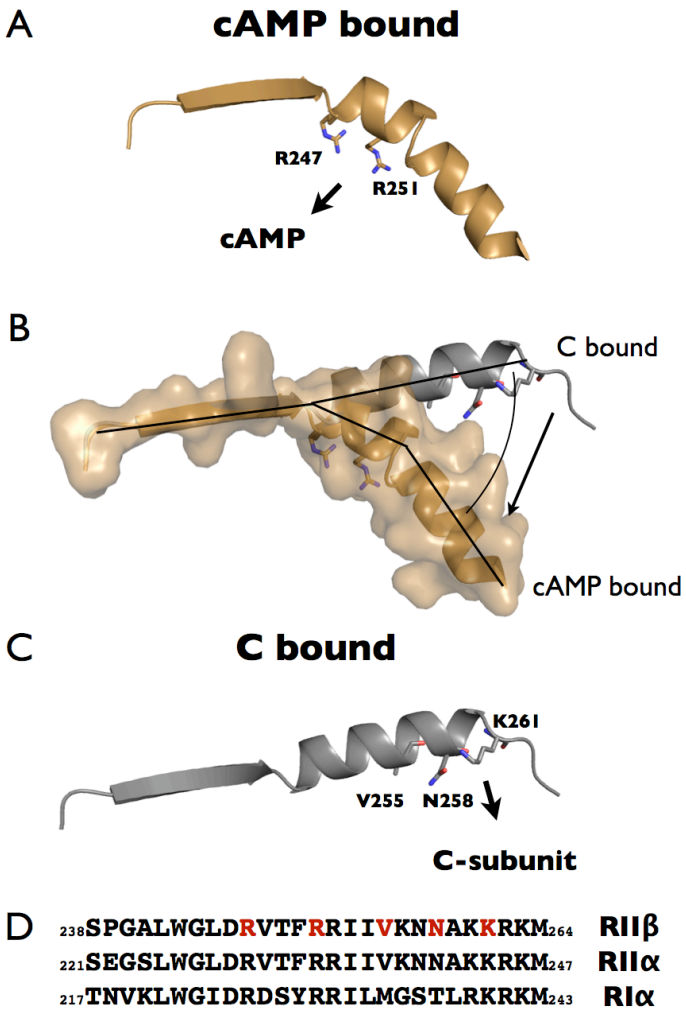

Figure 3.3: Conformational Changes of the B/C helix of RIIβ

Panel A shows the αB/C helix of RIIβ in the cAMP bound state with residues that interact with the PBC highlighted. Panel B compares the same helix in the cAMP-bound (tan) and C-bound (grey) states. Panel C shows the conformation of the αBC helix when it is bound to the C-subunit with interacting residues highlighted. Panel D shows the amino acid sequence of this region in RIα, RIIα, and RIIβ. Interacting residues are highlighted in red.

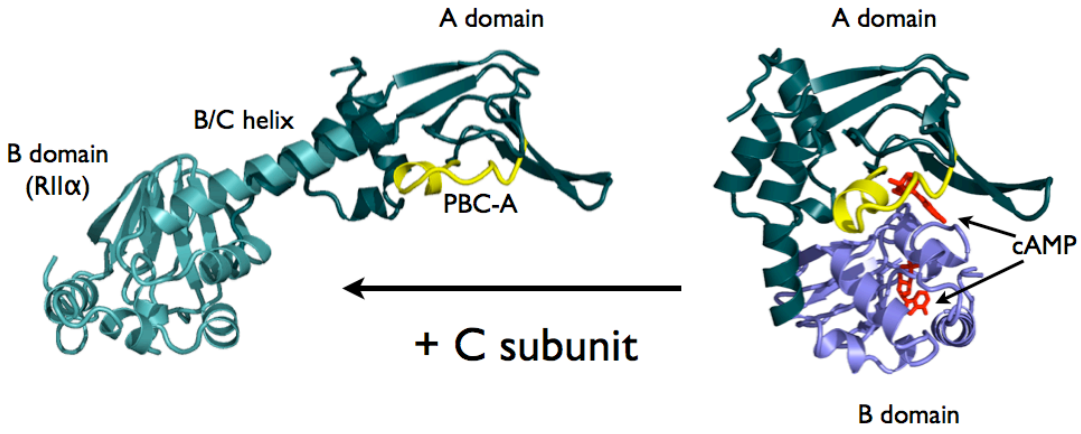

Figure 3.4: RIIβ Overall Conformational Change

A model of the overall conformational change of RIIβ. Shown on the right is a ribbon representation of RIIβ bound to cAMP (PDB ID 1CX4). CNB domain A (dark teal), CNB domain B (blue), and the PBC (yellow) are highlighted. Shown on the left is a model of the CNB domain A of RIIβ (108-268) bound to the catalytic subunit, with RIIα CNB domain B (PDB ID 2QVS) added to represent the overall conformational change of the R-subunit. RIIβ CNB-A and RIIα CNB-B were merged by alignment of the αC-helix.

In the holoenzyme complex, the extended C-helix of RIIβ is an integral part of the complex interface, sandwiched between the linker of RIIβ and the activation loop of the C-subunit. The C-helix nucleates important interaction networks in both the C-subunit bound and the cAMP bound RIIβ subunit and plays a role in the transfer of the cAMP signal from the PBC throughout the PKA molecule.

Important hallmarks of the PBC are two invariant residues necessary for cAMP binding; in RIIβ these are R230 and E221. Both residues are key for binding cAMP; R230 binds to the (exo)phosphate of cAMP while E221 is bound to the ribose. R230 is also part of an allosteric switch that transfers the cAMP signal [63]. Shown in Figure 3.5, D187 is in a position to be a direct sensor of cAMP binding to R230. In the cAMP bound form of RIIβ, R230 is hydrogen bonded to the phosphate of cAMP, and also to the side chain of D187 in β stand 3. R247 and R251 from the αBαC helix, and N227 and M225 from the PBC form a tight cluster, linking the αBαC helix and the PBC in the cAMP bound form of RIIβ.

These residues reorganize upon release of cAMP and binding to the C-subunit as shown in Figure 3.6. D187 flips away from R230 and instead binds to R247 from the C-helix. The flip of D187 also causes the tight hydrophobic cluster that links the PBC to the C-helix to be broken; the N227 – R247 link is entirely broken, while R251 and M225 stays in contact. The change in conformation of the PBC is transferred to the C-helix by a combination of

hydrophobic surface changes and salt bridge switches. The RIIβ holoenzyme structure defines a very specific for role of N227 in the PBC and it's importance for cAMP-induced conformational change and activation. This role that is unique to the RII subunits, since in RIα N227 is replaced by a glycine.

Mechanism for Inhibition of the Catalytic subunit: One of the most dynamic changes that occurs when the holoenzyme forms is that the inhibition site, which is highly disordered in the cAMP-bound state, locks into the active site cleft of the C-subunit. The basic mechanism of inhibition, whereby the inhibitor site binds to the active site cleft of the C-subunit, is conserved across all of the R-subunits and PKI inhibitors thus far solved in crystal structures. The inhibitor site forms a β strand that fits into the active site cleft forming an antiparallel β-sheet with the C-subunit. Two critical arginines at the P-2 and P-3 position in the inhibitor peptide bind to important subsites that form the active site cleft while the C-terminus of the inhibitor peptide (P+1 residue) docks to a hydrophobic pocket that is formed by the P+1 loop in the C-subunit. Interactions of the inhibitor site are shown in Figure 3.7.

Transition State Mimic: The RIIβ holoenzyme defines a new state for inhibition of the C-subunit. Through use of AMPPNP, the C-subunit has been trapped in a conformational state that in many ways resembles a transition state, as shown in Figure 3.8.

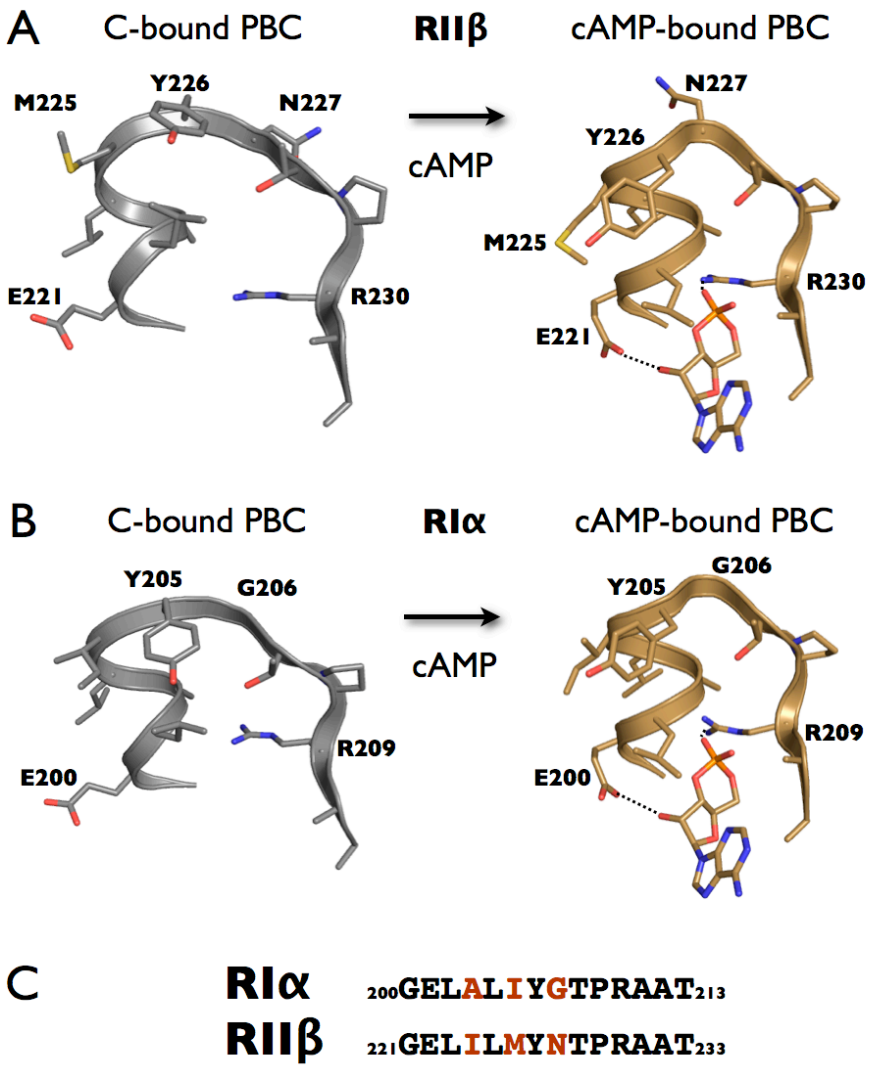

Figure 3.5: Conformational Changes of the PBC of RIα and RIIβ

Panel A shows critical cAMP binding residues in the phosphate binding cassette of RIIβ and demonstrates closure of the PBC around cAMP. Panel B shows the same region in RIα. Panel C shows the sequences of the PBC of RIα and RIIβ.

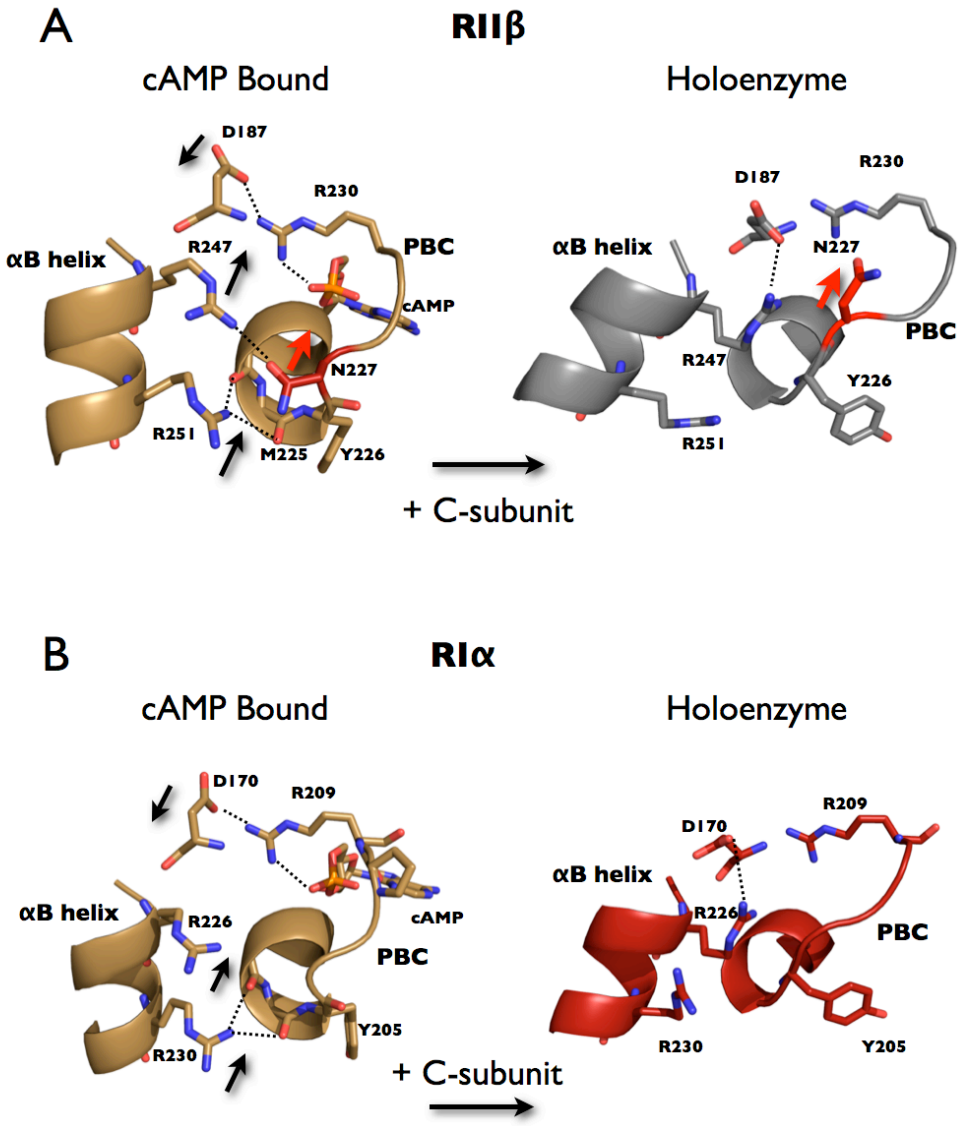

Figure 3.6: Role of Asn 227 in RIIβ Activation

Panel A shows the cAMP-bound and holoenzyme forms of RIIβ (108-268) and the conformational change of the phosphate binding cassette and the αB helix when catalytic subunit is bound. Panel B shows the same regions of RIα (91-376) in the cAMP bound and holoenzyme states. (PDB ID 1CX4)

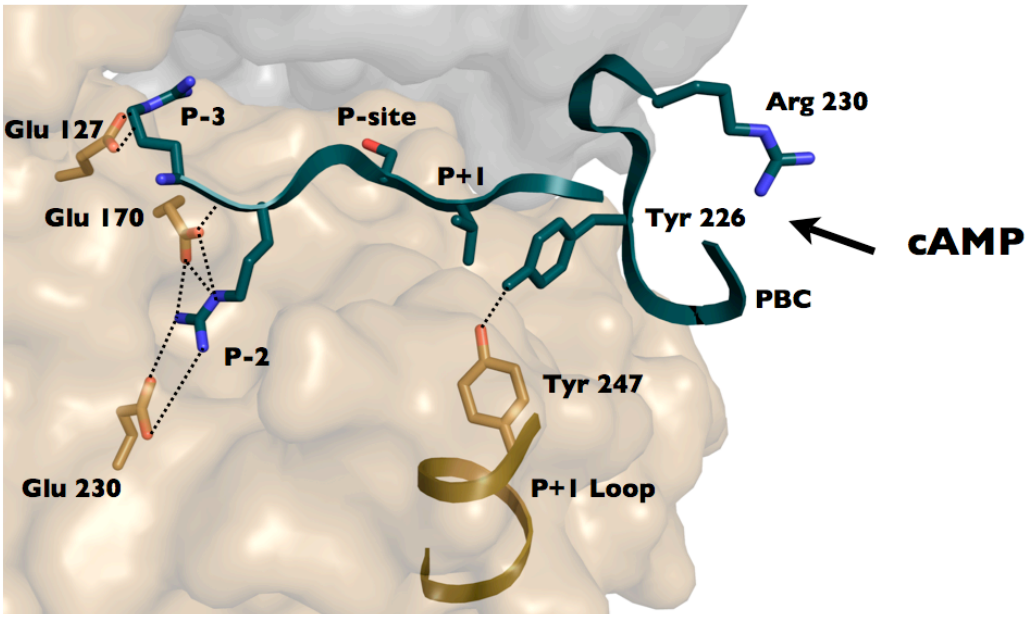

Figure 3.7: Mechanism for Inhibition of the Catalytic Subunit

The inhibitor peptide and the tip of the phosphate binding cassette of RIIβ dock to the inhibitor site of the catalytic subunit in the holoenzyme conformation of RIIβ. Two critical Arg residues at the P -2 and P-3 sites bind to conserved Glu residues in the large lobe of the C subunit. Tyr 226 from the PBC nucleates a hydrophobic interface with the P+1 Val from the inhibitor peptide and Tyr 247 from the P+1 loop of the catalytic subunit. cAMP activation involves a competition between cAMP and the C-subunit for binding the phosphate binding cassette of domain A.

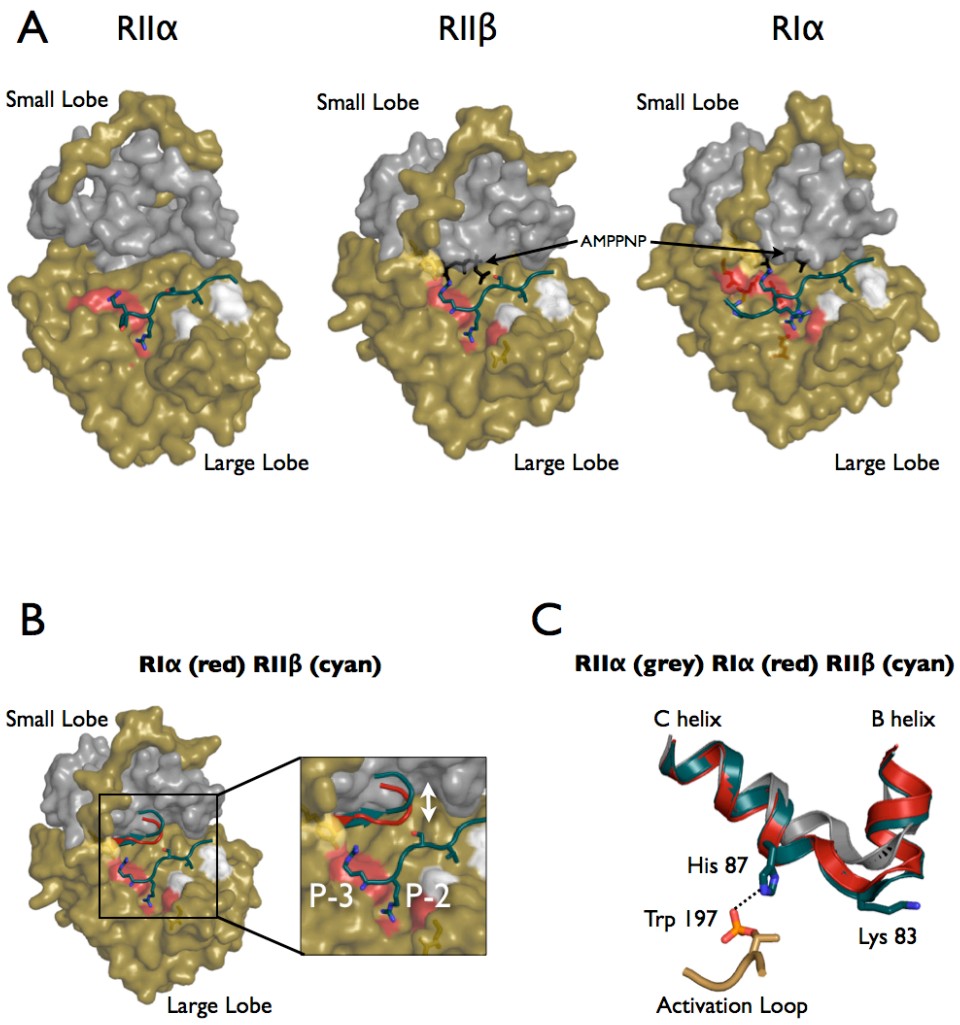

Figure 3.8: RIIβ Transition State

Panel A shows three holoenzyme structures demonstrating the trapped transition state that is present in the RIIβ structure. The RIIα holoenzyme is in a lobe open form. Both RIIβ and RIα are in a lobe closed form. Panel B shows that the glycine rich loop in the RIIβ complex is opened by 5 Å compared to the fully closed RIα structure. Panel C highlights the αB-αC helix of RIIα, RIIβ and RIα. RIIβ has been trapped into an RIα-like state by AMPPNP.

This RIIβ (108-268) holoenzyme structure represents the C-subunit in a form after the binding of ATP and the R-subunit, but before subsequent transfer of the phosphate. In the RIIα holoenzyme, crystallized in the absence of ATP, C-subunit is in an open conformation and is inhibited by interactions with only the large lobe. It is not clear whether in this state nucleotide can even bind to the complex. In contrast, the RIα holoenzyme shows a fully closed inhibited state of the C-subunit, primed for phosphoryl transfer but having no site to accept the γ-phosphate. The RIIβ represents another "trapped" transition state and demonstrates the importance of the closed conformation of the C-subunit, the role of ATP in this closure, and the positioning of the glycine-rich loop that is thought to be necessary for catalysis. In this conformation we are viewing the RIIβ subunit as a substrate while in the nucleotide free RIIα structure the R-subunit is seen only as an inhibitor. The catalytic states of the RII subunits are shown in Figure 3.9.

Contacts between the small lobe and the RIIβ subunit resemble contacts observed in the RIα A domain holoenzyme structure. The C-terminal tail of the catalytic subunit and the nucleotide have similar contact networks in RIIβ as compared to RIα. The P-3 IS site arginine engages both the small lobe and the nucleotide, similar to RIα and opposed to RIIα. Overall, the crystal structure of the C-subunit bound to RIIβ A domain highly resembles the structure that is seen in the RIα and PKI complexes.

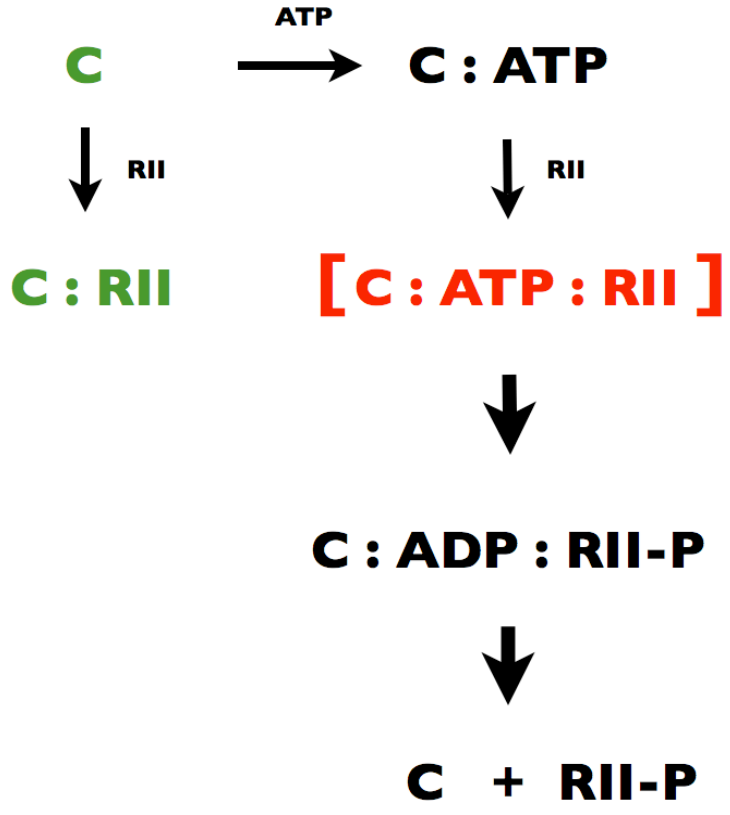

Figure 3.9: RII Catalytic Transition State

The crystal structure of RIIβ holoenzyme has been trapped in a transition like state with AMPPNP. This state is highlighted above in red. The RIIα holoenzyme structure and apo catalytic subunit structures represent the states highlighted in green. Phosphorylation of the RII subunit requires the presence of cAMP.

By using AMPPNP, the transition state for transferring the γ-phosphate of ATP to the P-site serine has been captured in the RIIβ structure.

In contrast to the holoenzyme structure of RIIα bound to the C-subunit, the structure of the C-subunit when it is bound to RIIβ has a significantly different conformation. In the RIIα PKA structure, RIIα (91-400) is bound to the C-subunit in the absence of nucleotide. The C-subunit is in a lobe open form, with the small lobe and C-terminal tail partially disordered. The entire contact surface for the R-subunit binding is on the large lobe of the C-subunit; there are almost no contacts between the small lobe and R-subunit. In the RIIα structure, it is the large lobe of the C-subunit that acts as a stable scaffold for binding of the R-subunit.

In the RIα holoenzymes, the inhibitor site peptide contains an alanine at the phosphorylation site that defines the RIα as a pseudosubstrate where the γ phosphate cannot be transferred. The RII subunits, in contrast, are all substrates and have a serine at the P-site of the IS. The RIIβ holoenzyme has been crystallized in a similar state where the γ phosphate of ATP is trapped at the active site cleft because the nitrogen of AMPPNP prevents the transfer of the γ-phosphate. While the RIα and RIIβ holoenzyme structures both capture closed and inhibited states of the C-subunit, only the RIIβ holoenzyme has been trapped in a state that is in a transition between two significant biological forms of the R-subunit.

The most significant difference between the RIα and RIIβ CNB domain A holoenzyme structures is the position of the glycine rich loop. The glycine rich loop is a highly conserved motif in the protein kinase core, critical in catalysis and necessary for nucleotide positioning. This loop positions the phosphates of ATP for optimal catalysis, and of critical importance is to trap the γ-phosphate of ATP between the tip of the glycine rich loop and Lys 168 in the Catalytic Loop. In the RIα structure the glycine rich loop is in a completely closed conformation where the γ-phosphate of ATP is trapped in precisely this way. Hydrogen bonding of the backbone of Ser 53 to the γ-phosphate of ATP is necessary for efficient catalysis [64, 65]. In the RIIβ structure the glycine rich loop is opened by 3 Å compared to RIα (2.9 Å from the γ-phosphate compared to 5.7 Å respectively) as shown in Figure 3.9. Complete closure of the glycine rich loop is observed in both RIα and PKI complexes containing ATP or AMPPNP but not in the RIIβ holoenzyme. It is also seen in the transition state mimic using ADP, AlF_3 and a substrate version of PKI (4-25) [66].

A clear link between the inhibitor site and small lobe in the RIIβ structure is the P-3 arginine. This residue is critical for inhibitor binding, and shifts in configuration between the RIIα and the RIIβ holoenzymes. In the RIIα, the P-3 arginine only interacts with the large lobe of the C-subunit. In contrast, when either RIα or RIIβ is bound, the tip of this arginine is shifted toward the small lobe where it forms hydrogen bonds with both the nucleotide and the glycine rich loop of the C-subunit. Binding of nucleotide to the C-

subunit may cause a shift of the P-3 arginine interactions towards the small lobe and facilitate closure of C-subunit.

The αB-αC loop of the C-subunit is another site of interaction that ties together the C-subunit Activation Loop, the linker of the R-subunit, and the small lobe of the C-subunit. In the RIIα structure, the small lobe is open and the αB-αC loop is distorted in order to maintain this R-C interaction. The majority of the small lobe of the C-subunit in the RIIα structure resembles the Apo PKA C-subunit, with the exception of this αB-αC loop. In RIIβ, this loop region is very similar to the RIα holoenzyme, as shown in Figure 3.8. The closure of the catalytic cleft of the C-subunit by AMPPNP induces this region to shift from an RIIα like form to a transition state conformation like RIα.

P-10 – P-5 Site: RIIβ (102-265) has 6 additional residues at the N-terminus corresponding to the P-10 to P-5 region of the inhibitor peptide. This is four residues longer than RIα and six residues longer than the RIIα holoenzyme structures. As was shown in Chapter 2, the addition of these 6 residues enhances the affinity for the C-subunit considerably. Shown in Figure 3.10, the structure of RIIβ (102-265) shows that this segment is positioned precisely onto the surface where the PKI helix docks but it is a strand, not a helix in RIIβ.

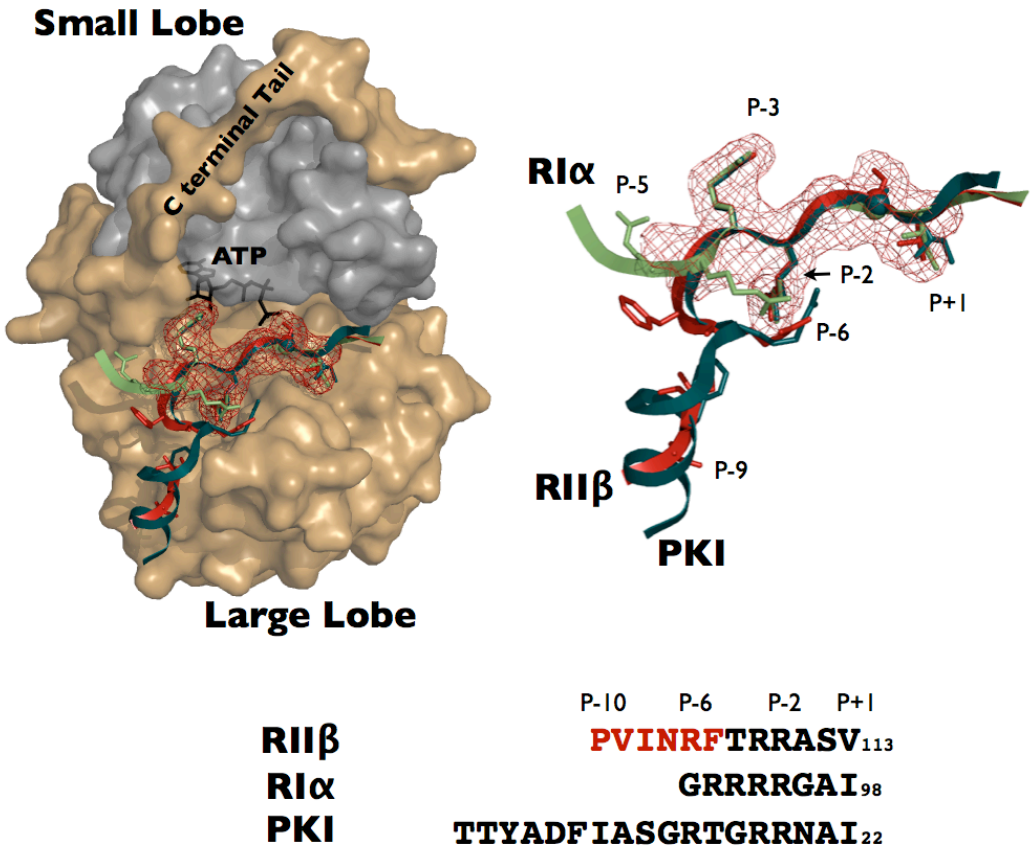

Figure 3.10: N-terminal Regions of RIIβ, RIα, and PKI

Highlighted N-terminal binding regions of PKI, RIα and RIIβ demonstrate differential binding between inhibitors. RIIβ and PKI dock to the C-lobe, while RIα docks to the C-terminal tail and N-lobe. Surface mesh representation is shown for highly conserved P-3 to P+1 region.

The RIIβ P-6 R106 is docking to the negative charged surface of E203 in the P+1 loop of the C-subunit. The P-5 Arg from RIα docks to the same surface, but the RIα residue approaches E203 from different angles. This result is consistent with the importance of the large lobe in both substrate and RII binding seen in earlier crystal structures but also expands our understanding of how the C-subunit can recognize different sequences that lie N-terminal to the inhibitor site.

The extended region of RIIβ from 102-105 makes mostly hydrophobic contacts with the large lobe of the C-subunit. The region of the C-subunit that contacts this segment of RIIβ is the αF-αG loop. This constitutes a hydrophobic pocket that is also used by PKI to achieve high affinity binding. This hydrophobic pocket is actually highly conserved in many kinases. The IP20 peptide from PKI forms an α helix in the P-8 to P-16 region and a hydrophobic surface nucleated by Phe 10 and Tyr 7 binds to the large lobe of the C-subunit. RIIβ binds to same hydrophobic surface on the C-subunit; however, instead of forming an α-helix, RIIβ forms a strand and the P-9 Val and P-8 Ile dominate the hydrophobic interaction. Like PKI, RII subunits have a P-6 Arg and in both cases this arginine binds to Glu203 in the P+1 loop. RIα has two additional arginines that precede that IS. However, the P-5 Arg goes to Asp328, while the P-4 Arg goes to Glu203. Thus the N-terminus of RIα further strengthens interactions with the C-terminal tail.

This region of RIIβ not only extends the modular nature of the binding of inhibitors to the C-subunit, but also further defines isoform differences. Previous work comparing binding of RIα and RIIα to mutant C-subunits showed significant differences between the isoforms. Mutation of the Arg133A on the large lobe decreased binding of only the RIIα subunit, while mutation of Asp328 decreased binding of the RIα subunit [67]. This result predicted that the region flanking the inhibitor site in RIα and RIIα would go in different directions, and that prediction is confirmed by RIα and RIIβ crystal structures. Interaction of the P-5 arginine of RIα with Asp328 explains the reduction of RIα affinity in the Asp328A mutant. In our structure the strand of RIIβ wraps over Arg133 of the large lobe, and mutation to an alanine might decrease RIIα binding as observed. In RIIα however, the P-4 threonine is replaced with an aspartic acid which would not only repel interactions with D328 but might also create an electrostatic interface with R133. Implications of the differential binding of the linker regions of RIα and RIIβ to the C-subunit will be discussed further in Chapter 4.

Summary: Crystal structures of RIIβ bound to the C-subunit of PKA have defined the mechanism for inhibition of PKA by RIIβ. The RIIβ holoenzyme structures define the overall binding surfaces and the conformational changes that take place upon formation of the RIIβ complex. The most striking feature of these structures is that the RIIβ holoenzymes

have trapped a conformation that resembles a transition state by the non-hydrolyzable AMPPNP nucleotide. This opens the possibility that other substrates could be trapped in a similar way.

Global conformational changes associated with holoenzyme formation appear to be conserved for all isoforms. Formation of holoenzyme has been a driving force for evolution and therefore PKA holoenzymes have more similarities than cAMP bound R-subunits. RIIβ holoenzyme structures reveal differences between isoforms in both the cAMP binding sites and in the P-10 region N-terminal to the inhibitor site. The cAMP binding sites differ between RIα and RIIβ in the surfaces that interact with cAMP and in the residue-specific conformational changes that occur. The regions N-terminal to the inhibitor site in RIα and RIIβ bind to different surfaces on the C-subunit, which has implications for the global organization of the tetrameric holoenzymes.

Methods:

Initial crystallization attempts were focused on RIIβ (108-402):C in the presence of AMPPNP. Although initial crystals were obtained and diffraction as high as 5 Å was achieved, a complete dataset was never obtained. Current attempts to solve this structure are ongoing and involve crystallization and cryo-freezing optimization as well as introducing point mutations into the R-subunit. Over 100 crystals have been screened but none of the crystals diffract to a resolution better than 5 Å so far. The smaller fragment RIIβ, (108-268) was chosen next as the minimal high affinity binding protein for crystallization based on previous results with RIα.

For crystallization of PKA type IIβ (108-268) Vapor Diffusion Under Oil (VDUO) crystallization was used. This technique incorporates a layer of oil over drops of crystallization regent and protein sample mixed together. By the use of round bottom 96 well plates, a reasonably fast throughput manual setup of crystallization trials can be obtained. Oil, sample and crystallization reagent additions were performed using multichannel pipettes allowing for fast, consistent setup.

Commercial PACT and JCSG+ crystallization screens were chosen for initial screening [68]. Crystals obtained under oil present a unique challenge to mount for data collection. The deep wells used for manual setup VDUO are too deep for traditional mounting techniques that are developed for glass

slides used in HDVD. In order to mount these crystals a bent loop was designed.

For later crystallography trials an Oryx robotic crystallization system was used. The advantages of the robotic crystallization system include a reduction of sample size from 1-2 μL per condition to 100 nL per condition, hands-off setup of crystallization trials, and increased speed and consistency of drops setup. Also, the optimization systems available in a robotic system highly exceed what can be setup by hand. The optimization techniques will be described in more detail below.

Robotic crystallization allows easy optimization through variation of all solution variables of the crystallization in a single plate. Using multivariate design on a two dimensional plate, all variables can be optimized in a single 2D plate. A 4D optimization was successfully used for RIIβ (102-265):C crystallization to improve crystal size and morphology, allowing growth of the diffraction quality crystal.

RIIβ (108-268):C Purification and Crystallization: RIIβ (108-268) and C-subunit were purified as described previously using cAMP resin and cGMP elution. [69] RIIβ was purified twice through Superdex 75 gel filtration for optimal purity and to remove cGMP. AMPPNP and $MnCl_2$ were added to the C-subunit, followed by a 1.2 fold molar excess of R subunit. The complex was spin dialyzed 3 times into the holoenzyme AMPPNP buffer. The complex was then run over S75 gel filtration in the above buffer to remove excess R subunit.

The final protein sample was concentrated to approximately 10mg/mL for crystallization.

A number of extra procedures were incorporated into the protein purification to maximize the chances of crystallization. As discussed previously, the non-hydrolyzable ATP analogue AMPPNP was incorporated into the crystallization buffer. The analogue was added to the buffer during the initial holoenzyme formation and was maintained during all following chromatography and sample preparation. Reducing agents were included in all phases of purification. Dithiothreitol (DTT) was incorporated in the initial cell lysis and purification steps, whereas the more stable reagent Tris (2-carboxyethyl) phosphine (TCEP) was used for final purification of the holoenzyme. Mn^{2+} was chosen as the metal ion to coordinate the AMPPNP, as it facilitates formation of a tighter inhibited complex instead of the physiological Mg^{2+}. In contrast to Mg^{2+}, Mn^{2+} also cannot be confused with a water molecule during crystal structure analysis. The final crystallization buffer consisted of 10 mM MOPS (Fluka) pH 7.0, 50 mM NaCl (Fluka), 0.2 mM ANPPNP (Calbiochem), 1 mM TCEP (Pierce) and 1 mM $MnCl_2$ (Fluka).

PACT and JCSG+ screens were obtained from Molecular Dimensions in a 96 well block format for use with SBS format multi channel pipettes. For this set of crystallization trials, 96 well plates of well volume of 250 μL were set up with 100μL of Al's Oil (Hampton Research) prior to sample addition. Crystallization plates were checked after 24 hours under the microscope and crystals were present in many wells of the PACT screen.

Conditions included:

C5: 100 mM Phosphate Citrate Buffer (PCB) pH 8.0, 25% PEG 1500

D11: 200mM Calcium Chloride ($CaCl_2$), 100mM Tris pH 8.0, 20% PEG 6000

E2: 200mM Sodium Bromide (NaBr), 20% PEG 3350

E7: 200mM Sodium Acetate (NaAc), 20% Peg 3350

G10: 200mM Na/KPO_4, 100mM Bis Tris Propane pH 7.5, 20% Peg 3350.

Cryo bases (Hampton Research) were used and mounted to an extra long cryo pin. This pin, 24mm in length compared to the standard 18mm length is long enough to reach the bottom of the VDUO well. However, in order to reach the bottom of the well and keep the crystal visible under the microscope, the pin needed to be at an angle compared to the cryo base. Therefore, the pin was bent at such an angle (~60) to allow access of the well and to keep the cryo loop and the end of the pin still at the correct angle for scooping. Using bent cryo pins, successful scooping of the new crystals was achieved. Once scooped from the well, the crystals were transferred into a drop containing the initial crystallization condition + 10% glycerol. This drop served to remove excess oil from the crystal and allowed the soaking of the glycerol cryo-protectant. Crystals were then flash frozen in liquid nitrogen for the duration of storage.

*Data Collection and Processing***:** Initial crystal screening was performed at 100 K at the UCSD chemistry home source. This source has a rotating anode CuK source emitting a wavelength 1.52 λ. Images were collected on a Mar 345 image plate detector. All crystals were screened on the home source

before shipping to the Advanced Light Sources (ALS) for data collection. The best diffraction was obtained from crystals grown at 4 C from crystallization solution E2. Three data sets were collected at the ALS at Lawrence Livermore National Lab beamline 8.2.2. Data collected at 1.63 Å was chosen for processing and analysis. Data was processed using HKL2000 (HKL Research) to a space group of C2. Initial phases were obtained used the Inhibitor Peptide (IP20) bound C-subunit (PDB code 1ATP) as a search model using the CCP4 package program PHASER. Initial density maps were obtained, and the model of RIα (91-244) was fit into the density for RIIβ (108-268). Initial refinement of the RIα model into the RIIβ density map was performed using the REFMAC5 program in CCP4. Model building continued by replacing all RIα residues with RIIβ residues and removing the poorly fit areas. Final refinements including TLS models in REFMAC5 yielded an R free of 22%.

*RIIβ (102-265):C Purification and Crystallization***:** Similar cloning techniques to the RIIβ (108-268) construct were used for RIIβ (102-265), PCR based cloning was used to produce an insert fragment from the full length RIIβ. Sites for Nde I and Xho I were engineered into the PCR primers, and the PCR product was cut and ligated into pREST vector cut by the same pair of enzymes. Sequences were checked through in-house sequencing using an ABI Prism 310 (Applied Biosystems) sequencer, and the successful clones were expressed in *E. coli*. BL21-DE3 cells. Following successful tests of expression, cultures were scaled up to 6 liters in YT media and purification

using the cAMP resin system was performed as described previously for RIIβ (108-268).

Holoenzyme was formed using the same techniques as described for RIIβ (108-268), and the final protein sample was concentrated to approximately 10mg/mL for crystallization. The Oryx 8 crystallization robot (Douglas Instruments) was utilized for crystallization trials of the RIIβ holoenzyme sample. The initial screens for crystallization were purchased in 96 well blocks, and the robot system was used to setup PACT, JCSG and Clear Strategy screens. 0.2μL drops were setup in 96-well plates and incubated under Al's oil. Initial screens indicated that the crystallization characteristics for RIIβ (102-265) were different than the slightly shorter (108-268). Best conditions from screening came from the PACT screen:

G7: 0.2M Sodium Acetate, 0.1M Bis Tris Propane pH 7.5, 20% PEG 3350
G8: 0.2M Sodium Sulfate, 0.1M Bis Tris Propane pH 7.5, 20% PEG 3350
F7: 0.2M Sodium Acetate, 0.1M Bis Tris Propane pH 6.5, 20% PEG 3350

Initial hits were too small and twinned for data collection; therefore optimization of the hits was initiated. First, drop ratio variation protein:precipitant concentrations using original hit reagents [70]. Both condition G8 and F7 did not yield crystals upon repeating, however great improvement was seem in the G7 condition, especially in the lower precipitant drops.

Second, the hit from the drop optimization was moved into full array optimization screening. Using the Oryx robot for optimization, a multivariate design was implemented to optimize the RIIβ (102-265):C crystals. Four variables were optimized: pH of Bis Tris buffer, protein concentration, precipitant (PEG 3350) concentration, and Sodium Acetate concentration. All permutations for a 4D factorial design were used for optimization, for a total of ~80 points. Multiple hits from the robot optimization grew significantly larger and better formed crystals. The best hit from the robot optimization is shown in Fig 2.3. Concentration in drop G11 consisted of: 6mg/mL RIIβ (102-265):C, 8% PEG 3350, 10 mM Bis Tris pH 7.2, 30 mM Bis Tris pH 7.6, 0.05 mM Na Acetate.

Multiple crystals from the factorial optimization screen were mounted into nylon loops and frozen in liquid nitrogen. The Douglas Instruments microbatch trays allowed scooping and freezing of the crystals directly out of the trays. Multiple crystals from the factorial optimization screen were mounted into nylon loops and frozen in liquid nitrogen. The Douglas Instruments microbatch trays allowed scooping and freezing of the crystals directly out of the trays.

Data Collection and Processing: Initial crystal X-ray screening was performed at 100°K at the UCSD chemistry home source. Images were collected on a Mar 345 image plate detector. A dataset of 176 images was obtained with 1° oscillations and 10-15 minute exposure time. Data was processed with HKL2000, statistics shown in Figure 3.1.

Multiple datasets were obtained at up to 2.2 Å at the ALS synchrotron. Unfortunately, following data collection none of the datasets were of high enough quality, and the home source dataset was chosen for final processing and model building. Current refinements yield an R free value of 29%.

Chapters 2 and 3 are in preparation for publication as it may appear as AMP-PNP Traps PKA RIIβ Holoenzyme in a Transition State Complex. Brown SHJ, Kim CW, Taylor SS. The dissertation author was the primary investigator and author of this paper.

Chapter IV

Engineering of a Truncated RIIβ Dimer

The R-subunits are modular and multifunctional. In addition to being inhibitors of the C-subunit, they also serve as major scaffolds for targeting the C-subunit to specific sites in the cell. A major mechanism for targeting PKA is through the dimerization domain at the N-terminus while the highly dynamic nature of the R-subunits is mediated in a large part by the linker region that joins the D/D domain to the inhibitor site or CNB domains. The linker regions are also very isoform specific.

Dimerization/Docking Domains: Anchoring proteins binding to the dimerization and docking (D/D) domain of the R-subunit achieve the localization of PKA to subcellular compartments and multiprotein signaling complexes. The D/D domain, consisting of the N-terminal 50 residues of the R-subunit, forms a dimer in both the free R-subunit and in the holoenzyme forms. The dimer interface is an X-type, four-helix bundle, with each pair of helices interacting in an anti-parallel fashion, forming primarily hydrophobic contacts. A hydrophobic groove formed by the pair of stacked helices 1 and 1' of the D/D domain is the binding site for the anchoring proteins. This hydrophobic grove is formed primarily by residues that are also involved in the dimer interface.

The AKAP AKB (A Kinase Binding) peptide is an amphipathic helix that docks into the hydrophobic groove of the D/D domain [71]. The 27-mer D-AKAP2 AKB peptide is a dual-specific peptide, binding to both RI and RII (K_D of 48 nM and 2 nM, respectively). D-AKAP2 has a domain organization

consisting of two tandem N-terminal RGS domains, the AKB domain, and a C-terminal PDZ domain [72]. In this study, we focused on the binding of PKA RIIα and RIIβ isoforms to the AKB of D-AKAP2 and asked specifically whether there are differences between RIIα and RIIβ.

High resolution structural information is available for the D/D domain of RIIα bound to different AKAP peptides. A crystal structure of RIIα (1-44) dimer bound to the D-AKAP2 AKB peptide, residues (631-649), was solved at 1.6 Å resolution [5], and is shown in Figure 4.1. Also, an NMR structure of RIIα (1-44) dimer demonstrated the role of individual residues in the binding of AKAP peptide Ht31 (493-515) [6].

Structural studies of the RIIβ subunit bound to AKAP peptides are currently ongoing, and preliminary results indicate small but significant differences between RIIβ and RIIα structures (P. Jennings, unpublished results). These structural differences indicate that isoform selectivity between RIIα and RIIβ may be achieved through modification of the D-AKAP2 peptide. Through the use of a peptide substitution array the amino acid determinates of high affinity binding for RIIβ and RIIα were identified.

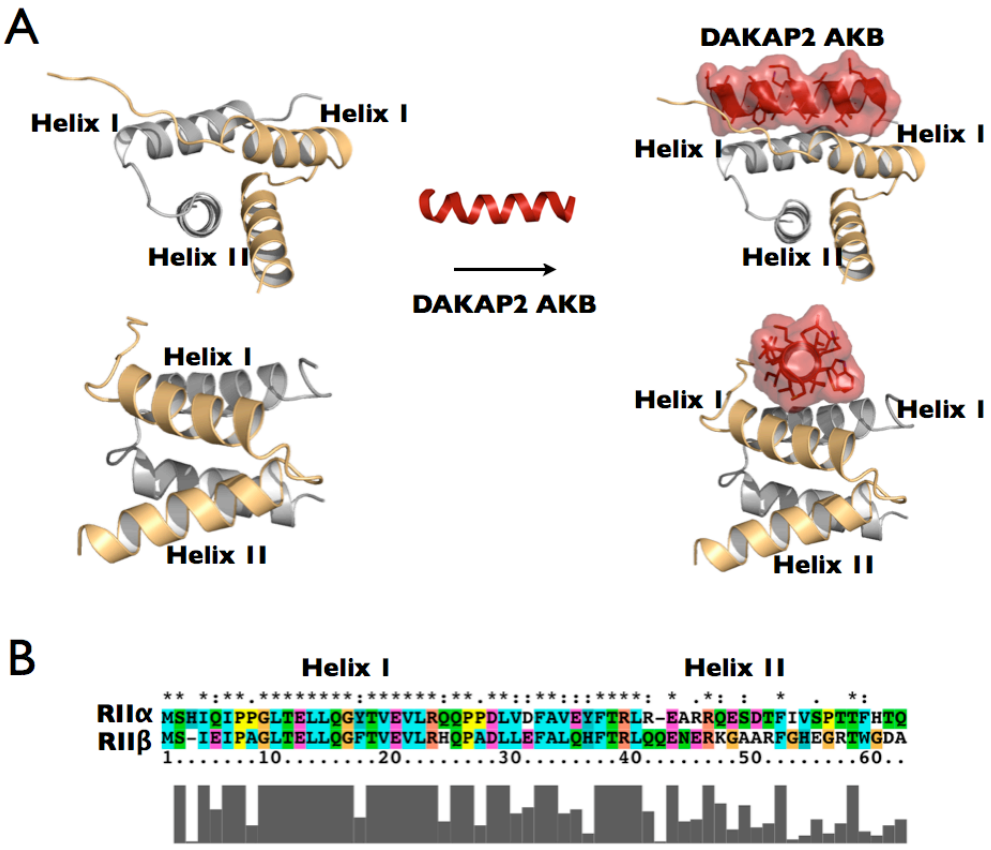

Figure 4.1: Comparison of RIIα and RIIβ D/D Domain

Panel A shows a ribbon representation of RIIα D/D domain bound to D-AKAP2 peptide. The D/D domain is shown in tan colors and the AKAP peptide is in red. Panel B shows the sequence homology between RIIα and RIIβ D/D domains.

Linker Regions: While we have been able to obtain structures of D/D and CNB domains, the structure of any full-length holoenzyme has remained elusive. This is likely due to the highly dynamic nature of the linker. Small angle x-ray scattering (SAXS) gives information about the global features of proteins in solution and can be used to generate basic models of protein shapes. Scattering data is inverse Fourier-transformed to a pair-distance distribution function (known as the *P(r)* function) that describes the probable distribution of vector lengths *(r)* between each pair of scattering centers within the scattering molecule. SAXS studies on full length R-subunits indicated RIIβ and RIIα are significantly different from RIα in overall shape [50, 51]. Shape restoration modeling of the SAXS data indicates that the IIα and IIβ isoforms of both free R-subunit dimers have an extended structure when free of the C-subunit, in contrast to the RIα subunit which is Y-shaped. However, while the RIIα subunit stays extended upon C-subunit binding, RIIβ undergoes a significant compaction to form a globular holoenzyme, shown in Figure 4.2. An insert in the linker region of RIIβ is the most significant sequence variation between the RIIα and RIIβ isoforms. Linker switch experiments where the extra linker insert from RIIβ was inserted into RIIα showed an intermediate structure between the RIIα and RIIβ holoenzymes [51].

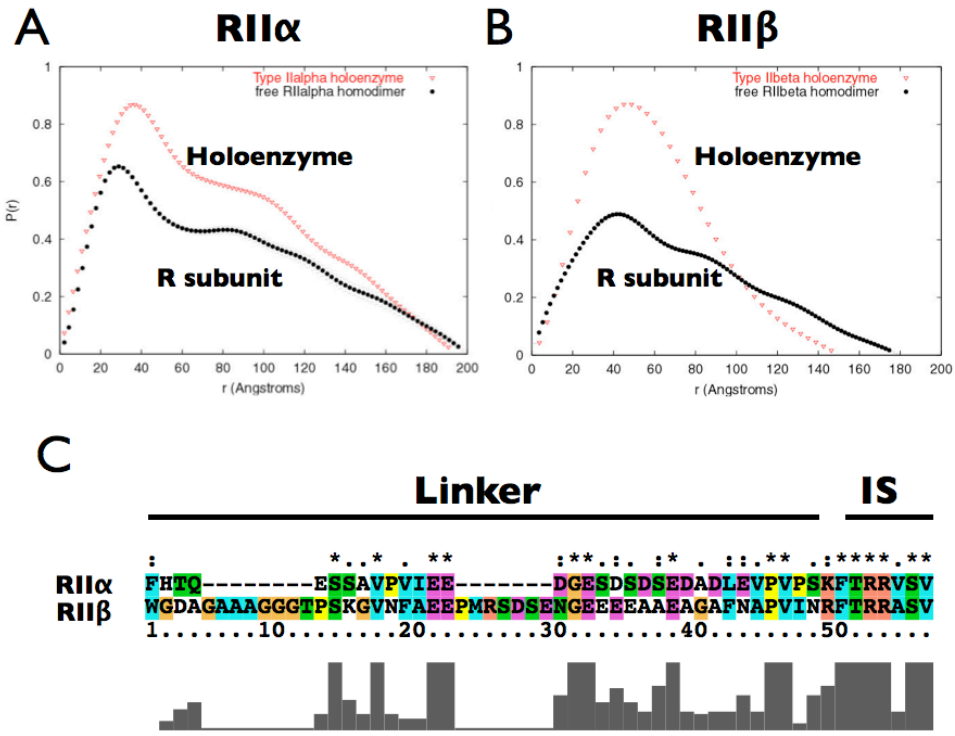

Figure 4.2: SAXS Analysis of PKA Type II linker

Panel A shows the P(r) functions of RIIα regulatory subunit bound to cGMP (black symbols) and holoenzyme (red symbols). Both conformations are highly extended. Panel B shows the P(r) functions of the same conformational states of RIIβ. RIIβ becomes more compact upon forming holoenzyme. Panel C shows the amino acid sequences of type II linker between the D/D domain and inhibitor site represented by single letter codes.

In the compact RIIβ holoenzyme form, it is likely that the linker is at least partially ordered and interacting with the CNB domain or the D/D domains.

Since a full-length RIIβ has not been successfully crystallized, we decided to engineer a smaller fragment of RIIβ that might be able to capture the global features of the full-length holoenzyme. We thus engineered a deletion mutant of both RIα and RIIβ that lacked CNB domain B. Only the RIIβ mutant was stable, and we characterized its biochemical properties and its overall shape free and bound to the C-subunit using SAXS.

Results:

Engineering Dimeric Deletion Mutants of RIIβ: To better understand interactions between the D/D domain and CNB domain A in RIIβ and RIα, two constructs were cloned and purified, RIα (1-244) and RIIβ (1-281). These constructs contain the single CNB domain A and the entire N terminus of the R subunit. Initial purification of RIIβ (1-281) and RIα (1-244) were surprisingly different. The RIα (1-244) showed significant aggregation, both during purification and during formation of holoenzyme. Samples of RIα (1-244) were never obtained at a high enough quality to allow for further characterization.

RIIβ (1-281), in contrast, behaved very differently during purification. The RIIβ protein was very stable and only showed small amounts of aggregation during purification. In fact, it was significantly more resistant to proteolysis and less prone to aggregation than full-length RIIβ. RIIβ (1-281) also formed a stable holoenzyme complex with the C-subunit even in the absence of ATP. Incubation of RIIβ (1-281) with C-subunit followed by gel filtration chromatography yielded a pure peak of RIIβ (1-281):C which was stable during subsequent experimentation. Due to the dimerization of the D/D domain, SPR analysis of the RIIβ (1-281):C interaction was not possible, but based on gel filtration of the holoenzyme, a much tighter complex is formed with RIIβ (1-281) than with RIIβ (108-281) in the absence of AMPPNP.

SAXS: While significant aggregation during purification and SAXS analysis prevented reliable data collection on the RIα (1-244) subunit, SAXS data was obtained for the type IIβ (1-281) subunit. Results are summarized in Figure 4.3. Isolated RIIβ (1-281) subunit in the presence of cGMP had a D_{max} of 159 Å and an R_g of 45.4 Å, while the R-subunit in complex with the C-subunit had a D_{max} of 132 Å and an R_g of 41.6 Å. The largest dimension of RIIβ (1-281) subunit thus becomes smaller by approximately 30 Å following binding to the C-subunit.

Peptide Array: To establish whether there might be isoform-specific differences in docking of the D-AKAP2 peptide to RIIα versus RIIβ, a peptide blot array was designed. This strategy was used successfully with RIα and RIIα to find binding determinants and design isoform-specific peptides [73]. Peptides were synthesized directly onto a cellulose membrane support using standard spot synthesis techniques [74]. The array was then overlaid with full-length RIIα and RIIβ.

Peptide arrays were designed using an amino acid substitution technique, where the peptide sequence is arrayed on a single axis, while each position is substituted on the second axis. This allows each position on the entire peptide sequence to be substituted for every amino acid. For RII isoform selectivity screening, a peptide length of 23-mer was chosen, including 2 glycines at the membrane surface for flexibility.

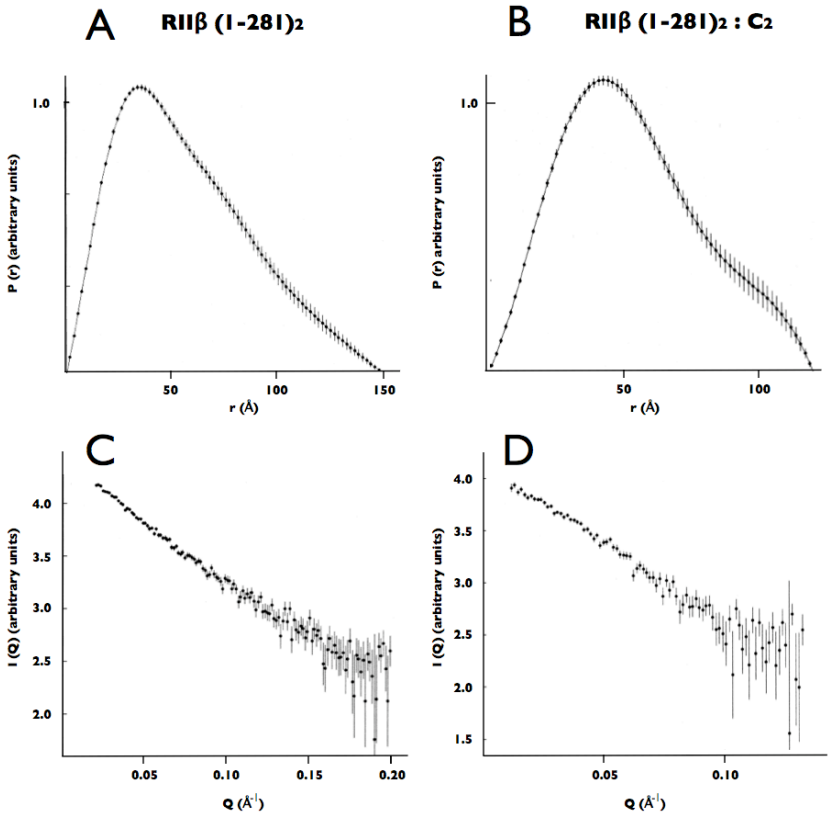

E

	Sample	R (g) Å	Dmax Å
A	RIIβ (1-281)2	45.4	159
B	RIIβ (1-281)2 : C2	41.6	132

Figure 4.3: SAXS Analysis of RIIβ (1-281)

Small angle X-ray scattering analysis of RIIβ (1-281) was measured in two states, bound to cGMP and bound to the catalytic subunit. Panel A shows the *P(r)* function for RIIβ (1-281) bound to cGMP. Panel B shows the *P(r)* function for RIIβ (1-281) bound to the catalytic subunit. Panels C and D show *I*(Q) versus *Q* profiles for RIIβ (1-281) bound to cGMP and catalytic subunit respectively. Panel E summarizes the R_g and D_{max} results derived from the *P(r)* analysis.

RIIβ and RIIα overlays of the blots demonstrated general conserved features for both RII subunits but also showed isoform selectivity as shown in Figure 4.4. The DAKAP-2 peptide is an amphipathic helix, and the binding surface of the helix can be recognized using the sequence patterns displayed by the array. Three hydrophobic regions, each separated by 2 residues, can be observed on the blot as binding regions with low tolerance for substitution. L5/A6, I9/A10, and I13/V14 regions all prefer hydrophobic residues and any change to a charged or hydrophilic residue reduced or abolished binding.

Substitution of an amino acid with a proline will diminish binding by disrupting the helix. Proline substitution in the helical region between E4 and M18 of the D-AKAP2 peptide abolishes binding. Proline substitution sensitivity and sensitivity to substitution in the hydrophobic regions indicate that the SPOT array peptide substitution method is a valid technique for mapping this helical motif.

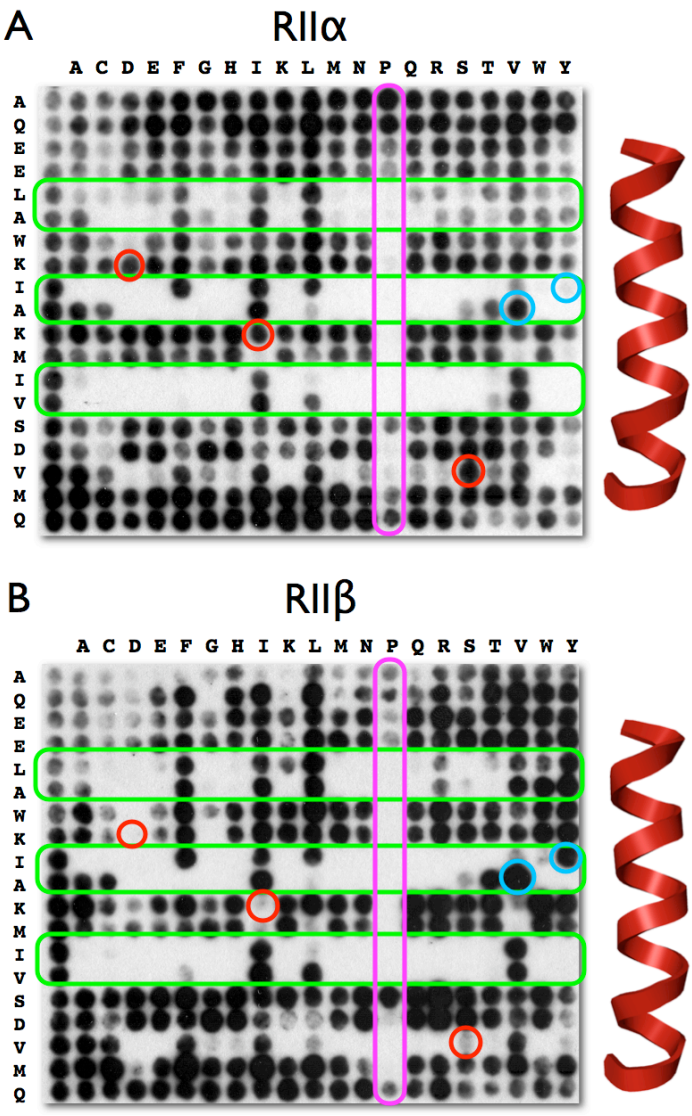

Figure 4.4: Peptide Array: RIIα and RIIβ Selectivity

Amino acid substitution blots of D-AKAP2 A kinase binding peptide overlaid with RII subunits. Panel A shows the RIIα overlay, and Panel B shows the RIIβ overlay. Hydrophobic docking regions have low tolerance for substitution as shown in green. Proline substitution abolishes binding as shown in purple. RIIβ specific mutations shown in red, and RIIα mutations in blue.

Comparison of RIIα and RIIβ overlays reveals selectivity between isoforms in binding to substitute peptides. Three locations on the overlays showed good selectivity for RIIα. Substitution at K8 or K11 with negatively charged residues are highly disruptive for RIIβ but not for RIIα. V17 substitution to a serine disrupts RIIβ but not RIIα. Two locations on the overlays demonstrated selectivity for RIIβ. Substitution of I9 with a tyrosine is a major disruptor for only RIIα. The converse is true for A10, where substitution with a valine significantly increases the binding to RIIβ while not affecting RIIα. Based on this array we are now engineering selective peptides that have preferred specificity for either RIIα or RIIβ.

Discussion:

A major goal of this project was to elucidate the global conformational dynamics of the subdomains of RIIβ and to understand how each subdomain interacts with the C-subunit. Three constructs, RIIβ (1-281), RIIβ (108-268), and RIIβ (108-402) can now be compared and their properties are seen to be significantly different with regard to three properties: 1) stability 2) global conformation of the free and holoenzyme states and 3) ATP dependence for holoenzyme formation.

Stability: The RIIβ (1-281) construct is resistant to both proteolysis and aggregation, which is in contrast to full-length RIIβ (1-416) and to the comparable fragments of RIα. During purification of full-length RIIβ, 30-60% of the protein is lost to aggregation and proteolytic degradation. Removal of CNB domain B in RIIβ reduced this tendency to aggregate and break down. This effect may be the result of cross talk between the D/D domain, linker insert and the CNB domain A of RIIβ, as shown in Figure 4.5.

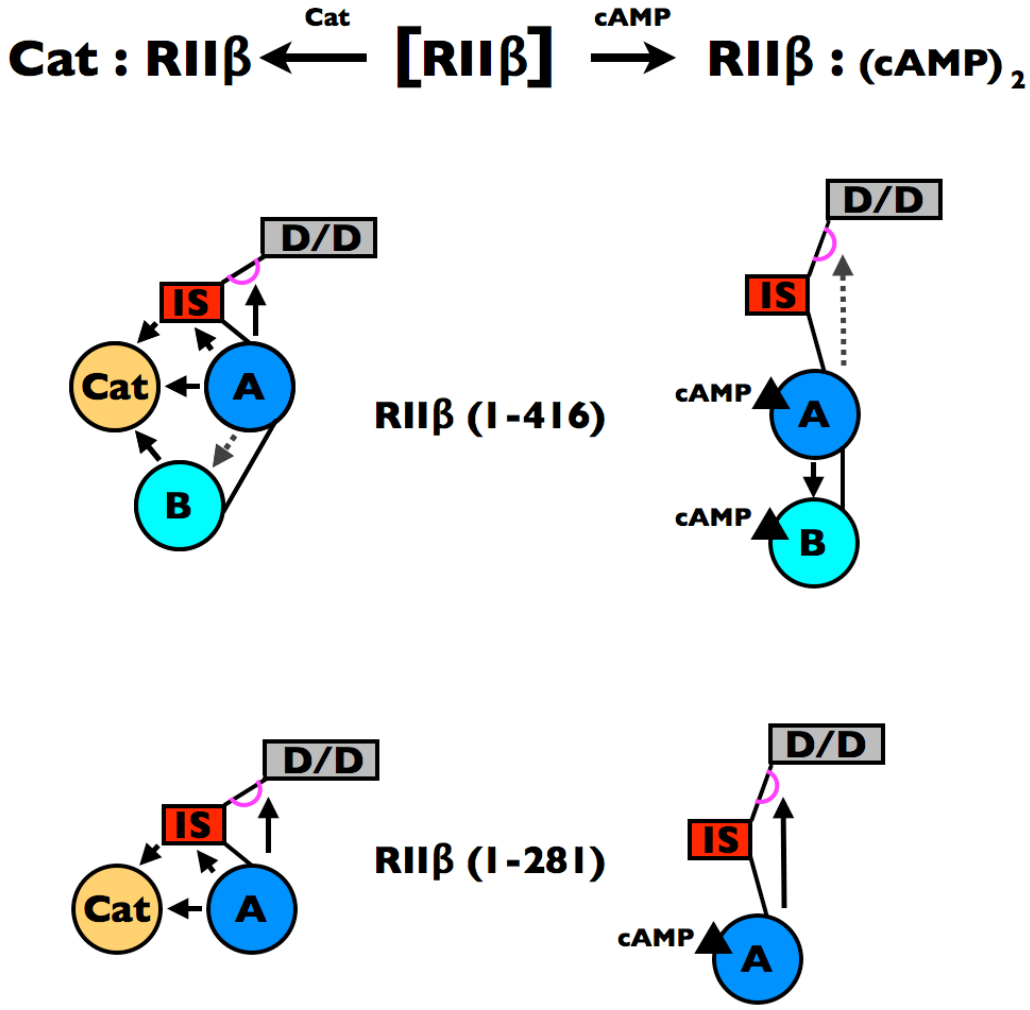

Figure 4.5: RIIβ Interaction Network

Intra-subunit and Inter-subunit communication in RIIβ holoenzymes shown on left. Intra-subunit interactions on cAMP bound regulatory subunits shown on right. Removal of Domain B in RIIβ (1-281) increases the strength of the Domain A – linker -- D/D interaction. Weak interactions are shown by dotted lines and the RIIβ specific insert is highlighted in magenta.

From cAMP-bound and holoenzyme crystal structures, it is known that the close interactions between the CNB domain A and CNB domain B are mostly abolished when C-subunit is bound and the R-subunit becomes extended. If there are interactions between the D/D, linker, and CNB domain A, it is possible that removal of the CNB domain B will change these interactions. The linker and CNB domain B, for example, may compete for interactions with CNB domain A. By removal of the CNB domain B in RIIβ (1-281), the competition is reduced and the CNB domain A interaction with the linker is strengthened. Therefore, the linker and D/D domain would then be more protected in RIIβ (1-281), thus explaining why this construct is less susceptible to aggregation and proteolysis.

Requirements for Changes in Global Conformation: The results of RIIβ (1-281) SAXS experiments demonstrate that the B domain is not required for compaction of the holoenzyme. For full-length RIIβ the D_{max} drops from 180 Å in the dimer form to 145 Å in the holoenzyme form. The maximal dimension of the RIIβ dimer thus is reduced by 35 Å when it binds to the C-subunit. The R_g values also decrease from 56 Å to 46 Å, indicating that the mass of the enzyme also is distributed closer to the center of the molecule. A simple shift in the D_{max} without a shift in R_g would indicate a small peripheral region of the protein is folding back towards the center of the molecule, while a R_g shift as

well as a D_{max} shift indicates that the body of the enzyme is undergoing a conformational change to a much more compact shape.

For RIIβ (1-281), the D_{max} decreases from 159 Å to 132 Å, and the R_g decreases from 45.4 Å to 41.6 Å when C-subunit binds. This difference is very similar that seen with the full-length RIIβ, with a 27 Å decrease in the D_{max} of the protein when C-subunit binds. The smaller change in R_g is indicative of a similar compaction as in the full-length protein, but starting from a somewhat more compact conformation for RIIβ (1-281). These SAXS results indicate that the compaction of the RIIβ subunit upon C-subunit binding does not require CNB domain B. The D/D domain, linker, IS and the CNB domain A appear to be sufficient to form a compact structure. RIIβ (1-281) is thus an excellent candidate for future structural studies of a tetrameric PKA holoenzyme.

ATP dependence for holoenzyme formation: The high affinity of the RIIβ (1-281) for the C-subunit in the absence of ATP is another indication of the importance of the linker region in the RIIβ-C interaction. Biacore results using RIIβ (102-265) showed significant improvement of affinity for C-subunit when the P-10 region is included, but AMPPNP was still necessary to get a high-affinity holoenzyme complex. During size exclusion chromatography of holoenzyme prepared using RIIβ (102-265), it was noted that the complex formed was incomplete, with a shoulder on the holoenzyme peak and the presence of unbound subunits in the SDS gel analysis. When a complex was

formed with RIIβ (1-281) in the absence of nucleotide and subjected to size exclusion chromatography, the complex ran as a symmetric peak and as a tight complex on SDS-PAGE. This confirms the importance of the linker region in RIIβ holoenzyme formation. Without the B domain and complete linker, RIIβ requires nucleotide to have high affinity for the C-subunit. When the B domain or the D/D domain and linker are present, the affinity for the C-subunit is increased and ATP is not required for holoenzyme formation.

The importance of ATP in the interaction of C-subunit with inhibitors is due entirely to the P-site residue in the R-subunit. In the presence of ATP, RIα and IP20 have high affinity for the C subunit (<1 nM), but in the absence of ATP the affinity drops to 125 nM and 2.3 μM respectively. In the absence of ATP both RIα and IP20 complexes can be readily be disassociated by physiological salt concentrations [58].

This basic change from a pseudosubstrate in RI to a substrate in RII also affects the dissociation of the R subunits in the cell [75]. When cAMP levels are raised in the cell, RI and C dissociate throughout the cell only when PKI or protein substrates are present. RII and C show the opposite behavior, with RII and C fully dissociating when an increase in cAMP level is induced. Mutation of the RII subunit to a pseudosubstrate changes the dissociation behavior to resemble RI. The converse is also true, i.e., introducing a phosphorylation site into RI causes it to behave like RII, with full disassociation of the complex by cAMP. These effects of the P-site of the R subunit in the R-C interaction have

also been observed in the R-C interaction with PrKX, the human X chromosome encoded PKA catalytic (C) subunit [76].

The fundamental change from a substrate in RII to a pseudosubstrate in RI is one of the most important functional distinctions between PKA isoforms. The absolute requirement for ATP in RI holoenzyme is also due to this single difference in the P-site residue. In RIα isoform the inhibitor site interaction with the catalytic cleft is completely dependent on the presence of ATP and 2 Mg^{2+} as observed in SPR affinity measurements [59]. Without ATP the small lobe of PKA is open and interactions with the inhibitor site region are reduced.

RII subunits use a larger set of features to bind to the C-subunit. When phosphorylated, the RII subunits still can bind the C-subunit, however with reduced affinity. The RII isoforms may use the B domain or the linker regions as an extra set of surfaces to maintain affinity when the R-subunit is phosphorylated. When cAMP is present, the CNB domain A and CNB domain B interactions with the C-subunit are lost, and the holoenzyme complex dissociates with either RI or RII. However, in holoenzyme complexes containing RI, the IS is still available for binding C-subunit, and will quickly rebind the C-subunit. The IS of RII will be phosphorylated after cAMP addition, decreasing the R-C affinity and allowing the RII subunit to diffuse away in the cell.

Methods:

SAXS: X-ray scattering data was acquired at 12 °C, using the X-ray instrument at University of Utah that uses CuK radiation (wavelength λ=1.54 Å) described previously [77]. Data were collected and reduced to $I(q)$ *versus* q ($q=4\pi(\sin\theta)/\lambda$, 2θ=scattering angle). The net scattered X-ray intensities for the proteins were determined by subtracting a normalized buffer blank from each protein data set. $P(r)$ was calculated as the inverse Fourier transform of $I(q)$ data using the program GNOM , which employs an indirect transform approach [78]. In addition to $P(r)$, GNOM also provides the radius of gyration, R_g, and the maximum linear dimension of the particle, D_{max}. The q-range employed for the GNOM analysis was 0.01–0.15 $Å^{-1}$. A smearing correction was applied to the data to correct for the slit geometry of the instrument. Guinier analyses showed a single linear fit at low q, consistent with there being no non-specific aggregation in the samples. Further, there was no concentration dependence of the scattering parameters of any sample, also consistent with the samples being aggregation-free and free of inter-particle interference effects that could otherwise distort the derived structural parameters.

Peptide Arrays: Peptide arrays were generated using the SPOT synthesis technique on a Multipep synthesizer (Intavis AG) [74]. Peptide arrays were washed with 100% ethanol (Rossville) for 5 min, followed by 2X washes in H_20 for 5 min and 1 min. Then blots were washed 1X with Tris Tween

Buffered Saline (TTBS) and then blocked with 5% milk in TTBS for 1 hr. Purified recombinant *E. coli*-expressed R-subunits were used to probe blots. Blots were made in duplicate and each protein incubation was performed only once on the blot. Protein was mixed with 5% milk at 3.7 μM concentration (1.85 μM dimer) and incubated overnight at 4 °C.

Blots were washed three times in TTBS for 10 min, followed by primary antibody incubation. All washing and antibody incubations were performed at room temperature. RIIα antibody (Santa Cruz Biotechnology) at 1:1000 and RIIβ antibody (Santa Cruz Biotechnology) at 1:2000 in TTBS were incubated shaking for 1 hr. Arrays were washed three times with TTBS for 10 min, and followed by a secondary anti-rabbit IgG peroxidase-labelled antibody (Santa Cruz Biotechnology) was incubated at 1:5000 and 1:10,000 for RIIα and RIIβ respectively for 1hr. Finally, blots were washed in three times in TTBS.

Quantification of RIIα and RIIβ binding to the peptide arrays was performed by using a chemiluminescent substrate (Sigma) and exposure of a series of films to the blots. The RIIα blot was incubated with the substrate for 3 minutes and the film was then exposed for approximately 5 seconds. The RIIβ blot was incubated with Femto substrate (Sigma) mixed at 1:50 with standard substrate, and the film was then exposed for approximately 20 minutes. These exposures produced blots with similar levels between each protein used. Films were scanned into digital format, and analysis was performed.

Chapter V

Hydrogen Deuterium / Mass Spectrometry Analysis of RIIβ-C

The highly dynamic nature of the regulatory subunits in their interactions with cAMP and the catalytic subunit create an ideal system to study using solution based techniques. The application of hydrogen deuterium exchange coupled with mass spectrometry (HD/MS) to probe both the R-C and R-cAMP interactions in solution have been very successful for PKA where we have both protein:protein and protein:ligand interactions [79-81]. HD/MS measures deuterium incorporation into backbone amides of the protein over time. Following deuterium incorporation, proteins are digested into peptides and changes in deuterium levels are quantified by mass spectrometry. Comparison of deuterium incorporation for liganded and unliganded states shows how the protein surface is affected by binding of the ligand.

Full length RIIβ was analyzed previously using HD/MS to elucidate solvent surface accessibility in the cAMP bound and C-subunit bound conformations [82]. For the holoenzyme, only peptides from the RIIβ subunit were characterized; the C-subunit peptides were not analyzed for deuterium incorporation. Three regions in domain A of RIIβ showed significant protection when bound to the C-subunit, while much of domain B showed increased solvent accessibility. The inhibitor site region of RIIβ (residues 102-115) showed reasonable protection in the holoenzyme. In addition, significant protection was observed in residues (150-152) corresponding to the 310 loop region, a conserved loop predicted to be a universal protein-protein interaction docking site [83]. Also, residues (253-268) from the αC helix was highly

protected extremely well from solvent by binding of the C-subunit. These results, summarized in Figure 5.1, were mapped onto the structure of cAMP bound RIIβ. All three regions that showed protection upon C-subunit binding correspond to interaction sites with the C-subunit in the RIIα holoenzyme.

HD/MS analysis of RIIβ defined the effects of cAMP and C-subunit binding on solvent accessibility of RIIβ. In order to fully understand the changes in solvent accessibility at the R-C interface, however, one needs to analyze both the C and R-subunits. We extended the HD study of the RIIβ holoenzyme by mapping changes in the C-subunit when it is bound to different R-subunit isoforms. In this chapter we describe the specific effects of binding RIIβ constructs and also the effects of AMPPNP. This work has been published and the key points are summarized here in Chapter V.

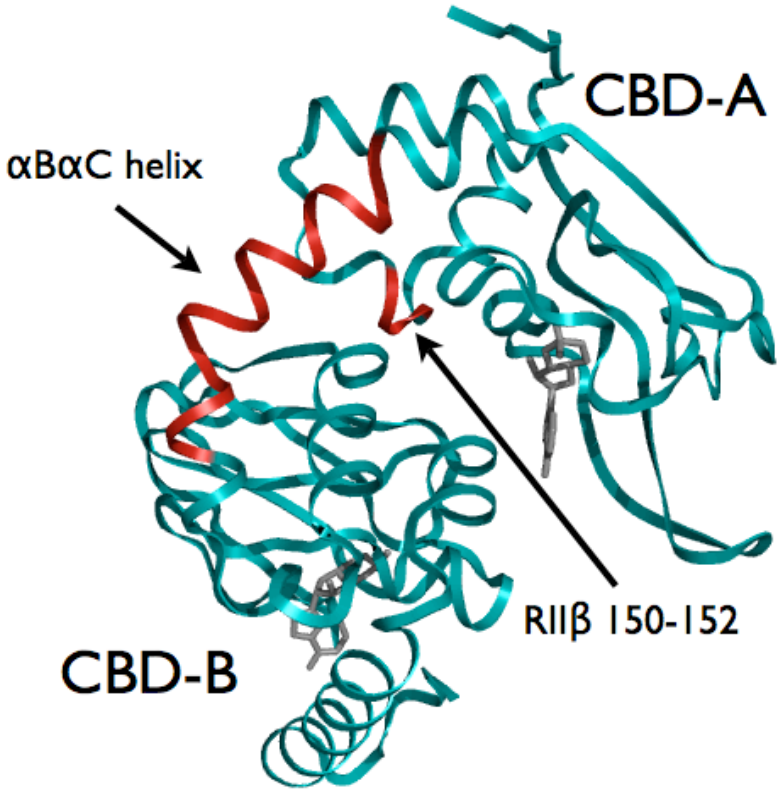

Figure 5.1: Protection of RIIβ in the Presence of Catalytic Subunit

The HD/MS analysis of RIIβ was carried out in the presence of cAMP and in the presence and absence of catalytic subunit (78). The protection that was afforded by the catalytic subunit is mapped here onto the cAMP bound conformation of the RIIβ subunit. cAMP is highlighted in grey.

Results:

HD/MS of RIIβ: While earlier HD/MS studies of RIIβ holoenzymes looked exclusively at protection in the R-subunits, here we looked at protection of backbone amides in both the C-subunit and in the RIIβ subunits. We used two RIIβ constructs, RIIβ (108-402) that contain both CNB domains A and B, and RIIβ (108-268) containing only CNB domain A. Peptides on both the R-subunit and C-subunit with the largest changes between the free and holoenzyme states are shown in Figure 5.2. Two peptides in the C-subunit showed significant changes upon binding to RIIβ subunits, and these will be discussed first. The peptides protected in the R-subunit then will be described.

Residues (44-54) in the C-subunit correspond to the tip of the glycine-rich loop in the N-lobe. HD/MS analysis of this peptide (44-54) is shown in Figure 5.3. This peptide is protected in the presence of RIIβ (108-402), but only when AMPPNP is present. RIIβ (108-268), which is missing the B-domain, gave no additional protection beyond AMPPNP alone.

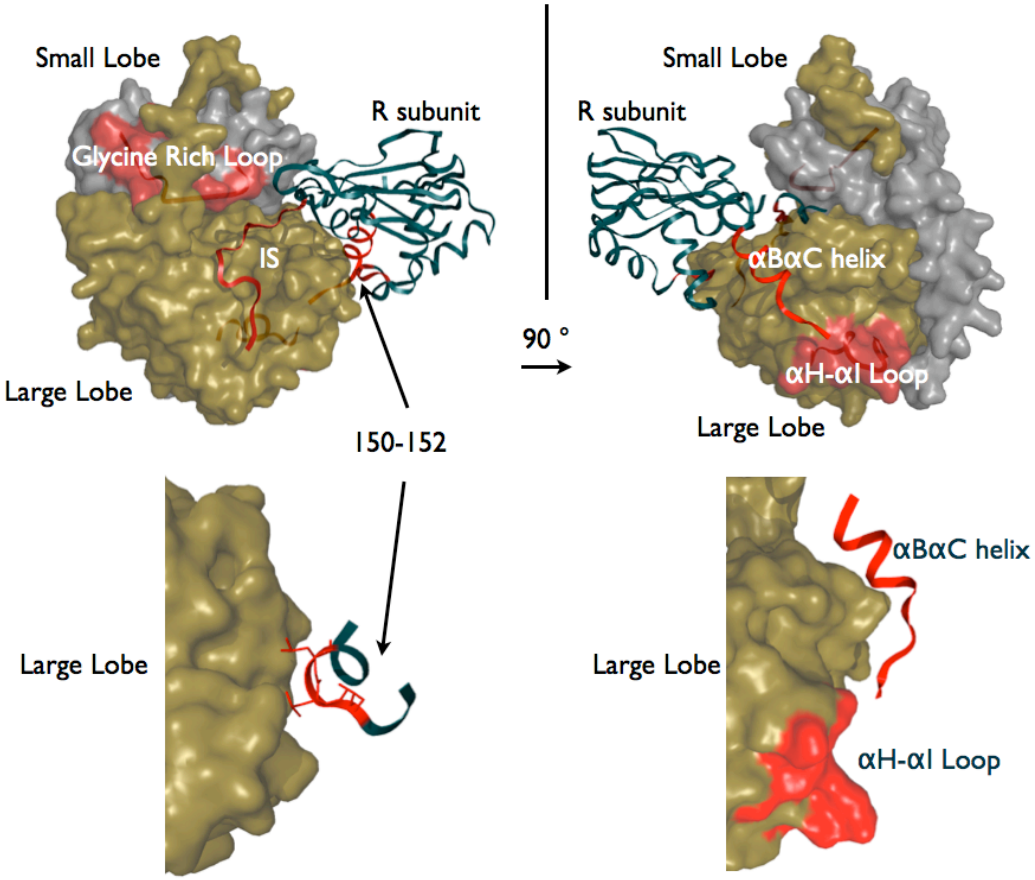

Figure 5.2: H/D Exchange RIIβ:C

Surface rendering of PKA C subunit in grey and tan, RIIβ rendered in dark cyan ribbons. Peptides that show changes in solvent accessibility shown in red. The IS and αB/C helix show decreased solvent accessibility in holoenzyme. The αH-αI loop is protected from solvent in the RIIβ (108-402) holoenzyme, and is highly solvent exposed in RIIβ (108-268). The glycine rich loop is slightly more solvent exposed in the RIIβ holoenzyme than in RIα.

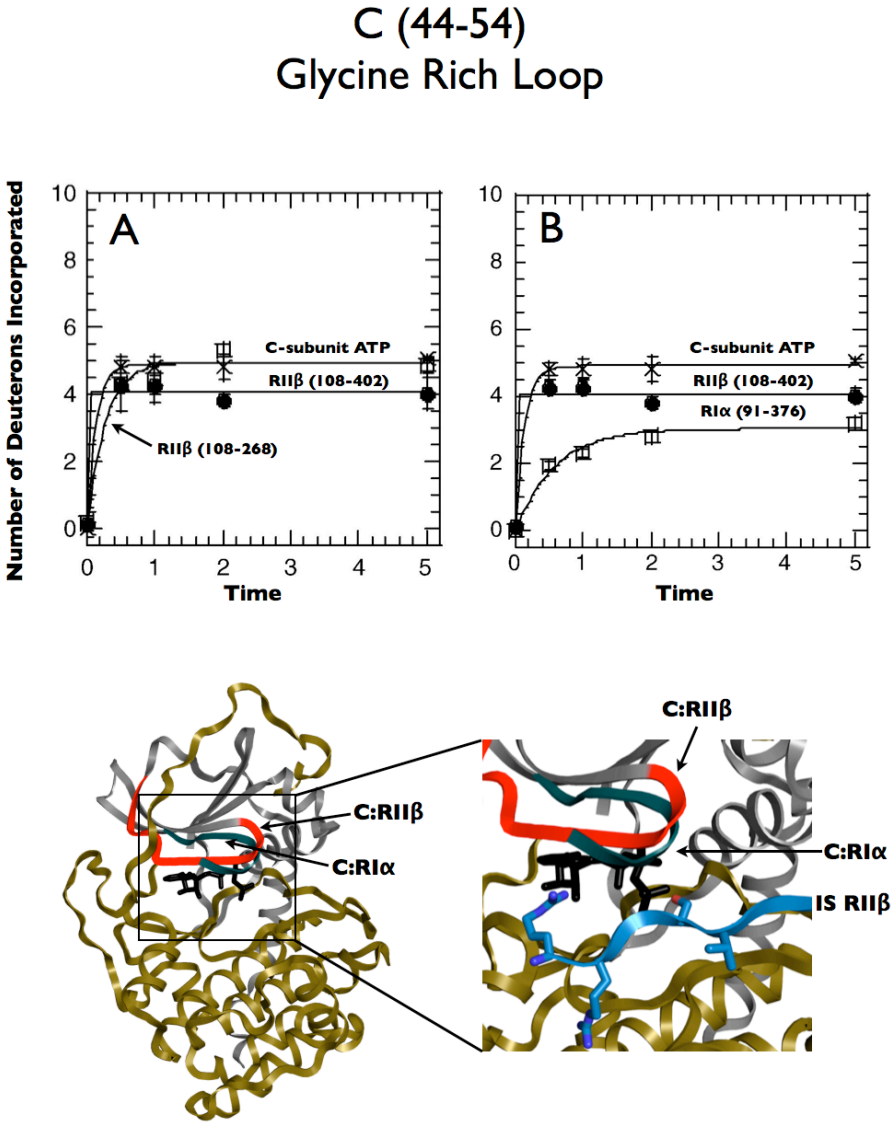

Figure 5.3: HD/MS Glycine Rich Loop of the Catalytic Subunit

Deuterium exchange of the glycine rich loop peptide of the catalytic subunit. As shown in Panel A, RIIβ domain B is required for protection of the glycine rich loop in RIIβ holoenzyme. Panel B shows comparison of protection in the glycine rich loop of RIIβ and RIα in complexes containing domain B.

Residues (278-289) in the C-subunit correspond to the αH-αI loop in the C-lobe. As seen in Figure 5.4, this peptide (278-289) showed nearly complete protection when bound to RIIβ (108-402), and unlike the glycine rich loop peptide, this protection was independent of AMPPNP. This protection is consistent with the structure of the RIIα holoenzyme where this site directly docks to domain B [15]. Analysis of the C-subunit when RIIβ (108-268) was bound showed that this site was extremely sensitive to the presence or absence of the B domain. Binding of RIIβ (108-268) caused a significant increase in the solvent accessibility of the αH-αI peptide. Even when compared to the C-subunit bound to AMPPNP alone, the solvent accessibility was increased. This surprising result highlights the potential importance of this site as an allosteric sensor.

Limited analysis of peptides from the R-subunit, due to low coverage, produced a single peptide that showed large protection in the holoenzyme complex. The peptide RIIβ (253-268) is protected by almost 10 amides when RIIβ (108-402) is bound to the C-subunit. This region corresponds to the αB/C helix of domain A that undergoes a major conformational change in going from the cAMP bound state to the holoenzyme state. This peptide showed comparable protection when full length RIIβ was bound [82]. When the B domain is missing from RIIβ, however, this region is not protected in the holoenzyme.

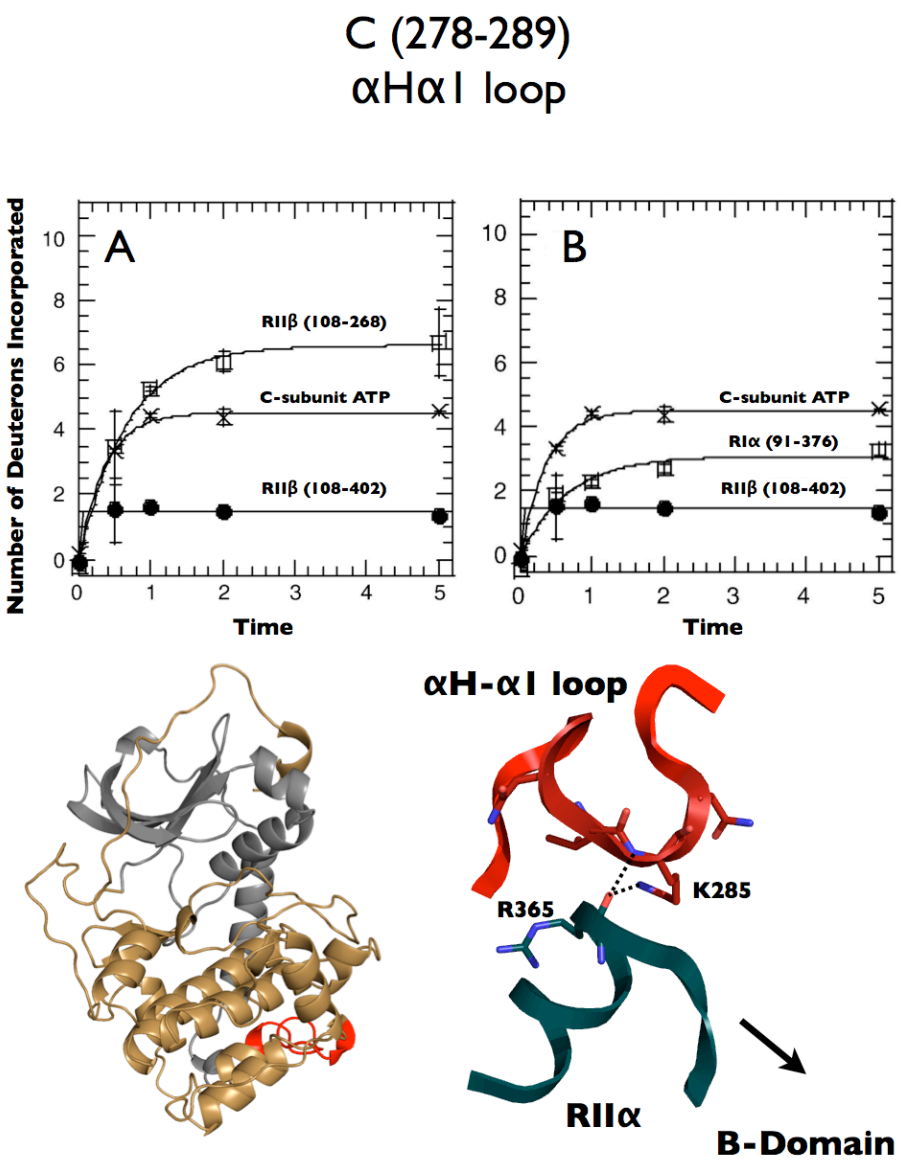

Figure 5.4: HD/MS αH-αI Loop of the Catalytic Subunit

Deuterium exchange of the αH-αI loop peptide of the Catalytic subunit. Lower right shows the interaction of the αH-αI loop in the RIIα holoenzymes, with hydrogen bonds between K285 in the catalytic subunit and R365 in the regulatory subunit highlighted.

Discussion:

HD/MS analysis of peptides from the RIIβ subunit demonstrated the importance of the RIIβ αB/C helix in the RIIβ-C interaction. This peptide, (residues 253-268), is a major docking site for the C-subunit in both the RIα and RIIα holoenzyme crystal structures, and is thus likely to play the same role in the RIIβ complex although we have not been able to crystallize an RIIβ holoenzyme complex when both A and B domains are present. While the corresponding peptide was also protected in the RIα holoenzyme, protection was much greater in the RIIβ holoenzymes.

This same RIIβ (253-268) peptide is not protected at all in the RIIβ (108-268) holoenzyme complex. The lack of protection observed in RIIβ (108-268) complex is likely due to a loosening of the R-C interaction in this region when the B domain is missing. As seen in Figure 5.2, the crystal structures show the αC helix unraveling at the C-terminus, and this confirms the lack of solvent protection of RIIβ (253-268) in the RIIβ domain-A holoenzyme. The presence of the RIIβ B-domain orders the αB/C helix against the C-subunit and decreases the solvent accessibility of this peptide in the RIIβ (108-402) holoenzyme, as it does in the full length holoenzyme.

In the RIIβ (108-402) holoenzyme complex the most significant protection was observed in the αH-αI loop of the C-subunit, shown in Figure 5.4. As seen in Figure 5.5 the αH-αI loop contains an essential conserved Arg, Arg 280, that interacts electrostatically with Glu 208 in the APE motif of the

activation segment. This region also contains a 5 residue insert (residues 282-286) that is a unique feature of the AGC kinases [84]. This region was shown in the RIIα structures to be the major docking site for the CNB domain B on the C-subunit. This interaction region is shown in Figure 5.5, which highlights the docking of the αB helix of RIIα to the αH-αI loop of the C-subunit. Comparison of peptide amide exchange between the C-subunit alone and the RIIβ (108-402) holoenzyme complex confirms the importance of the B domain for docking to this site. In the RIIβ (108-402) holoenzyme complex, peptide (278-289) is protected by three more amides than in the free C-subunit. This is significantly more protection than observed in the equivalent RIα experiment, where only a single amide was protected in the complex. The αH-αI loop thus senses isoforms differently.

The RIIα holoenzyme structure provides some clues about this critical RII docking site [15]. Arg 365 is completely shielded by the αH-αI loop; it is anchored by multiple hydrogen bonds to both its side chains and to its backbone carbonyl and through hydrophobic interactions. The side chain of Arg 365 of RIIα is interacting with the backbone carbonyl and the side chain of Thr 278 from the αH-αI loop of the C-subunit, and this interaction involves two hydrogen bonds between the two subunits. In addition, the backbone of Arg 365 is anchored strongly to the side chain and backbone amide of Lys 285. Arg 365 is thus firmly anchored to this site.

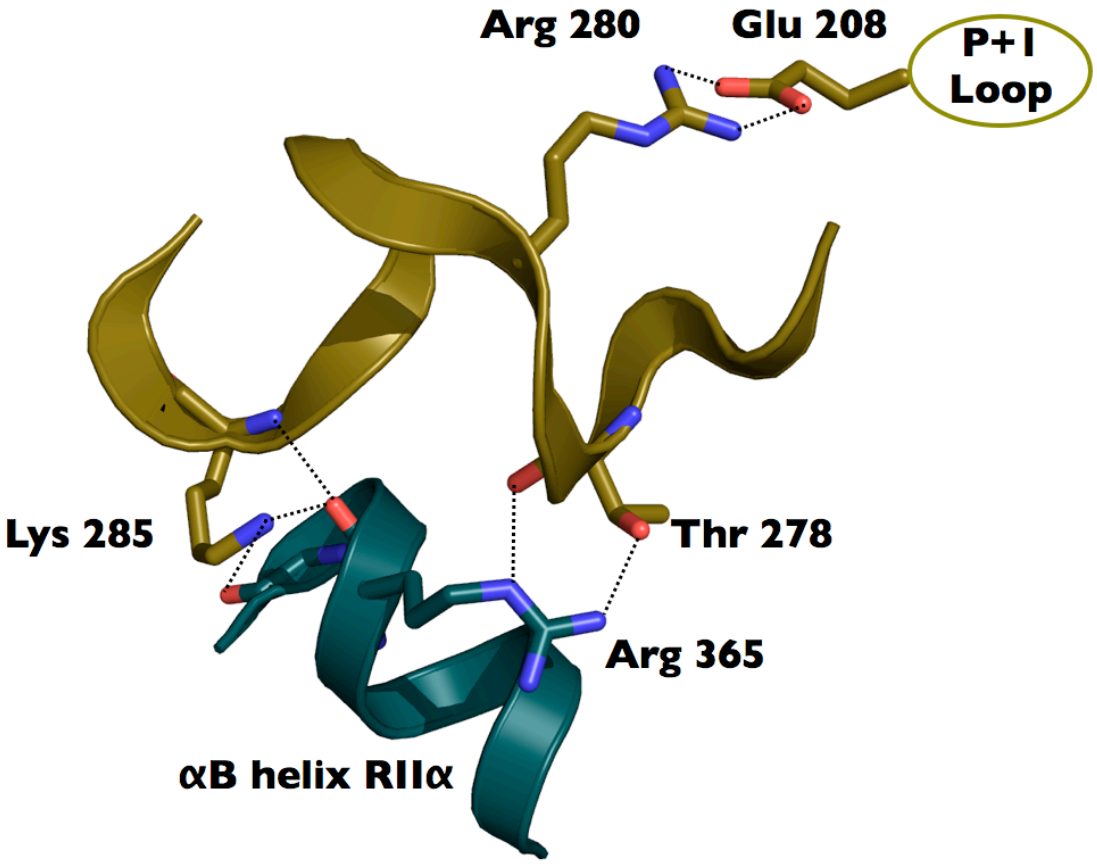

Figure 5.5: RIIα CNB-A Capping Residue Interactions with C-Subunit

The αB helix of RIIα (blue) CNB domain B interacts with the αH-αI loop of the catalytic subunit (tan). Arg 365 is both a major interaction partner with the C-subunit and is the hydrophobic cap for cAMP in CNB domain A of RIIα. (PDB ID 2QVS)

Arg 365 is also well shielded in the cAMP bound conformation where it serves as the capping residue for the adenine ring of cAMP bound to CNB domain A of RIIα. This capping function is conserved in RIIβ and RIIα, but is completely different in RIα where the capping residue comes from the A helix of domain B. Arg 365 thus has an important and unique role in regulating both the conformational states of RII; it is a key residue in the R-C interface and is also necessary for cAMP binding to the CNB-A. This residue corresponds to Arg 381 in RIIβ and is likely to play the same role in the interface of the RIIβ holoenzyme structure.

The protection of the αH-αI loop by the B domain of RIIβ highlights the importance of the RIIβ B domain for interactions with C-subunit. For RIIβ the affinity for C-subunit is nM when the B-domain is present but not measurable when the B-domain is missing. In the presence of AMPPNP we showed that the affinity was 11 nM when only the A-domain was present but 0.2 nM when the A and B domains were both present. Thus in both cases the B-domain is critical for high affinity binding of RIIβ to C-subunit, and HD/MS results correlate with this change in affinity to docking to the αH-αI loop.

When RIIβ domain A binds to the C-subunit, the αH-αI loop surprisingly becomes more solvent accessible, suggesting that this may indeed be an allosteric site. Binding of RIIβ A domain appears to prime the αH-αI region for binding of the B-domain. The αH-αI loop is thus a hotspot on the surface of the C-subunit. This study has identified this region as both a surface for RII

docking as well as a site for allosteric cross-talk in the C-subunit. Our structural and HD/MS studies that demonstrate the importance of this loop are reinforced by mutagenesis of K285 to proline. This mutation, which removes the hydrogen bonding of both the sidechain and the backbone, significantly decreased the binding of RII but had little effect for RI (Jie Yang, unpublished results). The αH-αI loop has also been independently identified as an important secondary surface for binding of substrates using a yeast genetic screen to trap kinase substrates [85]. Using point mutations in the αH-αI region of the Tpk1 yeast PKA, a catalytically impaired double mutant was found that traps protein substrates by preventing release. The αH-αI region has therefore been identified as a conserved hotspot for binding of substrates and mutations in this region reduce catalytic activity. The conserved Arg 280 at the end of the kinase core lies in this loop, and it makes a conserved contact with Glu 208 in the activation segment as shown in Figure 5.5. This contact is likely to be an important part of the allosteric network, and mutation of Arg 280 also leads to loss of activity (Jie yang, personal communication).

Temperature Factor Analysis: Shown in Figure 5.6 are temperature factor (B-factors) plots for the C-subunit in complex with RIIβ, RIα or RIIα. Both RIIβ and RIα structures were solved in the presence of AMPPNP and contain only the CNB domain A. RIIα was solved in the absence of nucleotide and contains both CNB domains A and B.

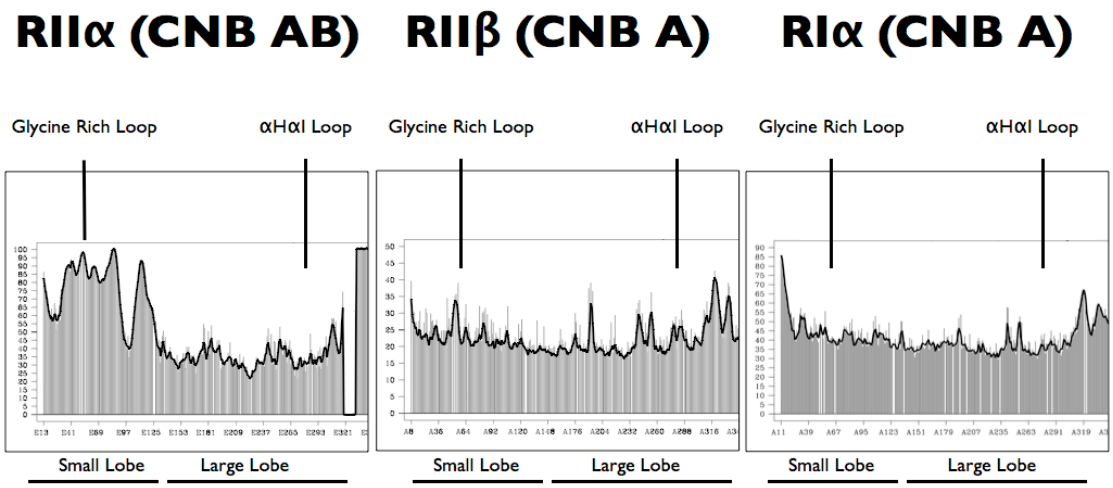

Figure 5.6: B-Factor Analysis of Holoenzyme C-Subunits

Temperature factor analysis of the catalytic subunit of three holoenzyme PKA crystal structures. Shown on the left is RIIα (91-400) : C in the absence of ATP. Shown in the middle is RIIβ (108-268) : C : AMPPNP. Shown on the right is RIα (91-244) : C : AMPPNP. The effects of AMPPNP and the B-domain of the regulatory subunits are highlighted.

Comparison of B-factors of the crystal structure models of the C-subunit reveals regions of relative disorder and order in the molecules. RIIβ (108-268) : C-subunit B-factors are relatively low throughout the structure and generally resemble the RIα holoenzyme. The RIIα structure has high B-factors in the small lobe, consistent with the disengagement of the small lobe from the rest of the molecule observed in the crystal structure.

Comparison of B-factors in RIα and RIIβ bound C-subunits reveals two key features that differ between the two isoforms. The B domain of RIIβ was shown to be important for high affinity binding to the C-subunit. Crystal structures of RIα and RIIα have defined the αH-αI loop region of the C-subunit as an interaction region with the R-subunits. The temperature factors for this loop have a spike in the RIIβ holoenzyme and are relatively flat in the RIIα and RIα holoenzymes. Docking of RIIβ domain A makes this loop region more dynamic, based on the B-factors, and this is exactly what was seen in the HD/MS experiments. In contrast, docking of RIα domain A did not prime this site based on the HD/MS experiments, and has flat temperature factors in this region. In RIIα holoenzyme the B domain is docked to this site and thus has low temperature factors.

The glycine rich loop of the C-subunit also can be identified on the B-factor plot. The region consisting of C-subunit residues (45-55) in the RIIβ crystal structure have a significant spike in the B-factors when compared to RIα. The glycine rich loop is demonstrated in the RIIβ crystal structures to be

partially disengaged from the inhibitor site when compared with fully closed crystal structures. This result of increased B-factors for this region in RIIβ compared to RIα is consistent with the glycine rich loop being dynamically flexible in the RIIβ structure whereas it is fully shielded in the RIα complex.

Methods:

HD/MS: Deuterated samples were prepared at 23 (±1) °C by diluting 5 μl of protein solution with 45 μl of deuterated buffer A (50 mM Mops, 50 mM NaCl, 1 mM DTT (pH 7.0), followed by "on-exchange" incubation for varying times (0–10 min) prior to quenching in 0.2% TFA (pH 2.5) at 0 °C. The exchange mixtures for the C-subunit in the presence of Mg^{2+} and ATP included 2 mM $MgCl_2$ and 0.2 mM ATP with buffer A. The exchange mixture for the RIIβ (108–402): C and RIIβ (108–268): C complexes contained 2 mM $MnCl_2$ and 0.2 mM AMP-PNP with buffer A. The quench buffer for free RIIβ (108–268), RIIβ (108–402) and RIIβ (108–402): C complex included 1 mM EDTA with buffer A.

Deuterium exchange at time *t* = 0, was determined by adding the protein solution in H_2O (5 μl) to a mixture of 0.5 ml 0.1% TFA and deuterated buffer A (45 μl). A portion of the quenched reaction (0.1 ml) was mixed with 50 μl of pepsin bead slurry (previously washed two times in 1 ml of cold 0.1% TFA). The mixture was incubated on ice with occasional mixing for 5 min, centrifuged for 15 s at 12,000 g at 4 °C, divided in aliquots, frozen in liquid N_2, and stored at -80 °C until analyzed.

Frozen samples were quickly defrosted to 0 °C, mixed with matrix (5 mg/ml a-cyano-4-hydroxycinnamic acid in 1:1:1 acetonitrile, ethanol, 0.1% TFA, final pH 2.5 at 0 °C), and 1 μl was spotted on a chilled MALDI target. The

target was quickly dried and analyzed on a Voyager DE STR Biospectrometry Workstation (Applied Biosystems Inc., Foster City, CA) as described.

The mass spectrometry data were analyzed using DEX software to remove the natural isotopic abundances for all but one peptide (residues 278–289 of the C-subunit). Centroid determination was calculated automatically for each sample by DEX, and checked manually for verification. The average number of deuterons exchanged and standard deviations reported were determined from at three independent experiments for most peptides. Averages and standard deviations were calculated with measurements from three independent experiments for most peptides. Due to high noise in data sets for certain peptides, fewer measurements were obtained and consequently no standard deviations were calculated.

Chapter 5 in part has been published as it may appear as R-subunit Isoform Specificity in Protein Kinase A: Distinct Features of Protein Interfaces in PKA Types I and II by Amide H/(2)H Exchange Mass Spectrometry. *J Mol Biol.* 374(2):487-99 (2007). Anand GS, Hotchko M, Brown SH, Ten Eyck LF, Komives EA, Taylor SS. The dissertation author was a secondary investigator and author of this paper.

Chapter VI

High Throughput Screening for cAMP Analogue Selectivity

Comparison of the cAMP bound and C-subunit bound conformations of the R-subunits reveal both the dramatic conformational changes of the R-subunit upon C-subunit binding, and the isoform specific differences between the cAMP bound and C-subunit bound conformations of RIα and RIIβ. Analysis of the cAMP bound RIα and RIIβ subunits highlighted differences in the cAMP binding networks in the CNB domains A and B for each R-subunit isoform, as well as in other cAMP binding modules [12, 69, 86]. Holoenzyme structures of RIIα, RIα, and RIIβ demonstrated the significant distortion of the cAMP binding sites that occurs upon C-subunit binding. Building on this foundation we sought to more comprehensively define isoform specific differences in cAMP activation.

Binding affinities of cAMP analogues to isolated regulatory subunits have been well characterized. Comprehensive studies over several decades characterized the binding of cAMP analogues to isolated R-subunits, testing the effects of substitution in the adenine and ribose rings and the phosphate moiety [87-89]. Studies on binding of cAMP analogues to the CNB domains of the R-subunits revealed a wealth of knowledge about the binding sites and site specific preferences for analogue binding, but did not systematically measure activation profiles of the cAMP analogues. Nor were these analogues systematically mapped against the crystal structures of RIα and RIIβ bound to cAMP. Crystal structures of RIα, RIIα, and RIIβ holoenzymes demonstrate large changes in the cAMP binding sites in the C-subunit bound conformation.

A systematic study into activation of PKA holoenzymes by cAMP analogues was initiated to investigate if isoform selectivity in activation of the holoenzymes differs from cAMP analogue binding selectivity of the free R-subunits.

The only known antagonists of PKA are analogues of Rp-cAMPS, where the equatorial oxygen on the phosphate is replaced with sulfur. The Rp compounds bind to the cAMP sites of the R-subunit in holoenzyme, but do not induce the conformational change necessary to displace the C-subunit. Therefore, the Rp cAMPS compounds act as competitive inhibitors of cAMP-induced PKA phosphotransfer activity. The alternate isomer is Sp cAMPS, where a sulphur atom has replaced the axial exocyclic oxygen. The Sp isomers act as agonists for PKA, indicating that equatorial oxygen plays a key role in initiating the conformational change that releases the C-subunit. Studies on the mechanism of this inhibition and the residues that are involved have been performed by NMR analysis [63, 90]. Substitutions of the adenine ring of the Rp-cAMPS molecule may show selectivity of inhibition of holoenzyme that is similar to cAMP substitution selectivity of activation. To determine the trends of substitution selectivity of antagonism by Rp-cAMP, an antagonism screening study of Rp-cAMPS molecules was initiated.

We used a florescence anisotropy (FA) assay that was developed to measure activation and inhibition of PKA in a high throughput (HT) mode [91]. Instead of measuring loss of PKA activity, the assay was developed to measure association and disassociation of the R and C-subunits. It thus

allows us to measure agonists and antagonists that are not simply competitive inhibitors of ATP which almost all other known assays do. The assay is based on Ligand Regulated Competition (LiReC). The readout for this assay is the measurement of an FA signal on a labeled IP20 peptide inhibitor. Peptide bound to the C-subunit has a higher FA signal than free peptide in solution due to the lower tumbling rate in solution. R-subunit competes with the labeled peptide, causing the peptide to disassociate from the complex and the FA decreases. The LiReC assay can be optimized for use in three modes by modifying the level of cAMP in the assay mix; activation mode, inhibition mode, and a screening mode that measures both simultaneously. To measure an agonist, cAMP is absent from the assay mix and disassociation of the complex is measured, as shown in Figure 6.1. In contrast, to measure an antagonist, cAMP is present in the assay mix and association of the complex is measured as a competition between the cAMP and the antagonist. To screen compounds from a random library, enough cAMP is added to give partial activation, and either agonist or antagonist response is measured, shown in Figure 6.1. The LiReC assay was modified here to screen in a dose response format, both for agonists and antagonists in RIα and RIIβ.

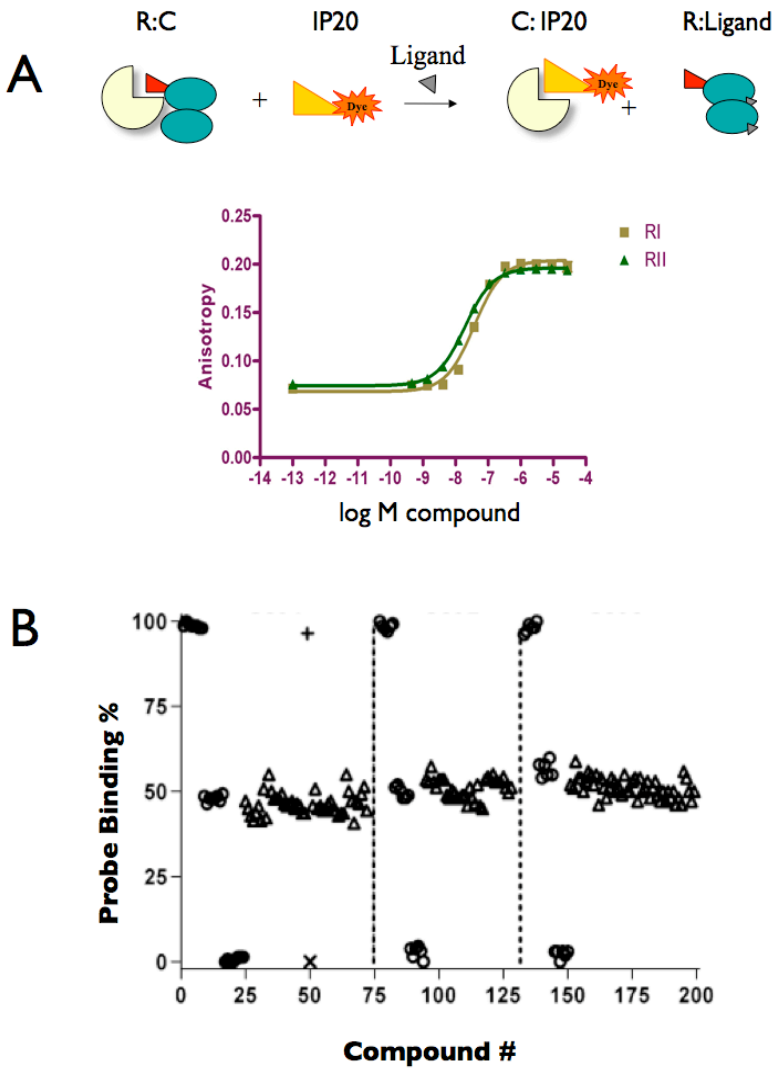

Figure 6.1: LiReC Assay Principal

Panel A shows the principal of LiReC assay in the agonist mode. PKA holoenzyme disassociates when an agonist is added, and labeled IP20 probe can then bind to the catalytic subunit. An example dose-response curve for cAMP disassociation of RIα and RIIβ is shown. Panel B shows the high throughput screening mode of the LiRec Assay. cAMP is added to give a half-maximal FP signal, and antagonists and agonists are measured. Panel B adapted from Saldanha et al.

Results:

Modification of the LiReC Assay for PKA Type II: While the LiReC assay could be used to screen for both activators and inhibitors of PKA RIα holoenzymes, we adapted the assay into two formats here that screen both RIα and RIIβ for dose-dependent activation or inhibition.

The initial challenge was to develop a suitable RIIβ construct that could be used for the LiReC assay. LiReC assay trials with RIIβ (108-402) yielded a poor FA response due to phosphorylation of the IS Ser. The assay was therefore modified by changing Ser 112 of RIIβ to an Ala to prevent this phosphorylation. RIIβ (108-402) S112A was tested for C-subunit inhibition under similar conditions to the LiReC assay. The mutant inhibited the C-subunit similar to the WT RIIβ (108-402) and RIα (91-379). RIα and RIIβ S112A have comparable EC50s for cAMP activation in the LiReC assay of approximately 36 nM and 18 nM, respectively. Both RIα and RIIβ subunits were truncated at the N-terminus to reduce the tendency for degradation and aggregation.

HT screening of commercial cAMP analogues: HT screening of dose-response activation of RIα and RIIβ by cAMP analogues was performed under the optimized assay conditions described. The analogues chosen represented the cAMP derivatives commonly used in cellular based studies.

The four main sites of modification are shown in Figure 6.2. A summary of EC50 values for compounds tested in the LiReC HT dose-response screening is shown in Table 6.1. Compounds have been grouped by substitution type and selectivity. EC50 for cAMP activation of RIα was 30-40 nM and of RIIβ was 15-22 nM under LiReC assay conditions.

Two significant trends in the activation results are the effects of the C8 and N6 substitutions of the cAMP molecule. These substitutions show distinct specificity trends for RI and RII isoforms of PKA. As shown in Figure 6.3, C8 compounds showed a preference for activation of the RI isoform (EC50s were 1.5 - 5 fold lower for RI versus RII). Conversely, N6 compounds prefer the RII isoform, as shown in Figure 6.4 (EC50s were 2-9-fold lower for RII versus RI). This preference held true for all compounds tested over IC50 ranges of 50 nM to 15 μM.

Rp cAMP Antagonists Selectivity: Four Rp cAMPS compounds were tested for their ability to reform a holoenzyme complex of RIIβ and RIα as shown in Fig 6.5. 100 nM cAMP was added to the assay mix to disassociate the holoenzyme complex, and compounds were then titrated into the assay. Both Rp cAMPS and Rp 6-Phe cAMPS have similar IC50 values for RIIβ and RIα. Rp cAMPS's substituted at the C8 position are 20-30 fold better inhibitors for RIα than RIIβ. The trend of C8 substitutions preferring RIα to RIIβ is exactly the same trend as observed for activation by cAMP analogues.

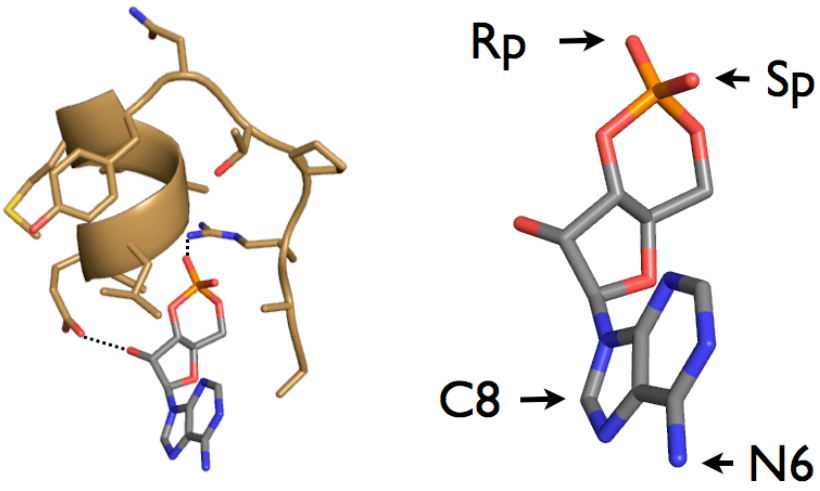

Figure 6.2: Modification Sites of cAMP

Four modification sites of cAMP were screened for selectivity of RIα versus RIIβ. Two modifications of the phosphate moiety were tested: Rp cAMP, substitution of the equatorial phosphorus for oxygen; and Sp cAMP, the substitution of the axial phosphorus for oxygen, shown above. Two modifications of the adenosine ring were tested, modification of the N6 position and modification of the C8 position, as shown above.

Table 6.1: Activation of PKA Isoforms by cAMP Analogues

Activation of PKA type I and type II PKA were measured using the LiReC assay. EC50 results are grouped according to substitution type and selectivity.

Compound	RIα EC50(nM)	RIIβ EC50(nM)	$\frac{RII\beta}{RI\alpha}$ selectivity
cAMP	36	18	2.0
cGMP	15000	5080	3.0
8-Cl cAMP	58	275	0.2
8-CPT cAMP	33	149	0.2
8-PIP cAMP	1020	3950	0.3
8-HA cAMP	358	1150	0.3
8-Br cAMP	81	184	0.4
8-MA cAMP	102	223	0.5
8-AHA cAMP	116	197	0.6
Sp cAMP	1590	2270	0.7
HE33	414	45	9.2
6-MBC cAMP	289	59	4.9
6-Bnz cAMP	170	35	4.9
6-Phe cAMP	92	20	4.6
Sp-5, 6-DCl BIMPS	344	83	4.1
6-MB cAMP	140	39	3.6
Sp-8-CPT cAMP	342	96	3.6
Sp-8-Br cAMP	1355	435	3.1
5, 6 DCl BIMPS	270	129	2.1
Sp-8-PIP cAMP	5048	2959	1.7
2-OMe cAMP	5666	n.d.	n.d.
2-AEA cAMP	8739	2652	3.3
2-Cl cAMP	42	45	0.9

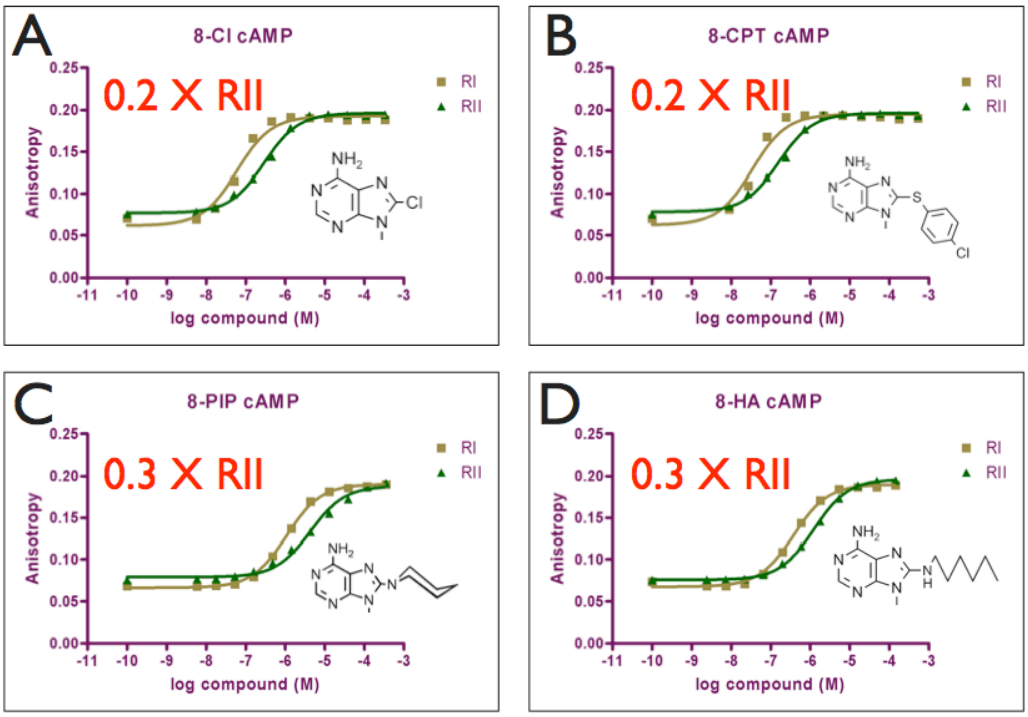

E

	Compound	RIα EC50(nM)	RIIβ EC50(nM)	RIIβ / RIα selectivity
A	8-Cl cAMP	58	275	0.20
B	8-CPT cAMP	33	149	0.20
C	8-PIP cAMP	1020	3950	0.30
D	8-HA cAMP	358	1150	0.30

Figure 6.3: C8 Substitutions Confer Type I PKA Selectivity

Substitution of the C-8 position of cAMP shows RIα selectivity for activation as measured by the EC50 in the LiReC assay. RIα activity is shown in brown, RIIβ in dark green. Panel A shows 8-Chloro-cAMP. Panel B shows 8-(4-Chlorophenylthio)-cAMP. Panel C shows 8-Piperidino-cAMP. Panel D shows 8-Hexylamino–cAMP. Panel E summarizes EC50 results and selectivity.

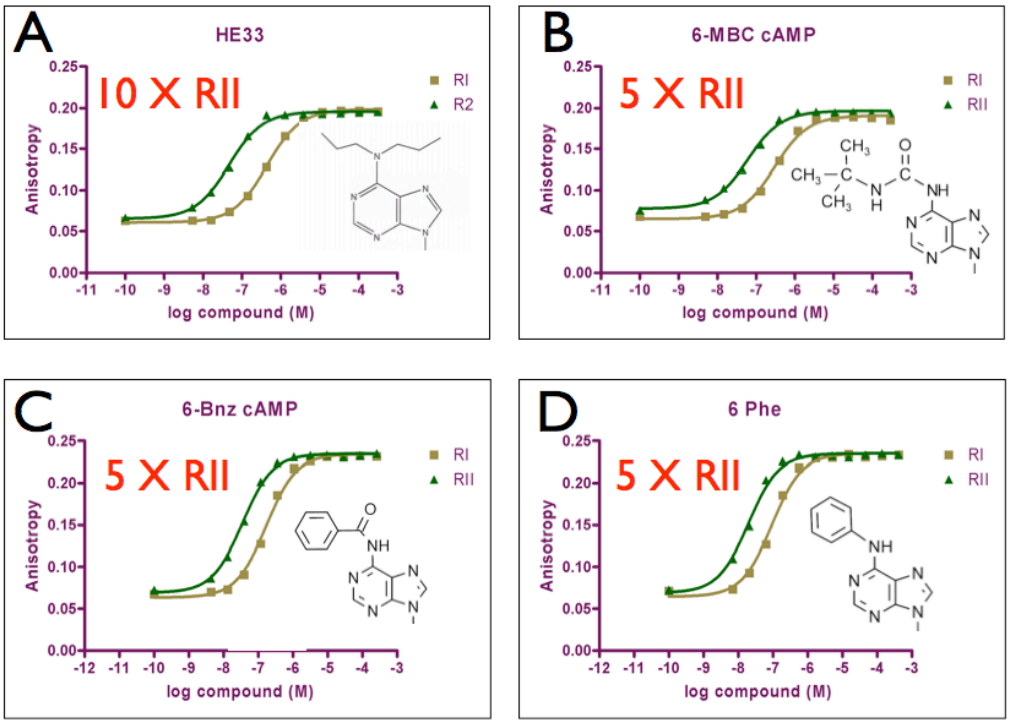

E

	Compound	RIα EC50(nM)	RIIβ EC50(nM)	RIIβ / RIα selectivity
A	HE33	414	45	9.2
B	6-MBC cAMP	289	59	4.9
C	6-Bnz cAMP	170	35	4.9
D	6-Phe cAMP	92	20	4.6

Figure 6.4: N6 Substitutions Confer Type II PKA Selectivity

Substitution of the N-6 position of cAMP shows RIIβ selectivity for activation as measured by the EC50 in the LiReC assay. RIα activity is shown in brown, RIIβ in dark green. Panel A shows HE33. Panel B shows 6-Mono-t butylcarbamoyl-cAMP. Panel C shows 6-Benzoyl-cAMP. Panel D shows 6-Phenyl-cAMP. Panel E summarizes EC50 results and selectivity.

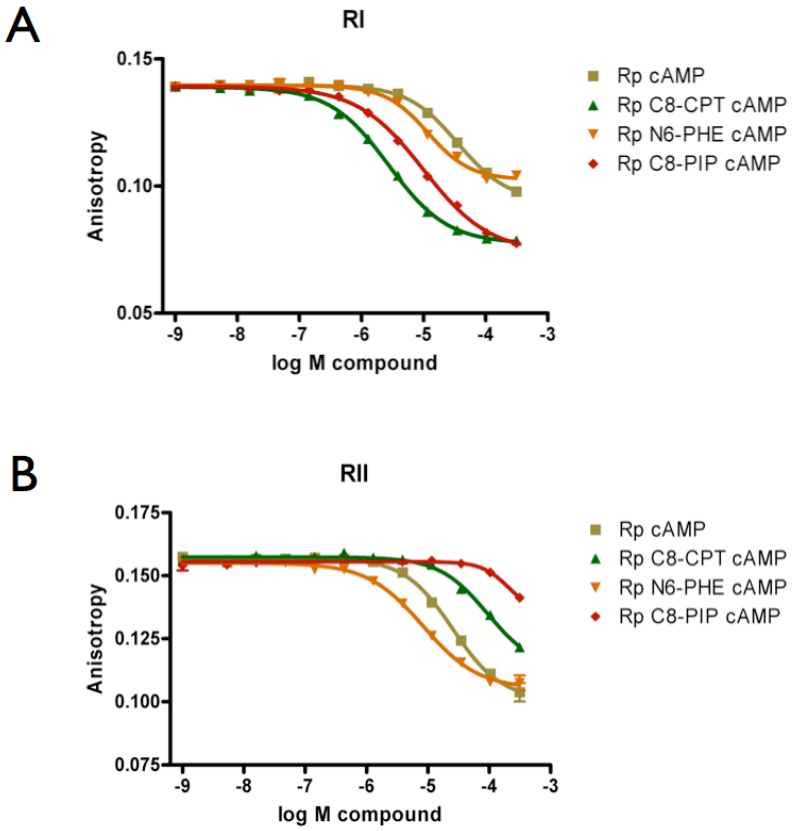

C

Compound	RIα IC50(uM)	RIIβ IC50(uM)	RIIβ / RIα selectivity
Rp-cAMP	36	25	1.44
Rp-6-Phe cAMPS	11	8.3	1.33
Rp-8-CPT cAMPS	3	95	0.03
Rp-8-PIP cAMPS	10	214	0.05

Figure 6.5: Inhibition of RIα and RIIβ by Rp-cAMPS Analogues

Inhibition of RIα and RIIβ by four analogues of Rp-CAMPS was measured using the LiReC assay in the antagonist mode. Panel A shows inhibition of RIα, Panel B shown inhibition of RIIβ. Panel C is a summary of the four compounds tested. C8 compounds are better antagonists for RIα than RIIβ.

Structure Solution of RIIβ (108-402) bound to HE33: The most selective compound from the LiReC assay is HE33, which is not commercially available. HE33 was developed as an analogue that may be clinically effective against Lupus. Initially found in an immunosuppressant screen, HE33 has been tested in Lupus model mice and was found to significantly increase the lifespan of mutant mice. (H. Cottam, personal communication) This compound, an N6 di-propyl substituted cAMP, was found to activate RIIβ with an EC50 similar to cAMP. In contrast, HE33 activated RIα with an EC50 5-fold higher than cAMP. Based on these results, HE33 was thus co-crystallized with RIIβ (108-402). The crystal structure of RIIβ (108-402) in complex with 2 molecules of HE33 was solved to 2.8 Å resolution. RIIβ (108-402): HE33 was refined to an R_{free} value of approximately 30%.

Discussion:

A major structural difference between RIα and RIIβ when cAMP is bound is the different interface between CNB domains A and B [48]. This shift in the relative orientations of the CNB domains changes the hydrophobic capping mechanism for cAMP-bound to CNB domain A, shown in Figure 6.6. Each CNB domain has a hydrophobic residue that caps the cAMP site and is critical for high affinity cAMP binding [69]. In RIIβ the capping residue for domain A is Arg 381 which is located in the αB helix of domain B. In contrast, in RIα the capping residue for domain A is Trp 260 which is located in the αA helix of domain B. In both cases, RIα and RIIβ, the capping mechanism for domain B is in the αC helix of domain B. The domain A capping mechanism is thus a major difference between RIα and RIIβ and is a critical feature that creates a very different interface between the A and B domains.

While each cap provides the same hydrophobic shield for cAMP and is in the same relative location in the cAMP-bound conformations, the position of the B domain relative to the A domain is quite different in the two cAMP-bound conformations. As discussed in Chapter 5, the capping residue for RIIβ CNB domain A is also a major interaction site for docking to the C-subunit. In contrast, the capping residue for RIα CNB domain A, Trp 260, only plays a minor role in the docking surface for the C-subunit.

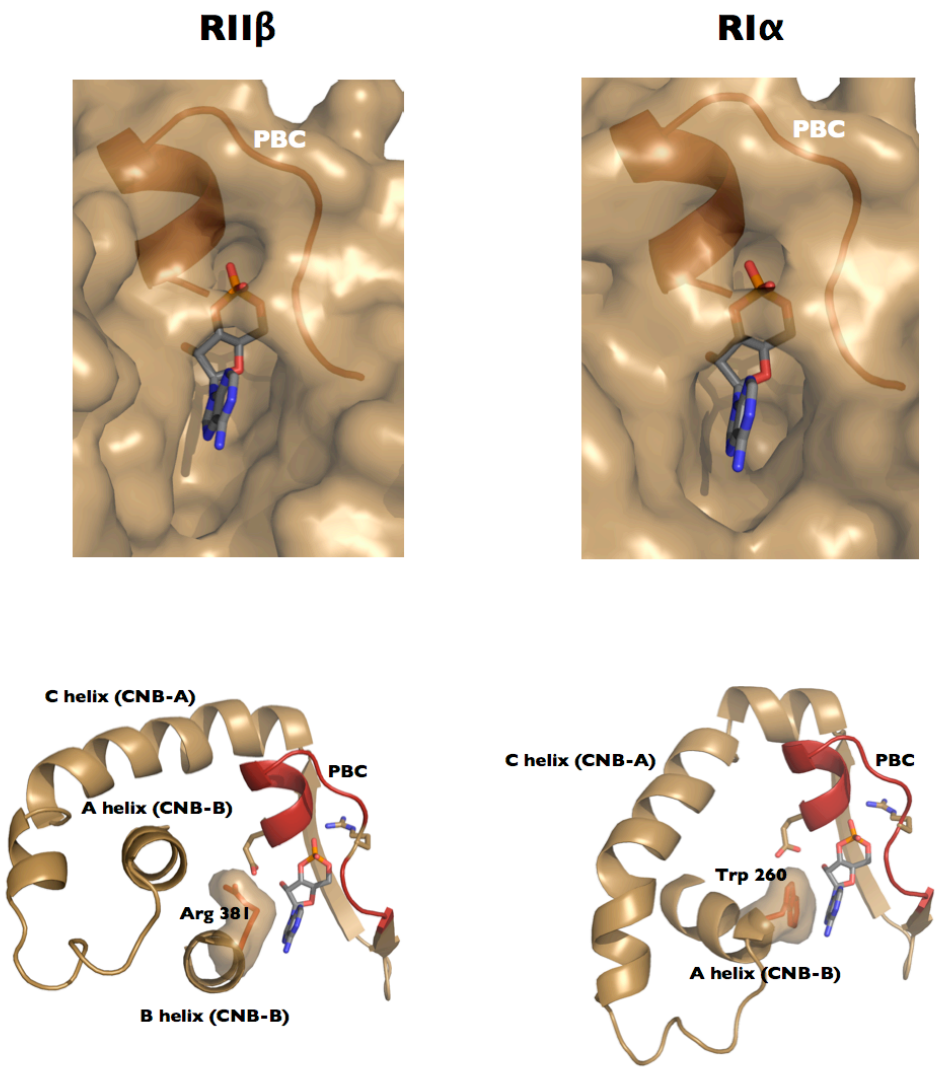

Figure 6.6: cAMP binding sites of Domain A in RIIβ and RIα

Shown in the top panel is a surface representation of the CNB-A cAMP pocket of RIα and RIIβ. The shape of the pocket differs between isoforms. Shown in the lower panel is the PBC and cAMP capping mechanism of CNB-A for RIIβ and RIα. The C-helix conformation and the relative orientation of the two cAMP binding domains is significantly different between isoforms.

Additionally, the cAMP bound structures of RIα and RIIβ demonstrate that the cAMP pocket differs between isoform. There is a significant pocket near the N6 position in the cAMP site of RIIβ that is not present in RIα, shown in Figure 6.6. Even though the conformations of the R-subunit in the two holoenzymes are similar for RIα and RIIα, the mechanism of capping the cAMP and the docking site for cAMP differ between isoforms.

The difference between the CNB-A cAMP binding sites of RIα and RIIβ has significant implications due to the importance of the A domain for holoenzyme activation. In both isoforms, cAMP must bind to the A site to induce activation. Mutations of the PBC binding sites have defined the stepwise binding of cAMP to RIα. cAMP must first bind to the B site of RIα before it can access the A site and induce activation [19]. In contrast, RIIβ holoenzyme does not require a stepwise binding of cAMP. RIIβ can be activated by binding of cAMP to only the A site when the B site is deficient in cAMP affinity [22].

The most significant result of screening cAMP analogues for selective PKA activation is the importance of the CNB domain A. In the LiReC activation assay, the N6 substituted compounds were selective for RIIβ, shown in Figure 6.3. C8 substituted compounds were selective for RIα, shown in Figure 6.4. ^{3}H-cAMP assays showed the exact same trends in cAMP analogue binding to the CNB domain A of RI and RII. The best binders for RI CNB domain A are C8 substituted compounds, while the best binders for RII

CNB domain A are N6 substituted compounds [92]. The trends of activation that are observed in the LiReC assay directly correlate with trends of cAMP binding to CNB domain A of the free R-subunits. The activation trends observed in the LiReC assay confirm the importance of the A domain for activation of holoenzyme by cAMP.

Rp cAMPS Antagonism: Similar trends of adenine ring substitution selectivity from the activation results were observed in Rp cAMP inhibition. 6-Phe Rp cAMPS and Rp cAMPS inhibited both RII and RI holoenzymes with similar IC50s. C8 substituted cAMPS analogues, however, are poor antagonists for RII.

cAMP binding to RIα causes a change in the off-rate of the holoenzyme complex. When cAMP is bound, the RIα-C complex disassociates approximately 150-fold faster while the on-rate remains the same. This leads to a 150-fold increase in Kd for the holoenzyme complex when cAMP is bound. In contrast, RIα bound to Rp cAMPS has a 5- fold slower disassociation rate of the complex when compared to RIα in the absence of cAMP (D. Johnson, personal communication). Therefore, Rp cAMPS is in fact a “super-antagonist”, not only acting as a competitive inhibitor for cAMP, but actually increasing the affinity of the R-subunit for the C-subunit. The Rp cAMPS is thus stabilizing the holoenzyme complex beyond when no cAMP is bound.

The critical site for inhibition of RIα by Rp-cAMPS has been shown to be CNB-domain A by mutation analysis. Arg 209 is critical for cAMP binding and is a major component of the cAMP activation mechanism as discussed in Chapter 3. The Rp sulfur substitution of the cAMPS molecule is in direct contact with Arg 209 in the PBC when bound to CNB domain A of RIα [61]. Binding of Rp cAMPS to PBC A cannot induce the conformational change necessary to disassociate the R-C holoenzyme. When this Arg is mutated to an Lys, Rp cAMPS acts as an activator [90]. In contrast, in the equivalent mutation of the B domain, Rp cAMP cannot activate RIα holoenzyme (C. Cheng, unpublished results). This confirms the importance of the A domain for activation of the holoenzyme.

Although the mechanism of antagonism is not entirely clear, it is likely to involve the electrostatic switch of Arg 209 and Asp 170, which in turn communicates ligand binding to the rest of the R-subunit and disassociates the complex. Rp cAMPS binding may stabilize the holoenzyme conformation of the PBC where Asp 170 is flipped away from Arg 209 as seen in the holoenzyme complexes.

Activation and antagonism assay trends can be extrapolated to design future antagonists. cAMP analogue screening can be used to find the isoform selectivity features in the adenine ring. These selectivity features can then be added to Rp cAMPS to generate selective antagonists. This study demonstrates that using selectivity features generated in the LiReC activation assay is a useful technique to generate isoform selective PKA inhibitors.

Crystal Structure of RIIβ (108-402) bound to HE33: The crystal structure of RIIβ (108-402) bound to two molecules of the selective analogue HE33 provides a possible mechanism for why RII subunits prefer N6 substituted analogues. The N6 position lies directly adjacent to the solvent exposed surface of the αB helix in domain B that is positioned by the capping of Arg 381 to the adenine ring. CNB domain A of RIIβ bound to HE33 is shown in Figure 6.7. Hydrophobic interactions between the di-propyl groups of HE33 and the αB helix of CNB domain B may maintain the binding of HE33 to RIIβ at levels similar to cAMP. These hydrophobic interactions are primarily with the aliphatic regions of the sidechains of Gln 377, Glu 380, and with the Arg 381 capping residue.

In contrast, in RIα CNB domain A, the equivalent residues are not available for hydrophobic interactions. The capping residue is located on the αA helix, and approaches cAMP from a different angle. In the RIα cAMP bound structure there are hydrophilic residues that are located in the region that the HE33 di-propyl groups would be located. This loss of hydrophobic interactions and increase in hydrophilic blocking in the αA helix of RIα may explain the increased EC50 for activation of RIα by HE33.

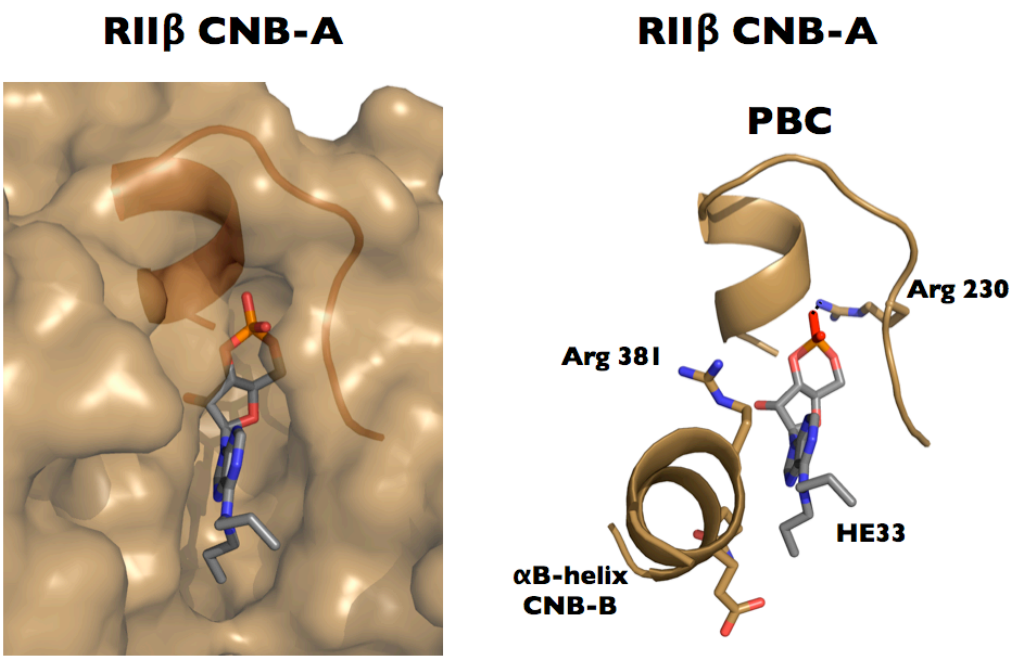

Figure 6.7: HE33 Docking Mode to A domain of RIIβ (108-402)

The cAMP analogue HE33 was crystallized with RIIβ (108-402). Shown on the left is a surface rendering of the cAMP binding site highlighting the pocket utilized by HE33. This equivalent pocket is not present in RIα. On the right a ribbon representation of the same site is shown highlighting the interaction between HE33 and αB helix of CNB-B. The CNB-A capping residue, Arg 381, is in close proximity to the HE33 alkyl groups.

As discussed previously, the cAMP binding site of RIIβ bound to cAMP has a pocket near the N6 position of cAMP. Shown in Figure 6.7, the di-alkyl substitutions of the cAMP analogue HE33 utilize this extra pocket in the N6 region.

The crystal structure of HE33 bound to RIIβ allows development of analogues with higher selectivity for RIIβ. Modification of the N6 position with larger hydrophobic groups is currently ongoing. cAMP analogues that can utilize the hydrophilic sidechains of the αB helix to increase binding to RIIβ also may show an increase in selectivity. Finally, the Rp cAMPS versions of HE33 and associated isomers are currently under development as selective antagonists for RIIβ holoenzymes.

Methods:

LiReC Assay: The Ligand Regulated Competition assay (LiReC) is based on the competition for the PKA C-subunit by multiple inhibitors [91]. The core component of the assay is a fluorescent labeled IP20 PKA inhibitor peptide probe. Fluorescence anisotropy (FA) of the label is used as the readout for the assay. In an FA assay, polarized light is used to excite the fluorophore on the probe; the extent to which the fluorophore retains the polarization during emission reflects the rotation rate of the probe. The molecular weight of the molecule attached to the probe affects the rotation rate of the dye molecule, and therefore changes the ratio of perpendicularly to parallel polarization of emissions. Measurement of the ratio of emission polarization generates an FA signal (Equation 1). Fluorescence polarization (FP) is a second way to describe the same polarization readouts and the equation is shown below (equation 2).

(1) FA = $r = \frac{I_{II} - I_{\perp}}{I_{II} + 2I_{\perp}}$ (2) FP = $P = \frac{I_{II} - I_{\perp}}{I_{II} + I_{\perp}}$

Theoretical ranges for FA signal varies a low of -0.2 to 0.4, however the practical values obtained in biological experiment vary from 0.01 for a free probe in solution, to ~0.3 for a probe bound to a large protein. The binding of the labeled probe to the C-subunit causes a large change in florescence

anisotropy due to the increase in apparent molecular weight of the probe. Unbound IP20 probe has an approximate *r* value of 0.08 while probe bound to the C-subunit has an approximate *r* value of 0.25.

When the IP20 probe is bound to the C-subunit a high FA signal is measured. When R-subunits compete with the probe for the C-subunit, the probe is displaced and the FA signal drops. The range of FA 0.1-0.25 over the course of the LiReC assay is adequate to generate accurate activation EC50 results. In the LiReC assay mode for activation, a preformed holoenzyme complex is formed and IP20 probe is added. Upon titrating in a ligand for the R-subunit, the R-C complex disassociates, and the IP20 binds to the C-subunit. The change in FA of the probe is measured and the activation EC50 is generated.

Modification of LiReC Assay into RI vs. RII selectivity screen: The LiReC assay was originally developed as an agonist and antagonist screen for RIα. This assay required modifications in order to screen RI versus RII PKA isoforms. The assay was originally designed and tested on the RIα (91-376) R-subunit using Fl-IP20. The dye was modified from Flourecine to a Texas Red to the decrease the affinity of the probe. Verification of assay effectiveness with RIIβ and the Texas Red (TR) dye was required. Truncation of the R-subunits N-terminal prior to the IS was required due the susceptibility of this region to aggregation and proteolytic cleavage.

TR-IP20 dye concentration was fixed at 3 nM and serial dilutions of C-subunit determined the affinity for the labeled probe. Assay mixtures contained 50 mM HEPES, 0.005% Triton X100, 2 mM ATP, 10 mM $MgCl_2$, 2 mM DTT, and 6.25% DMSO. The affinity of the TR-IP20 was found to be 5.5 nM under these assay conditions. In following LiReC compound screening assays a concentration of 6 nM PKA and 3 nM TR-IP20 was used.

Results of cAMP activation using RIα (91-379) with the TR-IP20 are consistent with the LiReC assay using FI-IP20, activation occurs at an EC50 of 53 nM. WT RIIβ does not behave well in the FA assay. The FA reading for the inhibited state is much higher for RIIβ, indicating that the RIIβ (108-402) cannot compete with IP20 for the C-subunit. Phosphorylation of the S112 of RIIβ is the most likely explanation for this affect. A mutation of the IS phosphorylation site, S112A, was made and tested in the LiReC assay. Site directed mutagenesis of the RIIβ S112 IS phosphorylation site to an alanine was performed in RIIβ (108-402). This protein was purified as described previously, and pure pools of protein were stored in 40% glycerol at -20 °C for future assays.

RIIβ (108-402) S112A performed very well under the assay conditions. The upper and lower FA values were similar between RIα and RIIβ S112A, and the EC50 values stayed consistent during the time course of the assay. In order to test whether the RIIβ mutation has affected the inhibition characteristics of the RIIβ, a coupled inhibition assay was performed. RIα,

RIIβ, and RIIβ S112A were all tested in a 96 well format coupled assay [93] for inhibition of WT C-subunit. All three isoforms of PKA have similar inhibition values under these assay conditions. Coupled assays were performed in a 96 well format coupled assay [93]. 5 nM PKA was used for all coupled assays and assay mix was incubated with the holoenzyme for ~20 min prior to cAMP addition. Plates were incubated for 20 min following cAMP addition and the reaction was initiated by addition of 5μL of kemptide using a 12-channel pipette into 24 wells. Reduction of signal was 340 nM was measured and the slope quantified as activity. RIα and RIIβ S112A have similar EC50 values of 57 nM and 60 nM respectively in the coupled assay. WT RIIβ has a much lower EC_{50} value of 19 nM. Results from the coupled assay are consistent with what was observed in the FA assay.

High Throughput Screening: All compounds were dissolved in DMSO and were diluted using 3 fold serial dilutions prior to assay setup. Compound stocks were made in 11 points from 5 mM – 85 nM, corresponding to final concentrations of 294 μM – 5 nM. cAMP stocks for all assays were made in H_2O at 9 mM concentration, frozen for storage, and diluted to 450 μM prior to serial dilution.

Assays were performed in 384 well Nunc flat black bottom plates. Assay mixture S1 composed of all buffer components plus C-subunit was made as a stock for all assays performed on the experimental day. S1 was split into two volumes and R-subunits were added, followed by a 5-minute

incubation at 4 °C. Then the TR-IP20 was added to the mixture and the mixture again incubated at 4 °C for 5 minutes. A multichannel pipette was used to add 75μL of S1 to the wells of the 384 well plate, followed by addition of the compounds. Also, 5μL of H2O was added to all compound wells, and 5μL of DMSO was added to the cAMP wells to keep DMSO concentration consistent across the plate.

Fluorescence readings were taken on a GenesisPro (Tecan, NC) plate reader at 570/20 nM excitation and 630/20 nM emission using the stock 510 nM dichromic mirror. Measurements were taken periodically over approximately 2 hours following addition of compound to the mixtures. Automatic gain optimization was used for each reading and each well was read 15 times per measurement set. A G factor of 1.0011 was used for the TR fluorophore. The raw polarization data was outputted into Excel and Graph Pad Prism was used to convert mP to FA and for data analysis. For screening results all data was fitted to a sigmoidal dose response curve with a fixed Hill slope of 1.0. EC50 values were calculated using Graph Pad sigmoidal data fitting algorithms.

To screen for isoform selectivity of Rp cAMPS molecules, Rp 6-Phe cAMPS, Rp 8-PIP cAMPS and Rp 8-CPT cAMPS were tested. These compounds were chosen due to the commercial availability and the selectivity of the cAMP equivalent selectivity of activation.

Setup of the Rp-cAMPS antagonism assay included the identical buffer and protein components, plus cAMP (Sigma). Concentration of cAMP was

chosen at a level that gave approximately 70% maximal activation of both isoform. cAMP levels of levels of 100 nM were found to give the most consistent cAMPS antagonism results. Rp compounds were added to the plate as described above following the addition of the assay mix.

Crystallization of RIIβ (108-402) and HE33: Selectivity of HE33 for RIIβ motivated attempts to crystallize RIIβ with the HE33 compound. Crystallization of RIIβ bound to cAMP used RIIβ (112-416), selected through analysis of degradation of longer RIIβ constructs. Even though the RIIβ:cAMP construct started at residue 112, the first ordered reside in the model was 130, indicating that the N-terminus is disordered and not playing a part in the crystallization.

The RIIβ (108-402) construct was selected for crystallization using the HE33 for two reasons: the improved stability of the (108-402) by removal of the C-terminal residues, and to allow simultaneous production of samples for use in RIIβ:C crystallization. Initial protein samples were eluted from a Superdex 75 (GE bioscience) column in 50 mM MES (Fluka), 200 mM NaCl (Fluka) 2 mM EDTA/EGTA (Fisher) and 5 mM DTT. HE33 was added to the protein sample, and after an overnight incubation the compound was removed by spin dialysis. This technique was adapted from crystallization of RIIβ [60].

All crystallization trials were set-up using the Oryx crystallization robot (Douglas Instruments) in modified microbatch mode. Commercial HT 96 well crystallization screens Index (Hampton Research), PACT (Molecular Dimensions) and JCSG+ (Molecular Dimensions) were used for crystallization

trials. Drop size of 0.4uL at 50% protein were used, and drops were covered with Al's Oil (Hampton Research) directly following mixing of reagents.

Initial hits were optimized both by hand and using the Oryx robot. The final crystallization condition included 20% PEG 4000, 80 mM Bis Tris 6.0, and 50 mM $MgCl_2$. Crystals were cryo frozen in the reservoir buffer with 10% glycerol.

Data Collection and Processing: Initial crystal screening was performed at 100 K at the UCSD chemistry home source. Images were collected for 15 minutes per image on a Mar 345 image plate detector. All crystals were screened on the home source before shipping to the Advanced Light Sources (ALS) for data collection. Two data sets were collected at the ALS at Lawrence Livermore National Lab beamline 8.2.2. Data collected at 2.8 Å was chosen for processing and analysis. Initial phases were obtained used the cAMP bound RIIβ subunit (PDB code 1CX4) as a search model using the CCP4 package program PHASER. Initial density maps were obtained and the model of RIIβ-cAMP was fit into the density for RIIβ-HE33. Initial refinement of the RIIβ-cAMP model into the RIIβ-HE33 density map was performed using the REFMAC5 program in CCP4. Current refinements in REFMAC5 yield R-free of ~30%.

Chapter 6 is in preparation for publication as it may appear as Protein Kinase A Isozyme Assays Reveal True Selectivity of Commonly Used cAMP Derivatives. Brown SHJ, Saldanha AS, Cottam H, Taylor SS. The dissertation author was the primary investigator and author of this paper.

Chapter VII

Conclusions

Signal transduction through the PKA pathway is regulated by the small molecule second messenger cAMP. The binding of cAMP to the R-subunit of PKA induces a massive conformational change of the R-subunit that in turn releases the PKA C-subunit from inhibition. PKA R-subunits act as both regulators and as scaffolds for the PKA C-subunit by inhibiting C-subunit activity while simultaneously anchoring the PKA complex to specific locations in the cell.

Determination of the functional and structural differences between PKA R-subunit isoforms was a major goal of this work. Crystal structures of the PKA RIIβ isoform bound to the C-subunit revealed for the first time the conserved and isoform specific features of the PKA holoenzymes. While many studies have focused on the roles of RIα and RIIα, relatively little is known about RIIβ. Surprising phenotypes of RIIβ knockout in mice indicate unique roles for RIIβ, and detailed structural information about each isoform will help elucidate the details of isoform diversity. Comparison of the isoform specific features of cAMP bound and C-subunit bound forms of the R-subunits allowed interpretation of the different roles of each subdomain of the R-subunit across PKA isoforms.

Measurements of the affinity between RIIβ and the C-subunit by SPR highlight the importance of two secondary binding domains of RIIβ in achieving high affinity binding to the C-subunit. The CNB domain B and the linker region N-terminal to the inhibitor site of the RIIβ subunit contribute to high affinity

binding of RIIβ to the C-subunit. The linker region of RIIβ near the inhibitor site was also shown previously to contain a flanking binding site for calcineurin, a partner phosphotase that is highly specific for RII subunits, shown in Figure 7.1. Future studies systematically extending the RIIβ linker and testing affinity for both the C-subunit and calcineurin will provide insight in the importance of the protein complex of each part of the linker. Details of the interaction between the RIIβ substrate, kinase, and phosphotase are currently unknown, and future structural studies of RIIβ holoenzyme will focus on solving this complex. The RIIβ linker region is the most isoform diverse region of the R-subunit, and structural knowledge of this linker and its binding partners will provide significant information about differences between PKA isoforms.

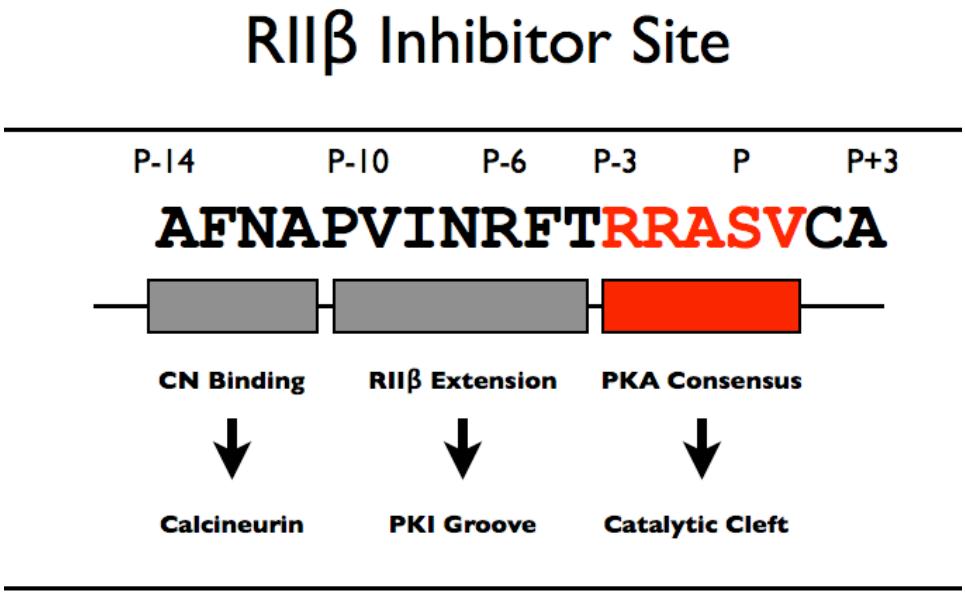

Figure 7.1: RIIβ Linker Interaction Sites

The linker region of RIIβ interacts with both PKA and Calcineurin. The interaction sites are shown above, including the PKA consensus site highlighted in red.

The non-hydrolyzable ATP analogue AMPPNP increased the affinity of RIIβ for the C-subunit and allowed us to confirm the importance of the additional residues on the RIIβ linker. This effect was especially pronounced for the single RIIβ CNB domain A. The use of AMPPNP allowed us to trap a substrate that on its own binds poorly, in this case the RIIβ A domain, in a transition-state complex. This is a trapping technique that may prove to be useful for other kinase substrates. Many kinase substrates have low binding affinity, especially after phosphorylation, and the use of AMPPNP to trap these substrates in a high affinity transition state complex would be an extremely valuable tool for structural studies of substrates of PKA and other kinases. Our work with RIIβ provides a template for achieving this long sought goal.

Two independent crystal structures of RIIβ CNB domain A constructs bound to the C-subunit confirm the molecular basis for the biochemical results. These structures reveal both the conserved and isoform specific structural features of PKA R-subunits and holoenzymes. The overall inhibition mechanism and general holoenzyme structures are conserved features across PKA isoforms. In contrast, the overall cAMP bound R-subunit conformations, the roles of specific residues in the PBC, and the importance of the region N-terminal to the inhibitor site are all isoform specific features of PKA R-subunits.

The RIIβ A domain holoenzyme structures are an important step in the goal of obtaining structural information about the full-length tetrameric PKA holoenzymes. The information obtained about the N-terminal linker of RIIβ highlights the importance of the previously ignored regions of the PKA R-

subunits. These flexible linker regions have often been regarded as disordered in the past. The (102-265) RIIβ holoenzyme structure presented here shows that the region up to the P-10 site is ordered, important for R-C affinity, and is a source of isoform diversity. In the future, extension of structural knowledge of this linker will provide insight into the global conformation of the PKA holoenzymes, reveal additional binding sites on the C-subunit, and allow identification of additional binding partners to this linker region.

The use of the solution based technique small angle x-ray scattering (SAXS) and allowed us obtain knowledge about the RIIβ holoenzyme that has not yet been observed in crystal structures. SAXS analysis demonstrated the role of the linker regions of the RIIβ subunit in the overall shape of the enzymes and the importance of this linker region for the compact nature of RIIβ holoenzyme. These results again reinforce that the linker region is important for PKA structure and function. Future SAXS studies will focus on the effects of phosphorylation and cAMP activation on the global shape of PKA holoenzymes.

A second solution based technique, peptide array screening, focused on the interactions between RIIβ subunit and the isoform specific targeting protein DAKAP2 which brings PKA to scaffolding proteins. Single residue mutations in the DAKAP2 PKA binding peptide that distinguish between RIIβ and RIIα have been identified in this study. Future studies expanding the knowledge of isoform specificity in AKAP interactions will clarify the role of the

different isoforms in the cell. This is of particular importance for the RII isoforms because most past studies have focused on RIIα and have not investigated the interactions between RIIβ and the AKAPs.

Hydrogen deuterium exchange (HDMS) experiments complement the crystallography and affinity data obtained for RIIβ. HDMS demonstrated a priming mechanism of the αH-αI loop region of the C-subunit after RIIβ binding. Changes in solvent accessibility of the surface of the C-subunit after RIIβ binding demonstrated an isoform specific allosteric communication mechanism across the C-subunit. Future HDMS studies with the PKA system will involve extensions of the RIIβ constructs to include the N-terminal linker region and continue investigation into the role of RIIβ binding and allosteric communication in the C-subunit.

The development of an isoform specific PKA activation assay to allow us to perform high throughput screening of small molecule kinase activators. Screening of commercial cAMP analogues against RIα and RIIβ identified two isoform specific trends of activation. Substitution of the C8 position of the cAMP molecule increased the selectivity of cAMP analogues for activation of RIα holoenzyme. Conversely, substitution of the N6 position of the cAMP molecule increased selectivity of the analogues for activation of RIIβ holoenzyme. These selectivity results demonstrate the importance of distinguishing between closely related isoforms and their differences in interaction with small molecules. The most selective analogue tested in the

activation screen was the cAMP analogue HE33. This compound has a clinical immunosuppressant affects on Lupus symptoms in disease model mice, and investigation is ongoing into the link between Lupus and PKA isoform selectivity found with this compound.

Future development of isoform specific analogues will focus on three techniques; crystallization of selective analogues with R-subunits, chemical synthesis of new compounds based on structural information, and development of screening techniques to include all four PKA isoforms. Additionally, currently ongoing development of a cell-based assay will allow the confirmation of analogue isoform selectivity in an in-vivo system. As discussed in the introduction, knockouts of RIIβ generate unique phenotypes related to expression RIIβ in adipose and brain tissues. Development of cAMP analogues to probe these tissue specific effects of RIIβ will be valuable to understand the importance of each isoform of PKA.

In conclusion, this dissertation has demonstrated the importance of isoform diversity in the PKA family. PKA isoforms are not functionally redundant, and although they are highly similar in both sequence and overall structures, isoform diversity is important for proper regulation and localization of PKA function. It has been demonstrated here that while the overall structures of PKA holoenzymes are similar, the details of both C-subunit inhibition and cAMP induced activation have functional isoform diversity in the PKA kinase family.

References

1. Manning, G., Whyte, D., Martinez, R., Hunter, T. & Sudarsanam, S. The protein kinase complement of the human genome. Science 298, 1912-34. (2002).

2. Manning, G., Plowman, G. D., Hunter, T. & Sudarsanam, S. Evolution of protein kinase signaling from yeast to man. Trends Biochem. Sci. 27, 514-520 (2002).

3. Knighton, D. R. et al. Crystal structure of the catalytic subunit of cyclic adenosine monophosphate-dependent protein kinase. Science 253, 407-14 (1991).

4. Banky, P. et al. Isoform-specific Differences Between the Type Ia and IIa Cyclic AMP-dependent Protein Kinase Anchoring Domains Revealed by Solution NMR. J. Biol. Chem. 275, 35146-35152 (2000).

5. Kinderman, F. S. et al. A dynamic mechanism for AKAP binding to RII isoforms of cAMP-dependent protein kinase. Mol Cell 24, 397-408 (2006).

6. Newlon, M. G. et al. The Molecular Basis for Protein Kinase A Anchoring Revealed by Solution NMR. Nat. Struct. Bio. 6, 222-7 (1999).

7. Michel, J. J. & Scott, J. D. AKAP mediated signal transduction. Annu Rev Pharmacol Toxicol 42, 235-57 (2002).

8. Dodge-Kafka, K. L., Langeberg, L. & Scott, J. D. Compartmentation of cyclic nucleotide signaling in the heart: the role of A-kinase anchoring proteins. Circ Res 98, 993-1001 (2006).

9. Li, F. et al. Consequences of cAMP and catalytic-subunit binding on the flexibility of the A-kinase regulatory subunit. Biochemistry 39, 15626-32 (2000).

10. Zawadzki, K. M., Pan, C. P., Barkley, M. D., Johnson, D. & Taylor, S. S. Endogenous tryptophan residues of cAPK regulatory subunit type IIbeta reveal local variations in environments and dynamics. Proteins 51, 552-61 (2003).

11. Diller, T. C., Madhusudan, Xuong, N. H. & Taylor, S. S. Molecular basis for regulatory subunit diversity in cAMP-dependent protein kinase: crystal structure of the type II beta regulatory subunit. Structure 9, 73-82 (2001).

12. Berman, H. M. et al. The cAMP binding domain: an ancient signaling module. Proc Natl Acad Sci U S A 102, 45-50 (2005).

13. Kim, C., Xuong, N. H. & Taylor, S. S. Crystal structure of a complex between the catalytic and regulatory (RIalpha) subunits of PKA. Science 307, 690-6 (2005).

14. Kim, C., Cheng, C. Y., Saldanha, S. A. & Taylor, S. S. PKA-I holoenzyme structure reveals a mechanism for cAMP-dependent activation. Cell 130, 1032-43 (2007).

15. Wu, J., Brown, S. H., von Daake, S. & Taylor, S. S. PKA type IIalpha holoenzyme reveals a combinatorial strategy for isoform diversity. Science 318, 274-9 (2007).

16. Hofmann, F., Beavo, J. A., Bechtel, P. J. & Krebs, E. G. Comparison of adenosine 3':5'-monophosphate-dependent protein kinases from rabbit skeletal and bovine heart muscle. J Biol Chem 250, 7795-801 (1975).

17. Taylor, S. S., Buechler, J. A. & Yonemoto, W. cAMP-dependent Protein Kinase: Framework for a Diverse Family of Regulatory Enzymes. Annu. Rev. Biochemistry 59, 971-1005 (1990).

18. Skalhegg, B. S. et al. Location of cAMP-dependent protein kianse type I with the TCR=CD3 complex. Science 263, 84-87 (1994).

19. Herberg, F. W., Taylor, S. S. & Dostmann, W. R. Active site mutations define the pathway for the cooperative activation of cAMP-dependent protein kinase. Biochemistry 35, 2934-42 (1996).

20. Cadd, G. G., Uhler, M. D. & McKnight, G. S. Holoenzymes of cAMP-dependent protein kinase containing the neural form of type I regulatory subunit have an increased sensitivity to cyclic nucleotides. J Biol Chem 265, 19502-6 (1990).

21. Gamm, D. M., Baude, E. J. & Uhler, M. D. The major catalytic subunit isoforms of cAMP-dependent protein kinase have distinct biochemical properties in vitro and in vivo. J Biol Chem 271, 15736-42 (1996).

22. Zawadzki, K. M. & Taylor, S. S. cAMP-dependent protein kinase regulatory subunit type IIbeta: active site mutations define an isoform-specific network for allosteric signaling by cAMP. J. Biol. Chem. 279, 7029-36 (2004).

23. Solberg, R. et al. Human regulatory subunit RI beta of cAMP-dependent protein kinases: expression, holoenzyme formation and microinjection into living cells. Exp Cell Res 214, 595-605 (1994).

24. Amieux, P. S. & McKnight, G. S. The essential role of RI alpha in the maintenance of regulated PKA activity. Ann N Y Acad Sci 968, 75-95 (2002).

25. Cummings, D. E. et al. Genetically lean mice result from targeted disruption of the RII beta subunit of protein kinase A. Nature 382, 622-6 (1996).

26. Schreyer, S. A., Cummings, D. E., McKnight, G. S. & LeBoeuf, R. C. Mutation of the RIIbeta subunit of protein kinase A prevents diet-induced insulin resistance and dyslipidemia in mice. Diabetes 50, 2555-62 (2001).

27. Czyzyk, T. A., Sikorski, M. A., Yang, L. & McKnight, G. S. Disruption of the RIIbeta subunit of PKA reverses the obesity syndrome of Agouti lethal yellow mice. Proc Natl Acad Sci U S A 105, 276-81 (2008).

28. Newhall, K. J., Cummings, D. E., Nolan, M. A. & McKnight, G. S. Deletion of the RIIbeta-subunit of protein kinase A decreases body weight and increases energy expenditure in the obese, leptin-deficient ob/ob mouse. Mol Endocrinol 19, 982-91 (2005).

29. Thiele, T. E. et al. High ethanol consumption and low sensitivity to ethanol-induced sedation in protein kinase A-mutant mice. J. Neurosci. 20, 1-6 (2000).

30. Weber, W. & Hilz, H. cAMP-dependent Protein Kinases I and II: Divergent Turnover of Subunits. Biochemistry 25, 5661-5667 (1986).

31. Griffin, K. J. et al. Down-regulation of regulatory subunit type 1A of protein kinase A leads to endocrine and other tumors. Cancer Res 64, 8811-5 (2004).

32. Lohmann, S. M. & Walter, U. Regulation of the Cellular and Subcellular Concentrations and Distribution of Cyclic Nucleotide Protein Kinases. Adv. Cyc. Nuc. Prot. Phos. Res. 18, 63-117 (1984).

33. Casey, M. et al. Mutations in the protein kinase A R1alpha regulatory subunit cause familial cardiac myxomas and Carney complex. J Clin Invest 106, R31-8 (2000).

34. Kirschner, L. S. et al. Mutations of the Gene Encoding the Protein Kinase A Type I-a Regulatory Subunit in Patients with Carney Complex. Nature Genetics 26, 89 (2000).

35. Kammer, G. M. Deficient protein kinase a in systemic lupus erythematosus: a disorder of T lymphocyte signal transduction. Ann N Y Acad Sci 968, 96-105 (2002).

36. Taimi, M., Breitman, T. R. & Takahashi, N. Cyclic AMP-dependent protein kinase isoenzymes in human myeloid leukemia (HL60) and breast tumor (MCF-7) cells. Arch Biochem Biophys 392, 137-44 (2001).

37. Bartlett, J. M., Hulme, M. J. & Miller, W. R. Analysis of cAMP RI alpha mRNA expression in breast cancer: evaluation of quantitative polymerase chain reaction for routine use. Br J Cancer 73, 1538-44 (1996).

38. Khan, I. U., Laxminarayana, D. & Kammer, G. M. Protein kinase A RI beta subunit deficiency in lupus T lymphocytes: bypassing a block in RI beta translation reconstitutes protein kinase A activity and augments IL-2 production. J Immunol 166, 7600-5 (2001).

39. Mishra, N., Khan, I. U., Tsokos, G. C. & Kammer, G. M. Association of deficient type II protein kinase A activity with aberrant nuclear translocation of the RII beta subunit in systemic lupus erythematosus T lymphocytes. J Immunol 165, 2830-40 (2000).

40. Kammer, G. M., Khan, I. U. & Malemud, C. J. Deficient type I protein kinase A isozyme activity in systemic lupus erythematosus T lymphocytes. J Clin Invest 94, 422-30 (1994).

41. Cho-Chung, Y. S. Role of cyclic AMP receptor proteins in growth, differentiation, and suppression of malignancy: new approaches to therapy. Cancer Res 50, 7093-100 (1990).

42. McDaid, H. M. et al. Increased expression of the RIalpha subunit of the cAMP-dependent protein kinase A is associated with advanced stage ovarian cancer. Br J Cancer 79, 933-9 (1999).

43. Tortora, G., Yokozaki, H., Pepe, S., Clair, T. & Cho-Chung, Y. S. Differentiation of HL-60 leukemia by type I regulatory subunit antisense oligodeoxynucleotide of cAMP-dependent protein kinase. Proc Natl Acad Sci U S A 88, 2011-5 (1991).

44. Tortora, G., Clair, T. & Cho-Chung, Y. S. An antisense oligodeoxynucleotide targeted against the type II beta regulatory subunit mRNA of protein kinase inhibits cAMP-induced differentiation in HL-60 leukemia cells without affecting phorbol ester effects. Proc Natl Acad Sci U S A 87, 705-8 (1990).

45. Neary, C. L. et al. Protein kinase A isozyme switching: eliciting differential cAMP signaling and tumor reversion. Oncogene 23, 8847-56 (2004).

46. Knighton, D. R. et al. Structure of a Peptide Inhibitor Bound to the Catalytic Subunit of Cyclic Adenosine Monophosphate-Dependent Protein Kinase. Science 253, 414-420 (1991).

47. Knighton, D. R. et al. Crystal Structure of the Catalytic Subunit of cAMP-dependent Protein Kinase. Science 253, 407-414 (1991).

48. Diller, T. C., Madhusudan, Xuong, N.-h. & Taylor, S. S. Molecular Basis for Regulatory Subunit Diversity in cAMP-dependent Protein Kinase: Crystal Structure of The Type IIB Regulatory Subunit. Structure 9, 73-82 (2001).

49. Diller, T. C., Xuong, N.-h. & Taylor, S. S. Type IIB Regulatory Subunit of cAMP-Dependent Protein Kinase: Purification Strategies to Optimize Crystallization. Protein Expression and Purification 20, 357-364 (2000).

50. Vigil, D. et al. Conformational differences among solution structures of the type Ialpha, IIalpha and IIbeta protein kinase A regulatory subunit homodimers: role of the linker regions. J Mol Biol 337, 1183-94 (2004).

51. Vigil, D., Blumenthal, D. K., Taylor, S. S. & Trewhella, J. Solution scattering reveals large differences in the global structures of type II protein kinase A isoforms. J Mol Biol 357, 880-9 (2006).

52. Heller, W. T. et al. C subunits binding to the protein kinase A RI alpha dimer induce a large conformational change. J Biol Chem 279, 19084-90 (2004).

53. Leon, D. A., Herberg, F. W., Banky, P. & Taylor, S. S. A stable alpha-helical domain at the N terminus of the RIalpha subunits of cAMP-dependent protein kinase is a novel dimerization/docking motif. J Biol Chem 272, 28431-7 (1997).

54. Su, Y. et al. Regulatory (RIa) Subunit of Protein Kinase A: Structure of Deletion Mutant with cAMP Binding Domains. Science 269, 807-819 (1995).

55. Herberg, F. W., Dostmann, W. R. G., Zorn, M., Davis, S. J. & Taylor, S. S. Crosstalk between Domains in the Regulatory Subunit of cAMP-dependent Protein Kinase: Influence of Amino-Terminus on cAMP-Binding and Holoenzyme Formation. Biochemistry (1994).

56. Li, F. et al. Consequence of cAMP and Catalytic-Subunit Binding on the Flexibility of the A-Kinase Regulatory Subunit. Biochemistry 39, 15626-15632 (2000).

57. Anand, G., Taylor, S. S. & Johnson, D. A. Cyclic-AMP and Pseudosubstrate Effects on Type-I A-Kinase Regulatory and Catalytic Subunit Binding Kinetics. Biochemistry 46, 9283-91 (2007).

58. Herberg, F. W. & Taylor, S. S. Physiological inhibitors of the catalytic subunit of cAMP-dependent protein kinase: effect of MgATP on protein-protein interactions. Biochemistry 32, 14015-22. (1993).

59. Zimmermann, B., Schweinsberg, S., Drewianka, S. & Herberg, F. W. Effect of metal ions on high affinity binding of pseudosubstrate inhibitors to PKA. Biochem J (2008).

60. Diller, T. C., Xuong, N. H. & Taylor, S. S. Type II beta regulatory subunit of cAMP-dependent protein kinase: purification strategies to optimize crystallization. Protein Expr Purif 20, 357-64 (2000).

61. Wu, J., Jones, J. M., Nguyen-Huu, X., Ten Eyck, L. F. & Taylor, S. S. Crystal structures of RIalpha subunit of cyclic adenosine 5'-monophosphate (cAMP)-dependent protein kinase complexed with (Rp)-adenosine 3',5'-cyclic monophosphothioate and (Sp)-adenosine 3',5'-cyclic monophosphothioate, the phosphothioate analogues of cAMP. Biochemistry 43, 6620-9 (2004).

62. Saraswat, L. D., Filutowics, M. & Taylor, S. S. in Methods in Enzymology (eds. Corbin, J. A. & Johnson, R. A.) 325-336 (Academic Press, Inc., New York, 1988).

63. Abu-Abed, M., Das, R., Wang, L. & Melacini, G. Definition of an electrostatic relay switch critical for the cAMP-dependent activation of protein kinase A as revealed by the D170A mutant of RIalpha. Proteins 69, 112-124 (2007).

64. Aimes, R. T., Hemmer, W. & Taylor, S. S. Serine-53 at the tip of the glycine-rich loop of cAMP-dependent protein kinase: role in catalysis, P-site specificity, and interaction with inhibitors. Biochemistry 39, 8325-32 (2000).

65. Valiev, M., Kawai, R., Adams, J. A. & Weare, J. H. The role of the putative catalytic base in the phosphoryl transfer reaction in a protein kinase: first-principles calculations. J. Am. Chem. Soc. 125, 9926-7 (2003).

66. Madhusudan, Akamine, P., Xuong, N. H. & Taylor, S. S. Crystal structure of a transition state mimic of the catalytic subunit of cAMP-dependent protein kinase. Nat Struct Biol 9, 273-7. (2002).

67. Cheng, X., Phelphs, C. & Taylor, S. S. Differential Binding of cAMP-dependent Protein Kinase Regulatory Subunit Isoforms Ia and IIB to the Catalytic Subunit. J. Biol. Chem. 6, 4102-4108 (2001).

68. Newman, J. et al. Towards rationalization of crystallization screening for small- to medium-sized academic laboratories: the PACT/JCSG+ strategy. Acta Crystallogr D Biol Crystallogr 61, 1426-31 (2005).

69. Wu, J., Brown, S., Xuong, N. H. & Taylor, S. S. RIalpha subunit of PKA: a cAMP-free structure reveals a hydrophobic capping mechanism for docking cAMP into site B. Structure 12, 1057-65 (2004).

70. Luft, J. R. et al. Efficient optimization of crystallization conditions by manipulation of drop volume ratio and temperature. Protein Sci 16, 715-22 (2007).

71. Burns-Hamuro, L. L., Barraclough, D. M. & Taylor, S. S. Identification and functional analysis of dual-specific A kinase-anchoring protein-2. Methods Enzymol 390, 354-74 (2004).

72. Huang, L. J., Durick, K., Weiner, J. A., Chun, J. & Taylor, S. S. D-AKAP2, a novel protein kinase A anchoring protein with a putative RGS domain. Proc. Natl. Acad. Sci. 94, 11184-11189 (1997).

73. Burns-Hamuro, L. L. et al. Designing isoform-specific peptide disruptors of protein kinase A localization. Proc Natl Acad Sci U S A 100, 4072-7 (2003).

74. Frank, R. The SPOT-synthesis technique. Synthetic peptide arrays on membrane supports--principles and applications. J Immunol Methods 267, 13-26 (2002).

75. Martin, B. R., Deerinck, T. J., Ellisman, M. H., Taylor, S. S. & Tsien, R. Y. Isoform-specific PKA dynamics revealed by dye-triggered aggregation and DAKAP1alpha-mediated localization in living cells. Chem Biol 14, 1031-42 (2007).

76. Diskar, M., Zenn, H. M., Kaupisch, A., Prinz, A. & Herberg, F. W. Molecular basis for isoform-specific autoregulation of protein kinase A. Cell Signal 19, 2024-34 (2007).

77. Trewhella, J., Carlson, V. A., Curtis, E. H. & Heidorn, D. B. Differences in the solution structures of oxidized and reduced cytochrome c measured by small-angle X-ray scattering. Biochemistry 27, 1121-5 (1988).

78. Svergun, D. I., Semenyuk, A. V. & Feigin, L. A. Small-angle-scattering-data treatment by the regularization method. Acta Cryst A44, 244-350 (1988).

79. Hamuro, Y. et al. Mapping intersubunit interactions of the regulatory subunit (RIalpha) in the type I holoenzyme of protein kinase A by amide hydrogen/deuterium exchange mass spectrometry (DXMS). J Mol Biol 340, 1185-96 (2004).

80. Anand, G. S., Hughes, C. A., Jones, J. M., Taylor, S. S. & Komives, E. A. Amide H/2H exchange reveals communication between the cAMP and catalytic subunit-binding sites in the R(I)alpha subunit of protein kinase A. J Mol Biol 323, 377-86 (2002).

81. Anand, G. S. et al. Identification of the protein kinase A regulatory RIalpha-catalytic subunit interface by amide H/2H exchange and protein docking. Proc Natl Acad Sci U S A 100, 13264-9 (2003).

82. Hamuro, Y. et al. Dynamics of cAPK type IIbeta activation revealed by enhanced amide H/2H exchange mass spectrometry (DXMS). J Mol Biol 327, 1065-76 (2003).

83. Kornev, A. P., Taylor, S. S. & Ten Eyck, L. F. A generalized allosteric mechanism for cis-regulated cyclic nucleotide binding domains. PLoS Comput Biol 4, e1000056 (2008).

84. Kannan, N., Haste, N., Taylor, S. S. & Neuwald, A. F. The hallmark of AGC kinase functional divergence is its C-terminal tail, a cis-acting regulatory module. Proc Natl Acad Sci U S A 104, 1272-7 (2007).

85. Deminoff, S. J., Howard, S. C., Hester, A., Warner, S. & Herman, P. K. Using substrate-binding variants of the cAMP-dependent protein kinase to identify novel targets and a kinase domain important for substrate interactions in Saccharomyces cerevisiae. Genetics 173, 1909-17 (2006).

86. Su, Y. et al. Regulatory (RIa) Subunit of Protein Kinase A: Structure of Deletion Mutant with cAMP Binding Domains. Science 269, 807-819 (1995).

87. Dostmann, W. R. et al. Probing the cyclic nucleotide binding sites of cAMP-dependent protein kinases I and II with analogs of adenosine 3',5'-cyclic phosphorothioates. J Biol Chem 265, 10484-91 (1990).

88. Dostmann, W. et al. Analogs of Adenosine Cyclic-3',5'-phosphorothioates: Probing the Cyclic Nucleotide Binding Sites of cAMP-dependent Protein Kinases I and II. J Biol. Chem. 265, 10484-10491 (1990).

89. Ogreid, D. & Doskeland, S. O. The kinetics of association of cyclic AMP to the two types of binding sites associated with protein kinase II from bovine myocardium. The kinetics of the interaction between cyclic AMP and the regulatory moiety of protein kinase II. Evidence for interaction between the binding sites for cyclic AMP. FEBS Lett 129, 287-92 (1981).

90. Dostmann, W. R. & Taylor, S. S. Identifying the molecular switches that determine whether (Rp)-cAMPS functions as an antagonist or an agonist in the activation of cAMP-dependent protein kinase I. Biochemistry 30, 8710-6 (1991).

91. Saldanha, S. A., Kaler, G., Cottam, H. B., Abagyan, R. & Taylor, S. S. Assay principle for modulators of protein-protein interactions and its application to non-ATP-competitive ligands targeting protein kinase A. Anal Chem 78, 8265-72 (2006).

92. Ogreid, D., Ekanger, R., Suya, R. H., Miller, J. P. & Doskeland, S. O. Comparison of the two classes of binding sites (A and B) of type I and type II cyclic-AMP-dependent protein kinases by using cyclic nucleotide analogs. Eur. J. Biochem. 181, 19-31 (1989).

93. Cook, P. F. Kinetic Studies To Determine the Mechanism of Regulation of Bovine Liver Glutamate Dehydrogenase by Nucleotide Effectors. Biochemistry 21, 113-116 (1982).